INTERACTIONS
BETWEEN
CADMIUM AND CALCITE

RENATA D. VAN DER WEIJDEN

Interactions between Cadmium and Calcite

Renata D. van der Weijden

Interactions between Cadmium and Calcite

Interacties tussen Cadmium en Calciet

(met een samenvatting in het Nederlands)

PROEFSCHRIFT

TER VERKRIJGING VAN DE GRAAD VAN DOCTOR
AAN DE UNIVERSITEIT UTRECHT
OP GEZAG VAN DE RECTOR MAGNIFICUS PROF. DR. J.A. VAN GINKEL
INGEVOLGE HET BESLUIT VAN HET COLLEGE VAN DECANEN
IN HET OPENBAAR TE VERDEDIGEN
OP DINSDAG 28 NOVEMBER 1995 DES NAMIDDAGS TE 4.15 UUR

door

RENATA DOROTHEA VAN DER WEIJDEN
geboren op 5 april 1962 te Doorwerth

To Mrs. Sprinkle

Contents

General introduction

1. Cadmium-Calcite Interactions

In this thesis the interactions between cadmium (Cd) and calcite ($CaCO_3$) are treated. Although the interactions with other minerals are interesting as well, it turned out that the interactions with calcite alone were complicated and intriguing enough to keep a scientist focused on these for many years. And still there can be no pretence whatsoever, that all is said and done now. The increase in the number of investigations on the interactions with calcite is not expected to diminish. This is partly due to the development of new scientific tools that will enable us to study the surface of minerals at (almost) atomic levels. It is also due to the fact that calcite is an important mineral in the geochemical environment, because of its wide abundance (7% of the earth's surface) and its role in many geochemical processes.

The geochemical fate of Cd is important for flora, fauna and humanity, because Cd is highly toxic. Though Cd may be appreciated for its use in alloys, batteries, pigments and thermoplastic stabilizers, its presence in e.g. phosphatic fertilizers and municipal waste, poses an environmental threat. Concentrations as low as 2.7×10^{-7} M in ground water may reduce the growth of plants by as much as 50%. Average concentrations of Cd in the earth's crust, ocean surface water, ocean deep water and river water are 1.4×10^{-6} M, 1×10^{-10} M, 1.1×10^{-9} M and 6×10^{-10} M respectively. The toxicity of Cd is directly related to its free aqueous activity. Assessment of the factors which may reduce or enhance Cd mobilization is therefore of great significance. The main factors by which the aqueous Cd activities and the Cd mobilization are controlled, appear to be sorption on, or incorporation in minerals and the formation of aqueous complexes. Examples of effective removal of Cd by $CaCO_3$ in the marine environment are the Cd uptake in biogenic calcite and in carbonaceous sediments during diagenesis.

A study on the interactions between Cd and calcite, contributes to the understanding of the ways in which minerals can serve as a sink for trace elements. Besides investigation of the influence on the aqueous concentration of Cd, in the light of a possible impact on the environment, additional aims were to evaluate the relative importance of the various interactions (e.g. sorption, incorporation, solid-state diffusion), to acquire a deeper understanding of the nature of these interactions, and to discover relationships between sorption and incorporation behavior.

In order to study the interactions between Cd and calcite, laboratory experiments simulating various aqueous environments were carried out. The great advantage of laboratory experiments over on-site research, is that system parameters are well defined and can be systematically varied. Furthermore, the possibility of employing radiotracer techniques, which are very accurate and by which subtle differences can be reliably detected, is a real advantage. The main difference with the actual geological setting is that (most) laboratory experiments are carried out in closed systems and that some processes proceed at a different rate than in the real world. Still, these experiments are a way to provide very valuable information concerning which parameters are important for sorption and incorporation of Cd under geological conditions.

2. Research outline

The thesis is composed of five chapters, some of which have been published or have been accepted for publication. The contents in some of the chapters may therefore slightly overlap, also because the subjects are closely related. The first two chapters focus mostly on the sorption of Cd on calcite, whereas the next two chapters are devoted to calcite growth and Cd incorporation during growth. In the fifth and final chapter, Cd sorption and incorporation is studied in an environment where calcite is formed, and where most of the factors dealt with in the previous chapters influencing calcite growth, Cd sorption and incorporation, are at play.

In *Chapter 1* the (im)mobilization of Cd in the estuary, where significant changes in the ionic strength, pH, and composition of water occur, is investigated. This is done by studying sorption of Cd on calcite using a ^{109}Cd tracer, in solutions simulating various mixtures of seawater and riverwater. The results are compared to sorption in mixtures of real seawater and nanopure water. In addition, the importance of the surface dynamics of calcite for removal of Cd by sorption and subsequent incorporation in these various solutions is investigated using a ^{45}Ca tracer.

Whereas in chapter 1 the effects of Mg^{2+}, Ca^{2+} and Cl^- on Cd^{2+} sorption are addressed, *Chapter 2* focuses on the influence of phosphate and sulfate. Both anions, present in seawater, are known to display affinity for the calcite surface. Their effect on the Cd sorption and the calcite surface dynamics is studied in solutions with an ionic strength of seawater over in the pH range 7 - 9.5. The pH range was also chosen in view of the carbonation process observed in municipal waste bottom-ash (chapter 5), during which a large decrease in pH occurs. Sorption of phosphate is studied separately with a ^{32}P tracer, because of the significance of the relationship between oceanic phosphate concentrations and Cd concentrations in biogenic calcite for reconstructing paleoceanic conditions.

Chapter 3 is devoted to the seeded-growth of calcite in supersaturated solutions at high (seawater) ionic strength. The influence of various total calcium and total carbonate concentrations on growth and growth rate is investigated using a chemo-stat system. The chemo-stat system allows for direct and accurate measurement of the outgrowth and growth rate of calcite. The influence of contaminants on the growth rate and the crystal morphology is also studied.

The same experimental method and solution conditions used for plain calcite growth, are applied in a study described in *Chapter 4* on the incorporation of Cd during calcite crystal growth. The influence of pH, growth rate, solution composition and calcite surface features on the Cd incorporation is investigated. Results of calcite crystal growth (rate) and Cd incorporation are discussed in the light of recent papers which contain new findings on the influence of the Ca/carbonate ratio on calcite crystal growth.

In a final study, described in *Chapter 5*, the importance of calcite formation resulting from carbonation of municipal incinerated solid waste bottom ash, for immobilizing Cd and other heavy metals, is investigated. The amount and composition of the precipitate after carbonation of filtered leachates are compared to the precipitate obtained from lime and aluminum hydroxide solutions. Besides the parameters influencing Cd sorption and incorporation, the parameters influencing calcite formation are considered as well.

For an overview of the most important experimental findings, the reader is referred to the *Summary*.

Chapter 1

Sorption and sorption reversibility of Cd on calcite under simulated riverine, estuarine and marine conditions

Abstract— Laboratory experiments using ^{109}Cd and ^{45}Ca tracers were carried out to study sorption and sorption reversibility of cadmium on calcite under simulated riverine, estuarine and marine conditions. Sorption of Cd on calcite increased with increasing sorption time, calcite surface area, aqueous Cd^{2+} activity, and decreasing aqueous Ca^{2+}, Mg^{2+}, and Cl^- activity. Electrostatic factors which could be influenced by the ionic strength, such as surface charge or double layer thickness, had little effect on the sorption behavior of Cd. Therefore Cd is considered to be chemisorbed and sorption data can be described with a Ca-Cd exchange model. Desorption experiments showed that Cd sorption on calcite is partly irreversible. The extent of reversibility depends on sorption time and pH. After short sorption times (< 1 week) desorption and rapid isotopic exchange experiments with ^{109}Cd showed that sorption reversibility decreases from pH = 8.3 to 7.9. At lower pH, Cd may merely be sorbed at the energetically most favorable sites like kinks and steps, because of the increased competition with Ca. After long equilibration times (2-6 months) the sorption reversibility decreases as a result of recrystallization. ^{45}Ca exchange experiments suggest that the recrystallization rate decreases from pH = 7.9 to 8.2. As a result thereof, the slow removal rate of Cd decreases as well. This study indicates that although at a pH of 8.3 more Cd is rapidly adsorbed, a pH of 7.9 seems favorable for more permanent uptake of Cd by calcite. Assuming residence times of suspended calcite in rivers (lower pH) are > 24 hours, the release of Cd in the estuary (higher pH) is expected to be limited.

1.1. Introduction

The heavy metal, cadmium, is introduced into the environment by natural sources (e.g. weathering of carbonaceous shales and of sphalerite), by industrial production (e.g. as a byproduct of the Pb-Zn industry), and by waste discharge (e.g. pigments, fly ash, phosphate fertilizers and phosphogypsum) (Korzun and Heck, 1990).

Since the toxicity of Cd is related to its free aqueous cation activity and not to its total concentration, it is important to know the aqueous speciation and the distribution of the metal between the aqueous and particulate phases (Buffle et al., 1990). Although the inorganic aqueous speciation of Cd in various aqueous environments has been studied in detail (e.g. Long and Angino, 1977; Mantoura, 1978; Turner et al., 1981), the interaction with solid phases is still an area of research.

This paper offers a systematic study of parameters which influence Cd sorption on calcite in the estuarine environment. The estuarine environment is of interest because of the drastic changes in pH, ionic strength, turbidity, composition, and sometimes redox conditions, and has therefore been a focus of attention (Windom et al., 1991; Elbaz-Poulichet et al., 1991; Harper, 1991). These changes in the aqueous conditions influence the Cd^{2+} activity, the Cd^{2+} aqueous speciation, the competition of Cd^{2+} with other cations for particulate phases, the surface speciation of particulate phases and thus the distribution and residence time of Cd in the estuarine environment.

Calcium carbonate was chosen as sorbent, because calcite can be a major constituent of riverine suspended material (e.g. Krka river, Yugoslavia, Elbaz-Poulichet et al., 1991) and a major solid in the marine environment. The interaction of Cd with calcite is of additional interest, because the Cd distribution in biogenic carbonates is thought to reflect changes in nutrient distributions due to altered oceanic circulation patterns (Boyle et al., 1988).

Davis et al. (1987) studied the effects of pH and magnesium concentration on Cd sorption on calcite at low ionic strengths. The study presented here, considers the effects of parameters influencing Cd sorption in the estuarine environment (e.g. sorption time, pH, Cd^{2+}, Cl^-, and Mg^{2+} activity) at ionic strengths ranging from 0.011 to 0.7. The relative importance of surface processes such as adsorption, recrystallization, surface precipitation, diffusion and solid-solution formation, which have been reported to control Cd sorption on calcite (McBride, 1980; Davis et al., 1987; Comans and Middelburg, 1987; Zachara et al., 1991) will be considered here as well.

1.2. Materials

Electrolyte solutions were prepared with nanopure water, filtered (0.22 mm) shelf-aged Doggersbank (North Sea) surface water containing less than 0.01 mM phosphate and less than 40 mM DOC, the reagent grade chemicals NaCl, $NaNO_3$, $MgNO_3$, and suprapure $CaCO_3$ and HNO_3.

Suprapure $CaCO_3$ (Merck) was used as sorbent and for achieving equilibrium with respect to $CaCO_3$ in all solutions. Due to repetitive experimenting, two batches of $CaCO_3$ were used as sorbent. SEM photography showed that the habit of the well crystallized $CaCO_3$ was rhombohedral, with grain sizes of 10 - 100 mm of intergrown rhombohedrons. The surface areas as determined with a micromeritics type PulseChemiSorb 2700, were 0.13 and 0.28 m^2/g for batch X and Y respectively, with a maximum error of 10%.

Carrier-free radioactive tracers (Amersham) used to study sorption and recrystallization were ^{109}Cd (as $CdCl_2$) diluted with 0.01 M HNO_3 and ^{45}Ca (as $CaCl_2$) diluted with nanopure water.

The pH of the solutions was measured with an Ingold microtip-electrode connected to a Knick pH-meter and calibrated with Ingold standardized buffers of pH = 7.00 and 9.21. The composition of the solutions was checked by means of Atomic Absorption Spectrometry (AAS, GFAAS) for major ions and Cd^{2+}. The concentration of Cd was below the detection limit (< 9 nM).

1.3. Methods

Before going into detail on how the various surface processes were studied, a description of the terminology used in this paper is given first. The term "adsorption" is used herein to mean the accumulation of a sorbate on a sorbent without the development of a three-dimensional structure (Sposito, 1986). The term adsorption also has a more general usage by which it refers to the forward sorption process, as opposed to the reverse desorption process (Comans, 1990). The term "recrystallization" as used in this paper concerns one phase only and includes Ostwald ripening (growth of larger crystals at the cost of smaller ones), the formation of agglomerates of crystals and surface renewal (fillup of faults etc.). The formation of a surface phase by propagation of a molecular unit in three dimensions is herein referred to as "surface precipitation" (Sposito, 1986). For surface precipitation to occur, the aqueous solution must be supersaturated with respect to the equilibrium solubility of a solid phase (Davis et al., 1987). The term "solid-solution" is used when the ion is actually incorporated in the crystal lattice, due to either one, or a combination of the processes mentioned above. Finally, the overall process of loss of Cd from solution to calcite, is herein called "sorption" (Sposito, 1984).

1.3.1. Sorption

Calculations were made with the chemical speciation code CHARON (De Rooij, 1990) to create solutions with the desired pH, ionic strength (I) and composition. The formation constants of the species used for these calculations are listed in Appendix 1. The composition of the solutions was chosen as to isolate the effects of single parameters and is given in Table 1. The effect of increasing I, Mg^{2+} or Cl^- activity, was studied in three sets of solutions, simulating various degrees of mixing between carbonate buffered riverwater and seawater, using pH = 7.9 and 8.3 as an average value for the respective endmembers. A fourth set of mixtures of nanopure and seawater was used to determine whether the previously addressed parameters could account for the sorption behavior in these mixtures.

Solubility equilibrium with respect to $CaCO_3$ was achieved by adding ± 8 g of $CaCO_3$ to, and bubbling H_2O saturated and filtered air through the solutions (1 l) until the pH stabilized (>1 week). In the fourth set of nanopure/seawater mixtures the pH did not increase with increasing salinity as would be representative for estuaries, but decreased instead. Because surface seawater is supersaturated with respect to calcite, the addition of $CaCO_3$ provided nuclei for crystal growth and caused calcite to precipitate (Chave and Schmalz, 1966). Therefore, the pH in seawater equilibrated with $CaCO_3$ was approximately 7.95 instead of 8.3.

4

Table 1. Composition and characteristics of the solutions used in this study.

Interactions between cadmium and calcite

Exp	NaCl (mM)	Ca(NO3)2 (mM)	Mg(NO3)2 (mM)	NaNO3 (mM)	S	pHs-pHf	I	γ Cd^{2+}	symbol
1A		3.30			~0	~7.85	0.011	0.661	▽
1B		5.85		100	5	7.86-7.79	0.118	0.336	△
1C		7.05		200	10	7.87-7.78	0.222	0.304	○
1D		8.55		400	20	7.82-7.77	0.427	0.286	□
1E		9.70		665	35	7.82-7.75	0.696	0.315	+
1F				700	35	8.37-8.26	0.704	0.314	◊
2B	100	5.85			5	7.96-7.93	0.118	0.067	△
2C	200	7.05			10	7.93-7.86	0.222	0.033	○
2D	400	8.55			20	7.87-7.81	0.427	0.014	□
2E	665	9.70			35	7.89-7.86	0.696	0.007	+
2F	700				35	8.27-8.24	0.701	0.006	◊
2F*	665				35	8.26	0.696	0.007	
3B		5.85	7.3	78.6	5	7.90-7.88	0.115	0.347	△
3C		7.00	14.6	157.3	10	7.91-7.85	0.222	0.286	○
3D		8.40	29.1	314.3	20	7.88-7.84	0.428	0.285	□
3E		9.60	51.0	515.2	35	7.88-7.83	0.699	0.305	+
3F			51.0	553.0	35	8.28-8.21	0.709	0.302	◊
	nanopure water (ml)	seawater (ml)							
4B	857.1	142.9			5	8.17-8.12	0.101	0.0805	△
4C	714.2	285.8			10	8.08-8.00	0.200	0.0406	○
4D	428.7	571.3			20	7.99-7.91	0.395	0.0186	□
4E	0	1000			35	7.95-7.87	0.690	0.0090	+

The activity coefficient (γ) of the free Cd^{2+} ion in solution is given as well as the figure symbols. pH$_s$ and pH$_f$ represent the pH at the start and at the end of the sorption experiment respectively. S is the simulated salinity based on the ionic strength (I) of seawater with corresponding salinity.

Prior to use, the solution was filtered through a 0.22 mm micropore filter. This procedure changed the pH of the solution by less than 0.05 pH unit. Eighty ml of the solution and 400 mg of dry suprapure calcite were allowed to pre-equilibrate in a teflon (PFA) vessel for at least 24 hours. After pre-equilibration, 160 ml of a mixture of ^{109}Cd in 0.01M HNO$_3$ and Cd carrier in 0.01M HNO$_3$ was added, as well as 0.8 ml of 0.001M Ca(OH)$_2$ to compensate for the addition of acid, yielding solutions with initial Cd^{2+} concentrations of 8.84, 44.0, 88.2 and 176.43 nM. All solutions were prepared in duplicate, the vessels were placed in a thermostated shakerbath, and kept at a temperature of 20°C ± 2°. At intervals during equilibration, subsamples were withdrawn under continuous stirring for measuring pH and for gamma-counting the ^{109}Cd activity of the liquid phase in 1 ml of supernatant after 20 minutes centrifugation at 4000 g in a Sorval-SS3 centrifuge. Subsamples containing ^{109}Cd were counted in polythene tubes on a Compugamma LKB 1280 gamma-counter with a 3 inch NaI well-type detector, producing results with a maximum deviation of 3% between duplicate samples. Aqueous and sorbed Cd^{2+} concentrations were calculated as described in the paper of Comans (1987). The slow Cd removal rate (SCRR) (after Davis et al., 1987) was calculated from the least square fit of sorption data for time greater than 190 hours.

The activity coefficient (γ) of the free Cd^{2+} ion in solution is given as well as the figure symbols. pH$_s$ and pH$_f$ represent the pH at the start and at the end of the sorption experiment respectively. S is the simulated salinity based on the ionic strength (I) of seawater with corresponding salinity.

Solubility equilibrium with respect to CaCO$_3$ was achieved by adding ± 8 g of CaCO$_3$ to, and bubbling H$_2$O saturated and filtered air through the solutions (1 l) until the pH stabilized (>1 week). In the fourth set of nanopure/seawater mixtures the pH did not increase with increasing salinity as would be representative for estuaries, but decreased instead. Because surface seawater is supersaturated with respect to calcite, the addition of CaCO$_3$ provided nuclei for crystal growth and caused calcite to precipitate (Chave and Schmalz, 1966). Therefore, the pH in seawater equilibrated with CaCO$_3$ was approximately 7.95 instead of 8.3.

1.3.2. Desorption

Desorption was initiated after *short* (< 1 week) and *long* (2-6 months) equilibration times to study sorption reversibility. A sorption reaction is considered 100% reversible if the ratios of the sorbed and aqueous species before and after desorption are equal (in the case of a linear isotherm).

Solutions with an ionic strength of 0.7 created with NaNO$_3$ and with a pH of 7.9 and 8.3 were replaced by Cd-free NaCl solutions with equal I and pH after short sorption times of 1, 2.5, 19 and 121 hours. After 50 minutes sorption time, rapid isotopic ^{109}Cd exchange experiments (as described in Davis et al., 1987) in identical NaNO$_3$ solutions were carried out as well, to support desorption results.

After long sorption times of 183, 81 and 74 days respectively, desorption was started in the solutions sets with increasing I, Mg^{2+} activity and in the various nanopure-/seawater mixtures. Hereto, the solutions were replaced with a Cd-free electrolyte of the same composition, except for the solutions with increasing I, which were replaced with a nanopure-/seawater mixture of $S = 5$ and subsequently with Doggersbank seawater ($S = 35$).

All solutions were replaced by transferring the remainder of the solutions after use for sorption studies to teflon (PFA) centrifuge tubes and centrifuging at 4000 g. The supernatant was removed and replaced with an equal amount of Cd-free electrolyte. The new electrolyte suspensions, were transferred back from the centrifuge tubes into the

reaction vessels. Desorption was followed with time by withdrawing subsamples as described under sorption.

1.3.3. ^{45}Ca isotopic exchange

In order to discriminate between the effects of adsorption and recrystallization, the latter process was studied with ^{45}Ca isotopic exchange. The effects of the variables which most likely influence recrystallization, pH, I and Mg (Davis et al., 1987) were studied in three sets of solutions also employed in the sorption/desorption studies. In teflon (PFA) vessels, 40 ml of solution and 0.5 g of suprapure calcite (batch Y) were allowed to pre-equilibrate one day or three months in the shakerbath. The experiment was started by addition of 40 ml of diluted ^{45}Ca tracer. Subsamples for pH monitoring and for ß-counting of ^{45}Ca were withdrawn under continuous stirring. After centrifugation for 20 minutes at 4000 g, 1 ml of the supernatant and 10 ml Instagel scintillation fluid were transferred to polythene counting tubes. The tubes were counted on a Philips β-scintillation counter. Davis et al. (1987) made a distinction between the short term ^{45}Ca exchange and the long term ^{45}Ca exchange rate, in this paper referred to as STE and LTER respectively. The STE was calculated as the mean of ^{45}Ca exchange of duplicate samples after 3.5 hours. The LTER was obtained by calculating the linear least square fit of single data for times greater than 28.5 hours.

1.4. Results

1.4.1. Sorption

In all sets of solutions a fast initial uptake ($t < 48$ hours) and a slow uptake region can be distinguished. The sorption percentages for the Cd concentrations of 8.84 - 176.43 nM/l are all equal, which implies a linear sorption isotherm in this concentration region. Papadopoulos and Rowell (1988) found the sorption isotherm to be linear up to 1 mmol Cd/g calcite. Figures presented here are for one concentration only, to enhance clarity.

Fig. 1 shows the Cd sorption behavior in solutions with increasing ionic strength. A decrease in Cd sorption is seen from $I = 0.011$ to $I = 0.118$. A further decrease from $I = 0.118$ to $I = 0.704$ is not observed. When plotting sorbed Cd versus free aqueous Cd^{2+} activity after 4 hours sorption time for a pH of 7.9 as interpolated from Fig. 1, the data conform to a single activity based isotherm (Fig. 2). For the activity coefficients, the extended Davies equation and Pitzer calculations were employed. In Fig. 3 the amount of initially sorbed Cd decreases as chloride increases. In Fig. 4 a plot similar to Fig. 2 is constructed from another experiment with increasing Cl⁻. From Figs. 2 and 4 it appears that Cd sorption depends on the free aqueous activity.

Initial fast sorption ($t < 48$ hours) decreases with decreasing pH. In Fig. 3, for instance, the initial amount of sorbed Cd at pH = 8.26 and $I = 0.7$ almost equals the sorbed amount at pH = 7.95 and $I = 0.118$, whereas the free aqueous Cd^{2+} activity in the latter case is higher by an order of magnitude. The pH also affects the slow Cd removal rate (SCRR). The SCRR decreases from pH = 7.9 to pH = 8.3. After 509 hours in Fig. 3, the amount of sorbed Cd at $I = 0.118$ and pH = 7.95 exceeds the amount of sorbed Cd at $I = 0.7$ and pH = 8.26, due to a higher uptake rate.
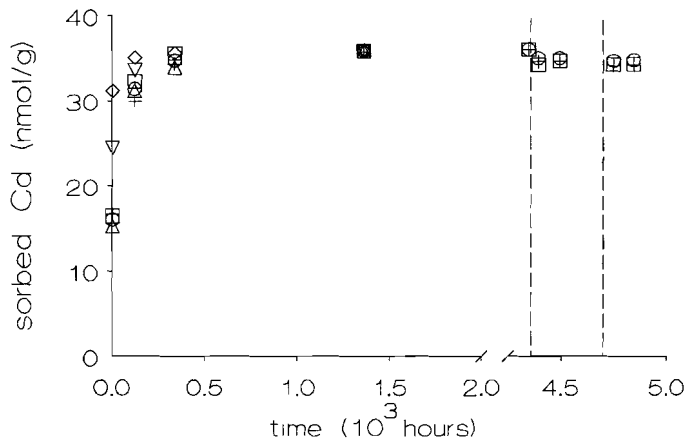
	NaNO₃ mM	I	pH
∇		0.011	7.85
Δ	100	0.118	7.83
O	200	0.222	7.83
□	400	0.427	7.79
+	665	0.696	7.78
◊	700	0.704	8.32

Fig. 1. Cadmium sorption on calcite versus time in solutions of increasing ionic strength. Calcite is batch Y, 4.94 g CaCO₃/l, 176.4 nM Cd. Desorption in a Cd-free nanopure-/seawater mixture with S = 5 (first dashed line) followed by desorption in Cd-fee seawater (second dashed line).
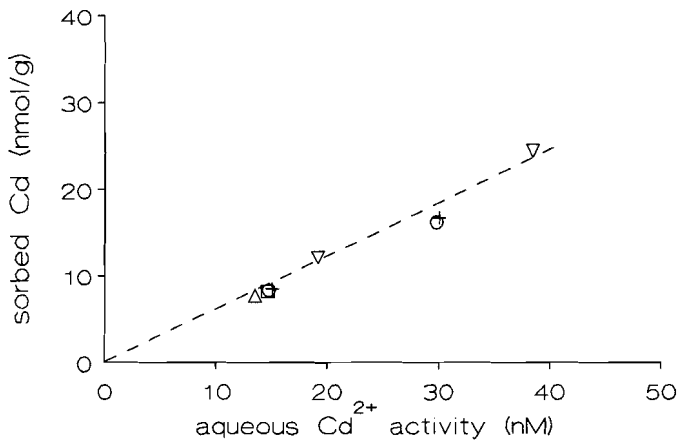
	NaNO₃ mM	I	pH
∇		0.011	7.85
O	200	0.222	7.83
+	665	0.696	7.78

Fig. 2. Sorbed Cd versus aqueous Cd^{2+} activity interpolated from Fig. 1: various NaNO₃ solutions of increasing ionic strength at pH = 7.9. The sorption time is 4 hours, calcite is batch Y, and Cd concentrations are 88.2 and 176.4 nM.
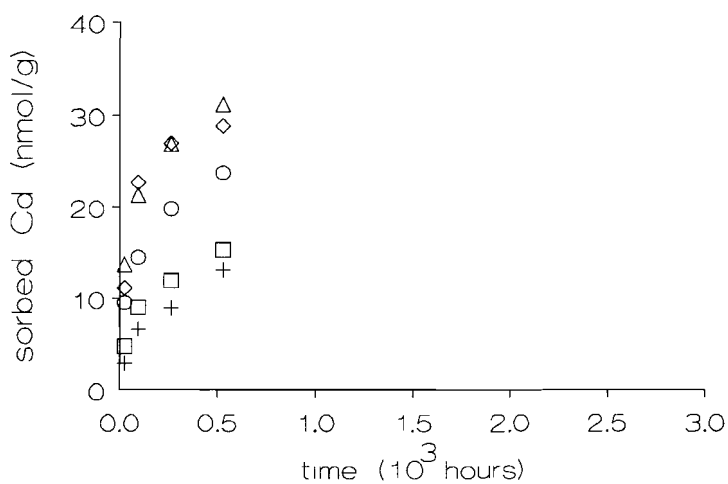
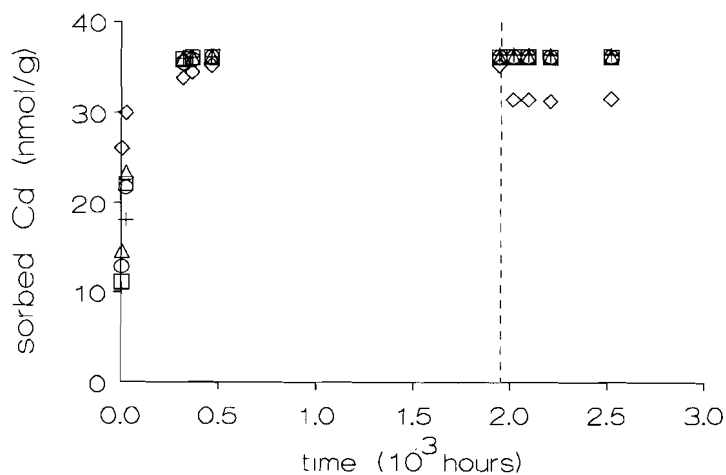|	NaCl mM	I	pH
Δ	100	0.118	7.95
O	200	0.222	7.89
□	400	0.427	7.85
+	665	0.696	7.87
◊	700	0.704	8.26

Fig. 3. Cadmium sorption on calcite versus time in solutions of increasing chloride concentrations and I. Calcite is batch Y, 4.94 g $CaCO_3$/l, 176.4 nM Cd.
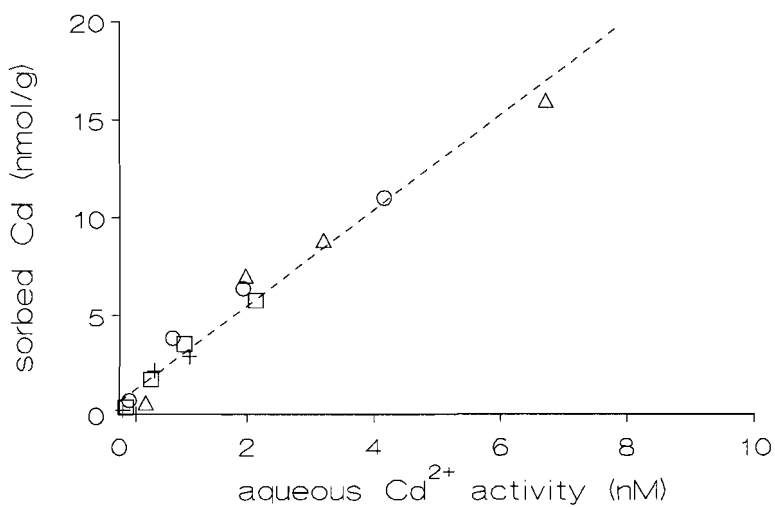
	NaCl mM	I	pH
Δ	100	0.118	7.95
O	200	0.222	7.89
□	400	0.427	7.85
+	665	0.696	7.87

Fig. 4. Sorbed Cd versus aqueous Cd^{2+} activity after sorption for 49 hours in solutions of increasing I and Cl^- activity at pH = 7.9. Calcite is batch X, 8.84, 44.1, 88.2 and 176.4 nM Cd.

The influence of increasing Mg^{2+} activities is very small (Fig. 5); Cd sorption decreases by only 7% when Mg increases from 7 to 51 mmoles at pH = 7.9. In the various nanopure-/seawater mixtures, the effects of I, Cl^-, Mg^{2+} and pH are combined. (Figs 6a and 6b). Initially, as chloride concentrations increase, the extent of Cd sorption decreases. After long sorption times, the differences in slow Cd removal rates as a result of different pH values become increasingly important. Fig. 6a shows the sorption results on calcite batch X after 1 day pre-equilibration time and Fig. 6b shows the sorption results on calcite batch Y after two weeks pre-equilibration time. Though the surface area estimate of batch Y as compared to batch X is twice as large (0.28 m^2/g versus 0.13 m^2/g), the percentage of Cd sorption is only 25% higher on batch Y after 24 hours. Experiments with batch X and Y in solutions with increasing I and chloride concentrations also yielded 25% more initial sorption for batch Y. Comparison of Fig 6a and 6b shows that not only the extent of Cd sorption but also the sorption pattern differs. A relatively high SCRR is observed at pH = 7.99 and 57% seawater with batch Y, but not with batch X. The values for the SCRR apparently also may be influenced by the particular batch of calcite and the pre-equilibration time, besides depending on pH.

	MgNO₃ mM	I	pH
Δ	100	0.118	7.95
O	200	0.222	7.89
□	400	0.427	7.85
+	665	0.696	7.87
◊	700	0.704	8.26

Fig. 5. Cadmium sorption on calcite versus time in solutions of increasing Mg concentrations and I. Calcite is batch Y, 4.94 g CaCO₃/l, 176.4 nM Cd. Desorption (at dashed line) in Cd-free Mg solutions with identical composition.

	% seawater in nanopure water	I	pH
Δ	14.29	0.101	8.18
O	28.58	0.200	8.12
□	57.13	0.395	8.03
+	100	0.690	7.95

Fig. 6a. Cadmium sorption on calcite versus time in various nanopure-/seawater mixtures. Calcite is batch X, 4.94 g CaCO₃/l, 176.4 nM Cd, pre-equilibration time is 24 hours.

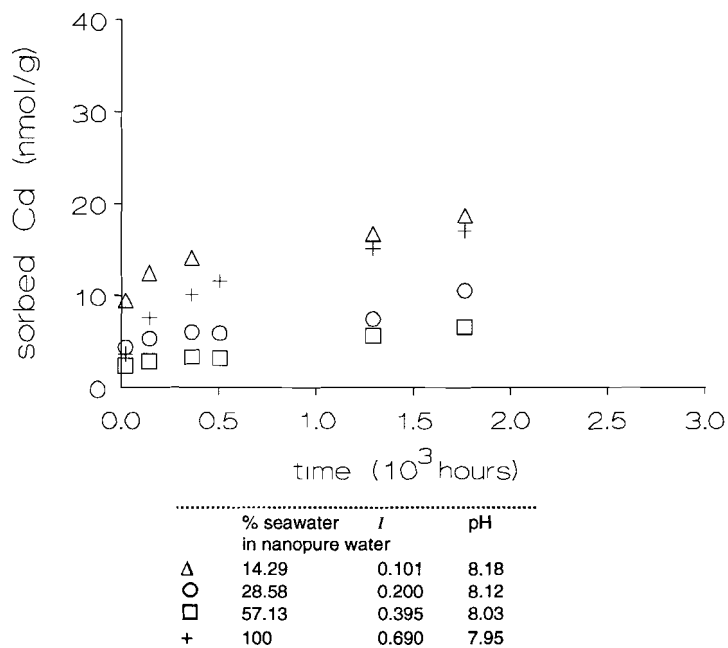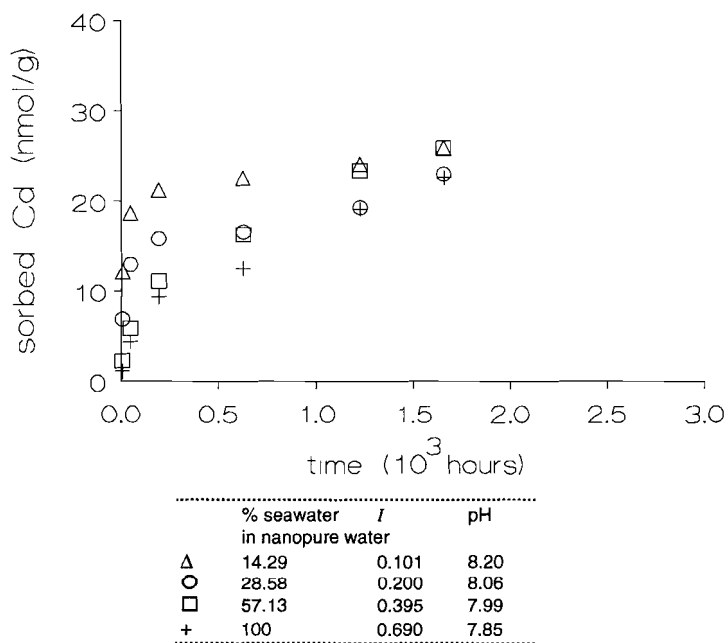|	% seawater in nanopure water	I	pH
Δ	14.29	0.101	8.20
O	28.58	0.200	8.06
□	57.13	0.395	7.99
+	100	0.690	7.85

Fig. 6b. Cadmium sorption on calcite versus time in various nanopure-/seawater mixtures. Calcite is batch Y, 4.94 g CaCO₃/l, 176.4 nM Cd, pre-equilibration time is 2 weeks.

1.4.2. Desorption

Fig. 7a shows desorption of Cd (pH = 7.9, I = 0.7) after sorption times of 1, 2.5, 19 and 121 hours. The results of an identical experiment at pH = 8.3 are shown in Fig. 7b. Chloride induces desorption quickly by complexation with Cd but, relatively, less of the total amount of sorbed Cd is desorbed at pH = 7.9 as compared to pH = 8.3. In Table 2 the ratios of sorbed and aqueous Cd at different times of desorption in NaCl solutions (from Fig. 7), as well as after different sorption times in NaCl (from Fig. 3) are given. From Table 2 it appears that the reversibility at pH = 8.3 is greater than at pH = 7.9, because at pH = 8.3 the ratios only differ by a factor of 2, whereas at pH = 7.9 this factor is greater than 100. Rapid isotopic exchange of [109]Cd after 50 minutes sorption in these NaNO$_3$ solutions, yielded 5% and 35% exchange within 5 minutes for pH = 7.9 and 8.3 respectively, also implying a greater reversibility at pH = 8.3.
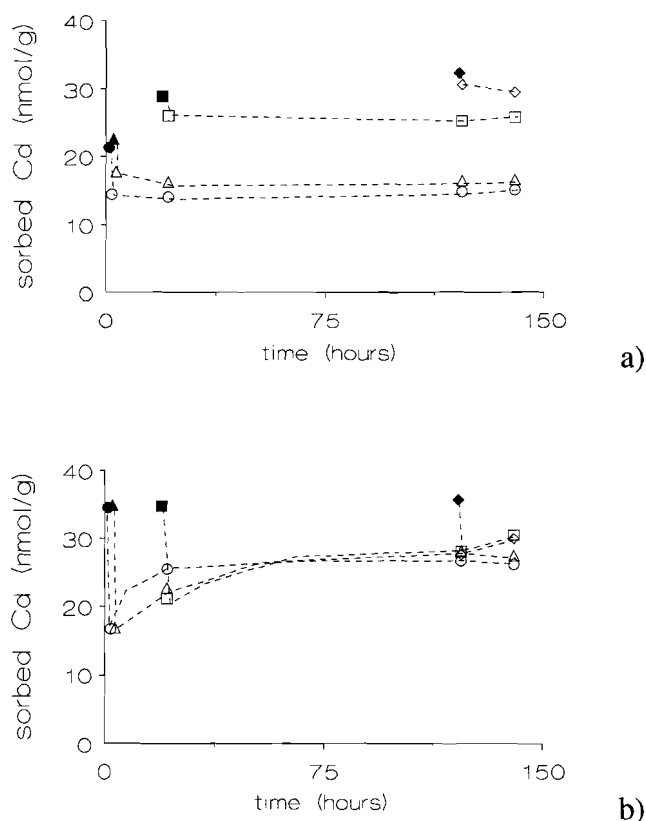

Fig. 7. Desorption of Cd in NaCl solutions after sorption times of 1, 2.5, 19 and 121 hours in NaNO$_3$ solutions (calcite is batch Y, 4.94 CaCO$_3$ g/l, 176.4 nM Cd, 2 days pre-equilibration time). The closed symbols represent sorption data after 1 (●), 2.5 (▲), 19 (■) and 121 (◆) hours, whereas the open symbols represent the corresponding desorption data. (a) Sorption in a solution with 665 mM NaNO$_3$, I = 0.7 and pH = 7.9 and desorption in a solution with 665 mM NaCl, I = 0.7 and pH = 7.9. (b) Sorption in a solution with 700 mM NaNO$_3$, I = 0.7 and pH = 8.3 and desorption in a solution with 665 mM NaCl, I = 0.7 and pH = 8.3.

Table 2. The dependence of the reversibility on pH after short adsorption times (Figs. 7a and 7b).

sorption time (h)	Cd_s/Cd_{aq} (l/g) after adsorption	Cd_s/Cd_{aq} (l/g) after desorption	Cd_s/Cd_{aq} (l/g) after adsorption (Fig. 3)
in 1E	in 1E	in 2E	in 2E
(1E = 665 mM NaNO3, pH = 7.9)		(2E = 665 mM NaCl, pH = 7.9)	
1	0.291	0.423	
2.5	0.337	0.629	
19	0.810	1.838	0.018
121	2.047	3.569	0.011
in 1F	in 1F	in 2F*	in 2F
(1F = 700 mM NaNO3, pH = 8.3)		(2F*= 665 mM NaCl, pH = 8.3)	
1	4.858	0.188	
2.5	4.858	0.187	
19	4.858	0.181	0.090
121	10.10	0.675	0.346

Ratios of Cd_s/Cd_{aq} (l/g) just before and after desorption after 1, 2.5, 19 and 121 hours equilibration in solutions with $I =$ 0.7 and pH = 7.9, and $I = 0.7$ and pH = 8.3 and desorption in solutions with $I = 0.7$, pH = 7.9, and NaCl = 665 mM, and $I = 0.7$, pH = 8.3, NaCl = 665 mM respectively. For exact conditions of 1E, 1F, 2E and 2F*, see Table 1.

Table 3. The dependence of the reversibility on pH after adsorption for 81 and 74 days respectively (Figs. 5 and 8). Cd_s/Cd_{aq} ratios (1/g) just before and just after desorption.

Exp	Cd_s/Cd_{aq} (l/g) adsorption	Cd_s/Cd_{aq} (l/g) desorption	pH
Mg-series			
7.3 mM MgNO3	1012	∞	7.90
29.1 mM MgNO3	2024	∞	7.86
51 mM MgNO3	503	∞	7.85
51 mM MgNO3	7.6	1.9	8.25
% seawater in nanopure/seawater mixtures			
14.29	0.31	0.33	8.15
28.58	0.07	0.13	8.04
57.13	0.12	2.24	7.96
100	0.25	70.5	7.91

Figs. 5 and 8 show desorption in Cd-free solutions with increasing Mg^{2+} concentration and in nanopure/seawater mixtures respectively. Adsorption times were 81 and 74 days respectively in solutions of the same composition. The relative amount of Cd released is greater at pH = 8.3 than at pH = 7.9. This results in much lower ratios of sorbed and aqueous Cd after desorption for the higher pH values as compared to the lower pH values (Table 3).

The release of Cd to nanopure/seawater mixtures after 183 days of sorption in solutions with increasing I is very small (Fig. 1). The greater part, 3 - 4% of desorbable Cd, is released immediately upon suspension in a nanopure-/seawater mixture with $S = 5$ (first dashed line). Only about an extra 0.5 - 1%, as compared to the initially sorbed amount of Cd, is desorbed after subsequent suspension in seawater with $S = 35$ (second dashed line). These results, simulating the path of suspended calcite from the riverine to the estuarine and marine environment, suggest that little Cd is remobilized after long interaction times of Cd with calcite in the riverine environment.

Desorption after both short and long sorption times is fast (< 24 hours) in all experiments and often results in a small pH increase (< 0.3 pH unit). The amount of Cd released to the solution decreases with time in most cases due to the slow Cd uptake, which is associated with recrystallization as we will learn in the next paragraph.
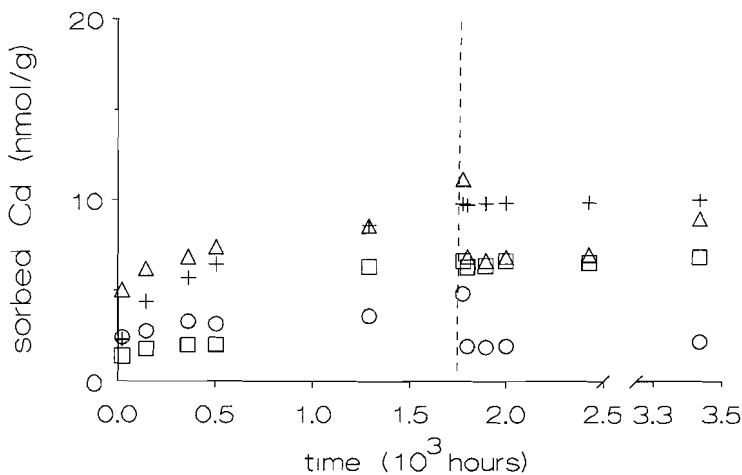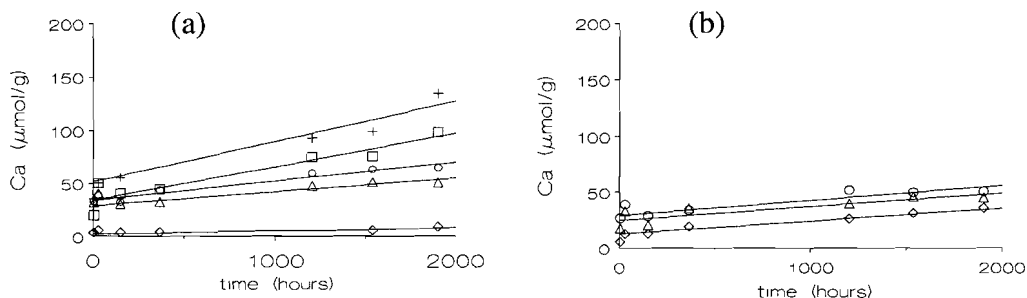

	% seawater in nanopure	I	pH
Δ	14.29	0.101	8.18
O	28.58	0.200	8.12
□	57.13	0.395	8.03
+	100	0.690	7.95

Fig. 8. Desorption (at dashed line) in Cd-free nanopure/seawater mixtures after sorption in identical solutions with Cd. Calcite is batch Y, 4.94 g $CaCO_3$/l, 88.2 nM Cd.
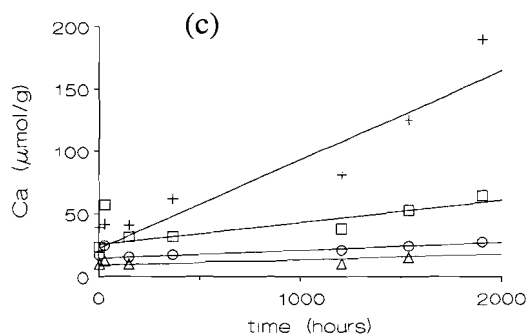
1.4.3. ^{45}Ca isotopic exchange

Fig. 9 shows the results of the ^{45}Ca exchange experiments in solutions with increasing I (9a), increasing Mg^{2+} concentrations (9b), and in various nanopure-/seawater mixtures (9c). For clarity, only the means of duplicates are plotted in Fig. 9. The mean deviation between duplicate samples is 1.33%. This deviation is relatively large compared to the total decrease in aqueous ^{45}Ca which ranges from 3% to 30% after 1903 hours of exchange. Statistics would probably have been somewhat better if a smaller L/S ratio had been used, which would have yielded more exchange.

	NaNO₃	I	pH
Δ	100	0.118	7.95
O	200	0.222	7.93
◊	700	0.704	8.23

	MgNO₃	I	pH
Δ	7.3	0.115	7.98
O	14.6	0.222	7.96
□	29.1	0.428	7.91
+	51.0	0.709	8.18
◊	51.0	0.709	8.18

	% seawater in nanopure water	I	pH
Δ	14.29	0.101	8.18
O	28.58	0.200	8.12
□	57.13	0.395	8.03
+	100	0.690	7.95

Fig. 9. ^{45}Ca isotopic exchange for solutions with increasing I (a), increasing Mg concentrations (b), and in nanopure/seawater mixtures (c) (see Table 1) after 24 hours pre-equilibration (calcite is batch Y, 12.5 g CaCO₃/l). Lines for LTER are calculated by linear least-square fits of single data with times greater than 28.5 hours. Only the mean values of duplicate data are plotted here.
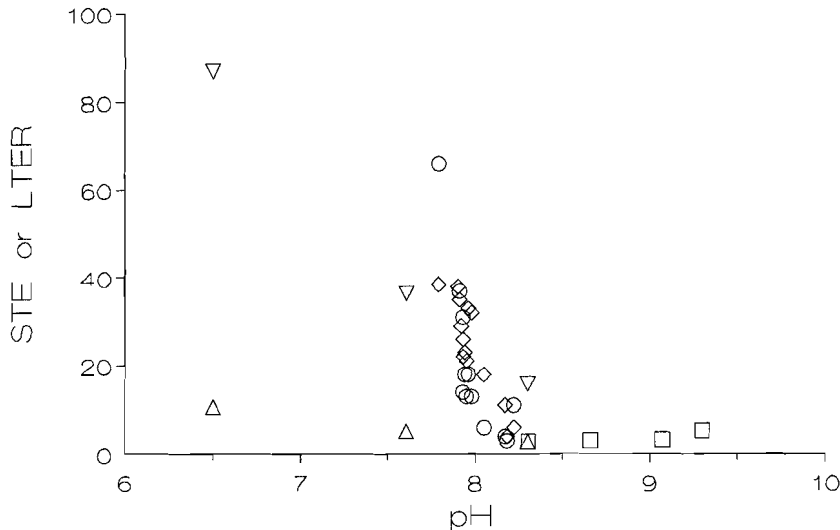
Fig. 10. Short term ^{45}Ca exchange (STE) and long term ^{45}Ca exchange rate (LTER) in this and other studies. ◊ = STE and ○ = LTER in this study. □= STE in Zachara et al. (1991). Δ = STE and ▽ = LTER in Davis et al. (1987).

The values, calculated for the short term exchange (STE) and the long term exchange rate (LTER), are listed in Table 4. The STE is thought to represent the total exchangeable amount of Ca at the surface, whereas the LTER is related to the recrystallization rate, as a result of which Ca is constantly removed from and added to the easily exchangeable Ca at the surface (Davis et al., 1987). In Fig. 10 the STE and LTER values of this and other studies are plotted. Considering the wide range of conditions covered in these studies, the agreement is satisfactory, as the order of magnitude of our data is similar to previous work.

From Table 4 it can be seen that the pH exerts a strong influence on the STE and LTER. For example, at equal I and Mg^{2+} concentrations (3E and 3F), STE and LTER are 35 mmol/g and 37 nmol/g×hr at pH = 7.9, whereas these values are 4 mmol/g and 3 nmol/g×hr respectively at pH = 8.18. The presence of Mg^{2+} seems to produce a small decrease in STE and LTER (compare Exp. 1F and Exp. 3F in Table 4), although one might argue about its significance given a mean deviation of 1.33%. Despite the increasing Mg^{2+} concentrations in the solutions (Fig. 9b) the LTER increases. Therefore, the effect of the decrease in pH values must outweigh the effect of increasing amounts of Mg^{2+}. The effect of increasing I, if present at all, is masked by the large effect of pH on STE and LTER, though one could expect a larger exchange with a larger Ca_T in solution. The pre-equilibration time (1 day or 3 months) has no significant effect, as the STE has remained practically the same (Table 4). The slow Cd removal rate (SCRR), calculated from the linear least square fit of data after 190 hours sorption time (Fig. 6b) is also given in Table 4. The SCRR increases with increasing LTER, which means that Cd is removed from solution faster if the recrystallization rate increases.

Table 4. Short term ^{45}Ca exchange (STE), long term ^{45}Ca exchange rate (LTER), slow Cd removal rate (SCRR), and pH in various solutions (see Table 1) after different pre-equilibration times (1 day or 3 months).

Exp	pH	STE Ca (μmol/g)		LTER Ca ((nmol/g)/hr)	SCRR Cd ((pmol/g)/hr)
		1day	3months	1day	2 weeks (Fig. 6b)
1B (5)	7.95	21	22	13	
1C (5)	7.93	27	25	14	
1D	7.92	29	36*)	**)	
1E	7.86	38	46*)	**)	
1F (10)	8.22	6	7	11	
3B (10)	7.98	32		13	
3C (10)	7.96	33		18	
3D (10)	7.93	22		31	
3E (9)	7.91	35		37	
3F (8)	8.18	4		3	
4B (4)	8.17	10	12	4	4
4C (10)	8.05	18	18	6	5
4D (8)	7.95	23	24	18	12
4E (8)	7.79	38	39	66	11

*) pH was ~ 0.15 lower
**) large deviation between duplicate samples

The LTER and SCRR were calculated as the least square fit of single data for times greater than 28.5 and 190 hours, respectively. The number of data points used for calculation of LTER is given in parentheses, whereas the number of data points used for SCRR is 4 in all cases. Only the mean values of duplicate samples are plotted. For exact experimental conditions, see Table 1.

1.5. Discussion

1.5.1. Parameters influencing Cd sorption

Reviewing the influence of the various parameters on Cd sorption and desorption, it appears that pH, sorption time and aqueous Cd^{2+} activity determine the degree of Cd sorption and desorption most, whereas the Mg^{2+} concentration and electrostatic factors appear to be of minor importance.

The influence of pH on the fast initial uptake, which is thought to be governed by adsorption (Davis et al., 1987), is related to the free Ca^{2+} activity, as Cd^{2+} competes with Ca^{2+} for surface sites. Competition at pH = 7.9 is greater than at pH = 8.3 in these experiments. A change in surface charge towards slightly positive values at pH = 7.9 could also contribute to the decrease in Cd sorption, because the zero point of charge of calcite as determined in $NaClO_4$ solutions is estimated to be 8.2 (Mishra, 1978). However, the data do fit the Ca-Cd exchange model, discussed later on, as proposed by Zachara et al. (1991), which does not take electrostatic effects into account. Therefore, the influence of ionic strength on the double layer or surface charge must be of minor importance. In the paper of Van Cappellen et al. (1993) the small influence of the ionic strength on surface charge and apparent surface stability constants is explained by a high capacitance of the calcite - aqueous solution interface.

The effect of the pH on the reversibility of fast initial uptake is also related to competition with Ca at non-uniform sorption sites. At higher pH and low Ca competition Cd could also adsorb on sites where it has a less stable configuration (e.g. on the flat surface or on less favorable crystal faces), whereas at lower pH and high Ca competition Cd possibly only sorbs on sites where it has a more stable configuration (e.g. kinks). Another indication that not all sites are equally favorable for Cd sorption is the fact that when the surface area is doubled, only 25% more Cd is initially sorbed. The decrease in reversibility with decreasing pH is not a result of recrystallization, since the contributions of recrystallization after 121 hours at pH = 7.9 and pH = 8.3 as estimated from Table 4 are only 1.45 nmol and 0.25 nmol respectively. This is less than 5% and 1% of the total amount of Cd that remains sorbed after 121 hours. Rapid isotopic exchange with ^{109}Cd also indicates a greater reversibility at higher pH. Results of similar experiments by Davis et al. (1987) suggest the opposite to be true, but they used the complexant EDTA in their experiments, which reverses the Cd sorption dependence on pH. The increase in irreversibility with time can be due to recrystallization and diffusion of Cd sorbed on a flat surface to kinks and steps (surface diffusion). This latter process has also been described for crystal growth (Zhang and Nancollas, 1990), where ions diffuse up to the surface, enter the adsorption layer, diffuse over the surface and integrate into a kink site.

The pH influences the slow Cd removal rate (SCRR) in an opposite manner as compared to the fast initial Cd uptake. At pH = 7.9 the recrystallization rate and the SCRR are higher than at pH = 8.3. This may be caused by the higher aqueous Ca^{2+} activity at a pH of 7.9, increasing the Ca flux to and from the calcite surface. Another cause may be the increase in HCO_3^- species at the surface. This facilitates the dissolution of small calcite particles, because at low pH the dissolution process is controlled by the rate of hydration of carbon dioxide, whereas at higher pH the dissolution rate is controlled by a surface process (Zhang and Nancollas, 1990; Van Cappellen et al., 1993). The dissolution and precipitation processes involved in the recrystallization process cause sorbed Cd to be buried. On the newly formed surface Cd can be sorbed again. Recrystallization contributes significantly to the Cd uptake after long interaction times as can be seen e.g. in Fig. 6b, where the Cd

uptake in seawater of $S = 35$ and pH = 7.85 is almost equal to the Cd uptake in a nanopure-/seawater mixture with $S = 5$ and pH = 8.20 after 1799 hours. The reversibility after long interaction times decreases as a result of recrystallization. The residence time and pH in the riverine environment are therefore important factors with respect to remobilization of Cd from suspended calcite.

Chloride drastically reduces the free Cd^{2+} activity even at $S = 5$ (Fig. 3 and 6). The main complexes formed in estuaries up to a salinity of 25 are (in order of importance) $CdCl^+$, $CdCl_2°$ and $CdCl_3^-$. At $S = 35$ the $CdCl_2^-$ complex becomes the dominating species (Mantoura, 1978). The amount of sorption is found to be independent of the dominating type of aqueous chloro-complex, and to depend only on the free aqueous Cd^{2+} activity (Fig. 4). Similar results were found by Comans and van Dijk (1988) for Cd sorption on riverine suspended material. The presence of chloride is merely a hindrance for Cd sorption (compare Fig. 1 with Fig. 3), because Cd is released from the chloro-complexes as sorption continues.

Magnesium, in contrast to Cl^-, could have a more permanent effect by changing the number and the characteristics of surface sites available for Cd. Though Mg has been shown to have a significant effect on e.g. Co^{2+} sorption on calcite (Kornicker et al., 1985), increasing Mg^{2+} activities affect Cd sorption only a little (Fig. 5). These results demonstrate the much greater affinity of Cd for the calcite surface as compared to Mg. This affinity depends on factors such as differences in ionic radius with Ca^{2+} ($rCd^{2+} = 0.97$ Å, $rMg^{2+} = 0.72$ Å versus $rCa^{2+} = 0.99$ Å, Burgess, 1978), the difference in the solubility product of the anhydrous metal carbonate ($K_{sp}CdCO_3 = 10^{-12.1}$, Stipp et al., 1992) versus $K_{sp}MgCO_3 = 10^{-8.91}$, Königsberger et al., 1992) and the single ion Gibbs free energies of hydration of both metals ($\Delta G_{hydr\ Cd} = -1812.4$ kJ/mol versus $\Delta G_{hydr\ Mg} = -1917.7$ kJ/mol, Millero and Sohn (1992)). All these factors are more favorable for Cd sorption, than for Mg sorption. Although the presence of Mg has been found to decrease both the STE and the LTER of ^{45}Ca (Davis et al., 1987), the effect of alteration of the calcite surface cannot be distinguished in these experiments. Cadmium can still be removed up to 100% as a result of slow Cd uptake within a reasonably short time.

The parameters (Cl^-), (Mg^{2+}), (Ca^{2+}) and (Cd^{2+}) seem adequate to explain the sorption behavior in nanopure/seawater mixtures (Figs. 6a and 6b). The difference in sorption patterns of Figs. 6a and 6b could be brought about by differences in pre-equilibration times and pH. Due to the reversed pH trend with respect to estuaries, the Figs. 6a and 6b give a somewhat distorted picture of sorption in the estuarine environment. The conditions under which Cd sorption is most favorable were estimated from Figs. 1, 3 and 5. Taking into account the relative effects of Cl^- and pH, the estimated order of increasing favorability for Cd sorption on calcite after fast initial sorption is; $S = 20 < S = 10 < S = 35 < S = 5 < S = 0.1$. After long sorption times this order can change, depending on differences in recrystallization rates.

The specific surface area of calcite appears to be a difficult parameter. One would expect a substantial extra amount of Cd to be sorbed when the surface area is doubled, not merely 25% extra sorption. Apparently, not only the magnitude of the surface area, but also the surface structure determines the number of sites favorable for Cd sorption.

1.5.2. Surface processes

Sorption isotherms were linear in the Cd concentration range 8.8 - 176 nM indicating a constant partition coefficient D, (eq 1);

$$D = \frac{(C_{Cd} / C_{Ca})_s}{(C_{Cd} / C_{Ca})_{aq}} \qquad (1)$$

Because more than one process is at play during Cd removal from solution, (adsorption, surface diffusion and recrystallization) the conclusion can be drawn that the influence of the various processes must be similar in the above mentioned concentration range. Equilibrium is not reached in these experiments, because the isotherms migrate with time, suggesting that the partition constants (eq 1) vary with time as well.

Fig. 11 shows plots of the data of Figs. 1 and 3 (no competition other than Ca^{2+}) after initial fast sorption using the Ca-Cd exchange model proposed by Zachara et al. (1991):

$$\log[(Cd^{2+})_{aq}/(Ca^{2+})_{aq}] = - \log K_{ex} + n\log[(NCdX)/(NCaX)] \qquad (2)$$

where $NCdX = Cd_s/X_t$, $NCaX = 1-(Cd_s/X_t)$, X_t = the total number of sorption sites, n is an empirical constant, and K_{ex} = the experimental exchange constant. A linear fit of the data could only be obtained by choosing a single value for X_t. In Fig. 11 a value of 2.3×10^{-6} mol Ca/g calcite was chosen for X_t based on the calcite surface area and the estimate of 5×10^{14} atoms Ca/cm^2 at pH = 8.3 (Möller and Sastri, 1974). The use of STE values from Table 4 for X_t at each specific pH (Fig. 11), yields lines with almost identical slopes but with different intercepts. Obviously, the K_{ex} value is strongly dependent on the chosen value for X_t. The increase of STE above pH = 9 or below pH = 8.3 has been attributed to adsorption of Ca on CO_3 surface sites (Zachara et al., 1991) or a thicker hydrated surface layer (Davis et al., 1987). The STE values found in this study at pH < 8.3 could not represent Ca in a hydrated surface layer, because this layer would then be at least 8 layers thick, which contradicts results with LEED (Stipp and Hochella., 1991). Since no suitable explanation for the high STE values at lower pH is found, direct substitution of STE for X_t in sorption models is not warranted.

In Fig. 11, plots of the sorption data in Figs. 1 and 3 using $X_t = 2.3 \times 10^{-6}$ yields intercepts of -3.02 and -3.12 (= $-\log K_{ex}$) respectively. These values are close to previous values reported for D (Davis et al., 1987) and surface exchange constants (Zachara et al., 1991). The slope of approximately 1 ($n = 1$) means that the exchange reaction may be considered ideal (Zachara et al., 1991). However, should an ideal solid-solution be formed in equilibrium with the aqueous phase, then $\log K_{ex}$ should be equal to $\log K_x = \log(K_{sp}$calcite = 8.43 $/K_{sp}$otavite = 12.1) = 3.7. The deviation between K_{ex} and K_x indicates that a possibly formed solid-solution is not in equilibrium with the aqueous phase, or that solid-solution formation is not the main process governing Cd sorption during the first 48 hours. Also, the small decrease in pH during sorption and the increase in pH during desorption suggest that substitution of Cd for Ca and vice versa might at least go partly via proton replacement (e.g. of surface CO_3H) which is not described with K_{ex}. Such a mechanism would be in agreement with observations of McBride (1979).
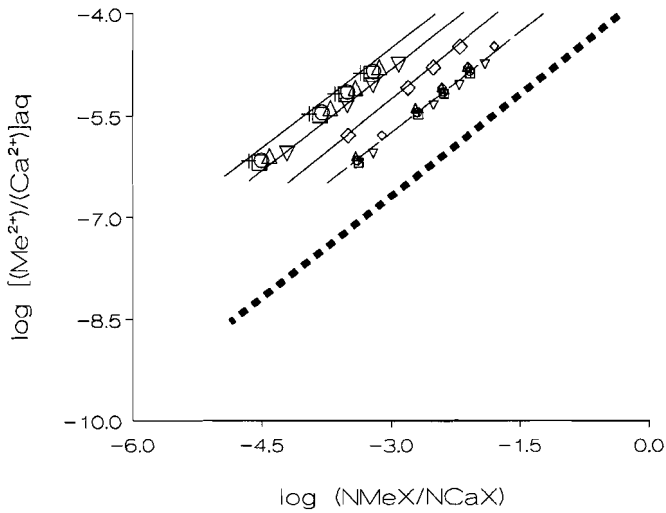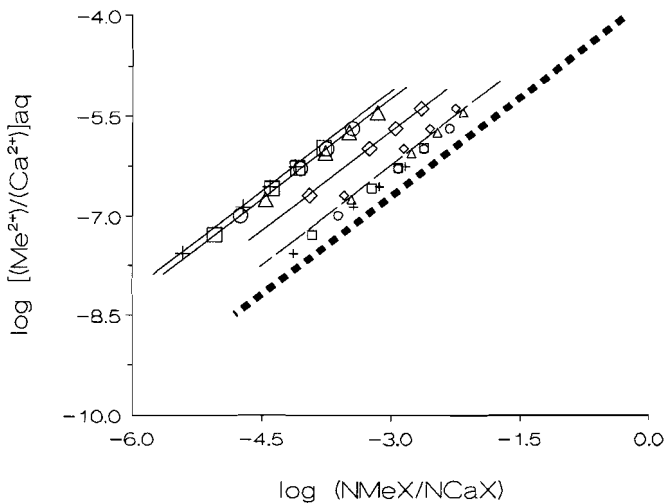
Fig. 11. Cadmium-calcium exchange isotherms based on Eq (2) during initial fast sorption ($t < 48$ hours). Using STE for X_t at the corresponding pH yields large symbols and solid lines (——). Using a constant value of 2.3×10^{-6} for X_t yields small symbols and broken lines (— —). The dashed line (■■■■) represents the isotherm for which the slope is 1 (ideal exchange) and the log K_{ex} equals 3.7 ($\log(K_{sp}\text{calcite}/K_{sp}\text{otavite})$). (a) Exchange isotherms for solution series with increasing I (see Fig. 1) after sorption for 4 hours. (b) Exchange isotherms for solution-series with increasing NaCl (see Fig. 3) after sorption for 24 hours.

The irreversibility displayed after just one hour sorption time (Fig. 7) needs some further consideration. Incomplete reversibility after short interaction times can be explained as being diffusion through a hydrated layer and subsequent solid-solution formation (Davis et al., 1987), solid-state diffusion into the crystal-lattice (Stipp et al., 1992) or surface precipitation (Comans and Middelburg, 1987). In view of the fact that the reversibility decreases with pH, these explanations are inadequate. It is unlikely that more Cd diffuses from the surface into the crystal when less Cd is adsorbed at the surface (pH = 7.9). In a paper by Das and Van der Weijden (1995), it is shown that solid-state diffusion under these experimental conditions is negligable. Also, the formation of a surface precipitate, as defined in the method section, would be more likely at pH = 8.3 and would result in a lower reversibility as compared to pH = 7.9 (Morel, 1983). Therefore, the explanation may simply be as stated above, that at lower pH, Cd is only sorbed at the most favorable sorption sites, due to the increased competition with Ca. Desorption from these sites may be extremely slow, which is hard to check because of the recrystallization process. In whatever way the pH dependence of the short term reversibility is interpreted, one has to be aware of its existence when comparing desorption data at different pH values (e.g. Zachara et al., 1991).

6. Closing remarks

Cadmium sorption on calcite can basically be explained as being a combination of an adsorption and a recrystallization process. Depending on the interaction time, either process may be of major or minor importance. Cadmium sorption in the estuarine environment could be adequately explained by considering the free Cd^{2+} activity, and the presence of Mg^{2+}, Ca^{2+} and Cl^-. The degree to which Cd can be remobilized in the estuary depends mainly on the pH and the contact time of Cd and suspended calcite in the riverine environment.

Acknowledgements

References

Boyle E.A., 1988. Cadmium: chemical tracer of deepwater paleoceanography. Paleoceanography vol 3, 4: 471-489.

Buffle J., Altmann, R.S., Filella M. and Tessier A., 1990. Complexation by natural heterogenous compounds: Site occupation distribution functions, a normalized description of metal complexation. Geochim. Cosmochim. Acta, 54: 1535-1553.

Burgess J., 1978. Metal Ions in Solution. Ellis Horwood Ltd., pp. 481.

Chave, K.E. and Schmalz R.F., 1966. Carbonate-Seawater interactions. Geochim. Cosmochim. Acta, 30: 1037-1048.

Comans, R.N.J., 1987. Adsorption, desorption and isotopic exchange of cadmium on illite: evidence for complete reversibility. Wat. Res., 21: 1573-1576.

Comans, R.N.J., 1990. Sorption of Cadmium and Cesium at mineral-water interfaces. Dissertation Utrecht University, pp. 169.

Comans, R.N.J. and Van Dijk, 1988. The role of complexation processes in cadmium mobilization during estuarine mixing. Nature, 336: 151-154.

Comans, R.N.J. and Middelburg, J.J., 1987. Sorption of trace metals by calcite: Applicability of the surface precipitation model. Geochim. Cosmochim. Acta, 51: 2587-2591.

Das, H.A. and Van der Weijden, R.D., 1995. Isotopic exchange experiments in batch adsorption and desorption experiments. J. Radioanal. Nucl. Chem., 191: 229-238.

Davis, J.A., Fuller, C.C. and Cook, A.D., 1987. A model for trace metal sorption processes at the calcite surface: Adsorption of Cd^{2+} and subsequent solid-solution formation. Geochim. Cosmochim. Acta, 51: 1477-1490.

Elbaz-Pouliche, F., Guan, D.M. and Martin, 1991. Trace metal behaviour in a highly stratified Mediterranean estuary, the Krka (Yugoslavia). Mar. Chem., 32: 221-224.

Harper, D.J., 1991. The distribution of dissolved cadmium, lead and copper in the Bristol channel and the outer Evern estuary. Mar. Chem., 33: 131-143.

Königsberger, E., Schmidt, P. and Gamsjäger, H., 1992. Solid-solute phase equilibria in aqueous solution: VI. Solubilities, complex formation, and ion- interaction parameters in the system Na^+ -Mg^{2+} -ClO_4^- -CO_2 -H_2O at 25°C. J. Soln. Chem., 21: 1195-1216.

Kornicker, W.A., Morse, J.W. and Damasceno, R.N., 1985. The chemistry of Co^{2+} interaction with calcite and aragonite surfaces. Chem. Geol., 53: 229-236.

Korzun, E.A. and Heck, H.H., 1990. Sources and fates of lead and cadmium in municipal solid waste. J. Air Waste Manage. Assoc., 40: 1220-1226.

Long, D.T. and Angino, E.E., 1977. Chemical speciation of Cd, Cu, Pb and Zn in mixed freshwater seawater and brine solutions. Geochim. Cosmochim. Acta, 41: 1183-1191.

Mantoura, R.F.C., 1978. Chemical speciation of Cd, Cu, Pb and Zn. Estuarine and Coastal Marine Science, 6: 387-408.

McBride, M.B., 1979. Chemisorption and precipitation of Mn^{2+} at $CaCO_3$ surfaces. Soil. Sci. Soc. Am. J., 43: 693-698.

McBride, M.B., 1980. Chemisorption of Cd^{2+} on calcite surfaces. Soil. Sci. Soc. Am. J., 44: 26-28.

Millero, F.J and Sohn, M.L., 1992. Chemical Oceanography. CRC Press Inc., pp. 531.

Mishra, S.K., 1978. The electrokinetics of apatite and calcite in inorganic electrolyte environment. Int. J. Mineral Processing, 5: 69-83.

Möller, P. and Sastri, C.S., 1974. Estimation of the number of surface layers of calcite involved in Ca-^{45}Ca isotopic exchange with solution. Z. für Phys. Chemie Neue Folge, 89: 80-87.

Morel, F.M.M., 1983. Principles of Aquatic Chemistry. John Wiley & Sons Inc., pp. 446.

Papadopoulos, P. and Rowell, D.L., 1988. The reactions of cadmium with calcium carbonate surfaces. Journal of Soil Science, 39: 23-36.

de Rooij, N.M., 1990. Charon speciation code. Delft Hydraulics. Delft, The Netherlands.

Sposito, G., 1984. The surface chemistry of soils. Oxford Univ. Press, pp. 234.

Sposito, G., 1986. Distinguishing adsorption from surface precipitation. In Geochemical Processes at Mineral Surfaces (eds. J.A. Davis and K.F. Hayes); ACS Symposium Series, 323, pp. 217-228.

Stipp, S.L. and Hochella, F.M., 1991. Structure and bonding environments at the calcite surface as observed with X-ray photoelectron spectroscopy (XPS) and low energy electron diffraction (LEED). Geochim. Cosmochim. Acta, 55: 1723 -1736.

Stipp, S.L., Hochella, M.F. and Parks, G.A., 1992. Cd^{2+} uptake by calcite, solid-state diffusion, and the formation of solid-solution: Interface processes observed with near-surface sensitive techniques (XPS, LEED, and AES). Geochim. Cosmochim. Acta, 56: 1941-1954.

Turner, D.R., Whitfield, M. and Dickson, A.G., 1981. The equilibrium speciation of dissolved components in freshwater and seawater at 25°Ca nd 1 atm pressure. Geochim. Cosmochim. Acta, 45: 855-881.

Van Cappellen, P., Carlet, L., Stumm, W. and Wersin, P., 1993. A surface complexation model of the carbonate mineral-aqueous interface. Geochim. Cosmochim. Acta, 57: 3505-3518.

Windom, H., Byrd, J., Smith, R., Hungspreugs, M., Dharmvanij, S., Thumtrakul, W. and Yeats, P., 1991. Trace metal-nutrient relationships in estuaries. Mar. Chem., 32: 177-194.

Zachara, J.M., Cowan, C.E. and Resch, C.T., 1991. Sorption of divalent metals on calcite. Geochim. Cosmochim. Acta, 55: 1549-1562.

Zhang, J.W. and Nancollas, G.H., 1990. Mechanisms of growth and dissolution of sparingly soluble salts. In Reviews in mineralogy (eds. M.F. Hochella, Jr. and A.F. White); volume 23, pp. 365-396.

Appendix 1. Aqueous speciation reactions and equilibrium constants (CHARON).

Reaction		$\log K$	Reaction		$\log K$
$H^+ + CO_3^{2-}$	$= HCO_3^-$	10.3	$K^+ + SO_4^{2-}$	$= KSO_4^-$	0.85
$2H^+ + CO_3^{2-}$	$= H_2CO_3^{\circ}$	16.72			
$H^+ + SO_4^{2-}$	$= HSO_4^-$	1.99			
$Ca^{2+} + CO_3^{2-}$	$= CaCO_3^{\circ}$	3.15	$Mg^{2+} + CO_3^{2-}$	$= MgCO_3^{\circ}$	2.98
$Ca^{2+} + HCO_3^-$	$= CaHCO_3^+$	1.00	$Mg^{2+} + HCO_3^-$	$= MgHCO_3^+$	1.1
$Ca^{2+} + H_2O$	$= CaOH^+ + H^+$	12.85	$Mg^{2+} + OH^-$	$= MgOH^+$	2.14
$Ca^{2+} + SO_4^{2-}$	$= CaSO_4^{\circ}$	2.31	$Mg^{2+} + SO_4^{2-}$	$= MgSO_4^{\circ}$	2.24
$Cd^{2+} + Cl^-$	$= CdCl^+$	1.97	$Na^+ + CO_3^{2-}$	$= NaCO_3^-$	0.6
$Cd^{2+} + 2Cl^-$	$= CdCl_2^{\circ}$	2.59	$Na^+ + CO_3^{2-} + H^+$	$= NaHCO_3^{\circ}$	10.5
$Cd^{2+} + 3Cl^-$	$= CdCl_3^-$	2.4	$Na^+ + SO_4^{2-}$	$= NaSO_4^-$	0.7
$Cd^{2+} + H_2O$	$= CdOH^+ + H^+$	10.1			
$Cd^{2+} + CO_3^{2-}$	$= CdCO_3^{\circ}$	4.1			
$Cd^{2+} + 2CO_3^{2-}$	$= Cd(CO_3)_2^{2-}$	4.6			
$Cd^{2+} + 3CO_3^{2-}$	$= Cd(CO_3)_3^{4-}$	6.22			
$Cd^{2+} + H^+ + CO_3^{2-}$	$= CdHCO_3^+$	12.4			
$Cd^{2+} + SO_4^{2-}$	$= CdSO_4^{\circ}$	2.45			
$Cd^{2+} + 2SO_4^{2-}$	$= Cd(SO_4)_2^{2-}$	3.44			

Chapter 2

Sorption and sorption reversibility of Cd on calcite in the presence of phosphate and sulfate

Abstract— The influence of phosphate and sulfate on the sorption of cadmium on calcite was studied in laboratory experiments at $I = 0.7$, pH = 7.4 - 9.5 and $PCO_2 = 10^{-3.5}$ atm. The effect was twofold: fast initial sorption of Cd decreased with increasing phosphate and sulfate concentrations, and slow Cd removal decreased because the Ostwald ripening rate was reduced by these anions. Since total phosphate and total sulfate sorption increase with decreasing pH as a result of reduced competition with carbonate, the effects on the sorption of Cd are most pronounced in the pH range 7.4 - 8.3. Both anions also affect the reversibility of Cd sorption. At pH = 8.3, the short term reversibility (< 24 hours) decreases, because a greater percentage of Cd is sorbed at the more favorable sorption sites. At pH = 7.4, the short term reversibility remains the same, because Cd is already sorbed at the more favorable sites without phosphate being present. The long term reversibility (> 144 hours) increases in the pH range 7.4 - 8.3, because the Ostwald ripening rate, which is related with the slow and more permanent removal of Cd, is reduced. Based on the reduction of the Cd/Ca ratios at the calcite surface and in the ripened calcite with increasing phosphate concentrations in sorption experiments, the relationship between Cd/Ca ratios in benthic foraminifera and phosphate concentrations in deep ocean water appears to result from biochemical, rather than chemical processes.

R.D. van der Weijden, J.A. Meima and R.N.J. Comans

2.1. Introduction

The distribution patterns of the trace metal cadmium and the nutrient phosphate in the oceanic water column are strikingly similar. Biogeochemical processes, such as mineralization in/from organic algal material, are mainly responsible for the relation between cadmium and phosphate in the water column (Saager, 1994). About 10% of cadmium in the water column is taken up in planktonic shells (calcium carbonate).

Boyle (1988) used the ratio of Cd/Ca in benthic foraminifera (calcium carbonate) as a tracer to reconstruct paleo phosphate concentrations of deep ocean waters. The tracer is only applicable if the partition coefficient (D) of Cd between these foraminifera and deep ocean water has remained constant in space and time, and the effects of P, T, depth, water composition, mineralization rate etc. on D are considered (Saager and De Baar, 1993; De Baar et al., 1994). The mineralization rate, for instance, can drastically affect D, as was shown in laboratory experiments investigating the purely chemical partitioning of Cd between calcite and simulated seawater at various calcite growth rates (Lorens, 1981).

In a previous paper (Van der Weijden et al., 1994) we discussed the influence of pH, ionic strength, equilibration time, magnesium and chloride on the Cd sorption on calcite. The fact that phosphate also displays a high chemical affinity for the calcite surface, gave reason to investigate the sorption behavior of Cd in the presence of phosphate under seawater-like conditions. For comparison, Cd sorption was studied also in the presence of sulfate, which after chloride, is the second most abundantly present anion in seawater. In addition to the effects of phosphate and sulfate on Cd sorption, the effect of these anions on the Ostwald ripening process of calcite, which is responsible for the slow removal of Cd by its burial in the growing calcite crystals (Davis et al., 1987; van der Weijden et al., 1994), was investigated by measuring the ^{45}Ca isotopic exchange rate. Sorption reversibility was considered after short (hours) and long (days) sorption times, to investigate remobilization of Cd. Finally, the chemical relationship that exists between Cd/Ca ratios on/in calcite and the aqueous phosphate concentration, was compared to the relationship that is believed to exist between biogenic calcite Cd/Ca ratios and paleonutrient concentrations in deep ocean water.

2.2. Materials

Electrolyte solutions were prepared with nanopure water and the reagent grade chemicals NaNO$_3$, Na$_2$CO$_3$, Na$_2$HPO$_4$.12H$_2$O, Na$_2$SO$_4$ and suprapure CaCO$_3$ and HNO$_3$ (Merck). Suprapure calcite was used as a sorbent and for achieving equilibrium with respect to calcite in all solutions. The surface area as determined with a micromeritics ASAP 2400 was 0.29 m^2/g ($\pm$ 10%). In ^{45}Ca experiments another batch of calcite with an area of 0.40 m^2/g was also used.

Carrier-free radioactive tracers (Amersham) used to study sorption and recrystallization were ^{109}Cd (as CdCl$_2$) diluted with 0.01M HNO$_3$, ^{45}Ca (as CaCl$_2$) diluted with nanopure water and ^{32}P (as orthophosphate) diluted with nanopure water. ^{109}Cd was counted on a Compugamma LKB 1280 gamma-counter with a 3 inch NaI well-type detector, producing results with a maximum deviation of 2% between duplicate samples. ^{32}P and ^{45}Ca were counted on a Philips β-scintillation counter.

The pH of the solutions was measured with an Ingold microtip-electrode, connected to a Knick pH meter and calibrated with Ingold standardized buffers of pH = 7.00 and 9.21.

2.3. Methods

Calculations for the speciations of the various solutions were made with the chemical speciation code MINTEQA2 (Allison et al., 1991). The formation constants of the species used in these calculations are given in Appendix 1. The total concentrations of the species in the solutions (ionic strength, $I = 0.7$) are shown in Table 1. Concentrations and activities are indicated with [ ] and ( ), respectively, in this paper. Activities were calculated with Pitzer coefficients using the speciation code WATEQX (Van Gaans, 1991).

Table 1. Composition and pH of the solutions.

	[Na$^+$] (mM)	[NO$_3^-$] (mM)	[CO$_3^{2-}$] (mM)	[Ca^{2+}] (mM)	[SO$_4^{2-}$] (mM)	pH
1	511	637	0.236	93.94		7.4
2	690	702	0.804	6.07		7.97
3	700	700	1.970	1.130		8.37
4	693	621	12.50	0.056		9.04
5	693	621	58.20	0.011		9.53
6a	511	637	0.294	63.15		7.50
6b	511	643	0.291	63.15	0.028	7.50
6c	512	643	0.291	65.14	1	7.50
6d	500	490	0.291	95.20	100	7.50
7a	511	637	0.721	8.7		8.01
7b	511	643	0.754	8.0	0.028	8.01
7c	512	640	0.754	8.0	1	8.01
7d	500	490	0.771	7.6	100	8.01
8a	700	700	2.10	1.13		8.38
8b	700	700	2.10	1.13	0.028	8.38
8c	700	698	2.10	1.13	1	8.38
8d	690	490	1.95	2.05	100	8.35
9a	700	690	12.46	0.058		9.04
9b	700	690	12.46	0.058	0.028	9.04
9c	700	688	12.6	0.058	1	9.04
9d	700	495	11.7	0.11	100	9.01
10a	684	615	63.4	0.095		9.53
10b	685	615	63.9	0.095	0.028	9.54
10c	684	614	61.8	0.097	1	9.54
10d	674	410	9.862	0.013	100	9.54

1-5: solutions for studying Cd sorption, phosphate sorption and Cd sorption at various phosphate concentrations, 6 - 10: solutions for studying Cd sorption at various sulfate concentrations.

2.3.1. Sorption

Since the microtopography and surface area are different for each batch of suprapure $CaCO_3$ (Davis et al., 1987; Van der Weijden et al., 1994), the sorption data of phosphate and cadmium from previous studies could not be quantitatively integrated in this study. Therefore, in addition to cadmium sorption in the presence of phosphate and sulfate, sorption of phosphate and cadmium were studied separately, to allow intercomparison.

Eighty ml of filtered (0.22 μm micropore filter) solution and 400 mg suprapure $CaCO_3$ were pre-equilibrated for > 48 hours in 100 ml teflon (PFA) vessels. Sorption was started by adding 100 μl of cadmium and/or phosphate tracer and/or carrier. The concentration of the Cd carrier was 1.2×10^{-9}, 9×10^{-9} or 4.5×10^{-8} M ([Cd] seawater = 5×10^{-8} M) and the concentration of the phosphate carrier ranged from 1.25×10^{-9} to 1.25×10^{-4} M ([PO_4] seawater = $1-4 \times 10^{-6}$ M). All solutions were prepared in duplicate, the vessels were placed in a thermostated shakerbath and kept at a temperature of 25°C ± 1°C. At intervals during equilibration, 2 ml subsamples were withdrawn under continuous stirring. Subsamples were centrifuged for 20 minutes at 20215 *g* and 1 ml of supernatant was used for counting the [109]Cd activity (gamma) in polythene tubes or the ^{32}P activity in 9 ml water in glass scintillation vials (beta). Aqueous and sorbed concentrations were calculated as described in Comans (1987).

2.3.2. [45]Ca isotopic exchange

The effect of different phosphate and sulfate concentrations on the Ostwald ripening of calcite was determined in duplicate experiments using [45]Ca isotopic exchange. In 100 ml teflon (PFA) vessels, 60 ml of solution and 2.1 gram of suprapure $CaCO_3$ were pre-equilibrated for more than 48 hours in the shakerbath at 25 °C. The experiment was started by adding 100 μl of [45]Ca tracer. At intervals during equilibration, subsamples for β-counting of the [45]Ca activity and pH monitoring were withdrawn under continuous stirring. After centrifugation for 20 minutes at 20215 *g*, 1 ml of the supernatant and 9 ml Instagel scintillation fluid were transferred to polythene scintillation vials. The vials were counted on a Philips β-scintillation counter. Short term exchange (STE, μmol/gram calcite) was calculated as the mean value of [45]Ca exchange of duplicate samples after 4 hours. The long term exchange rate (LTER, nmol Ca/(gram×hour)) was obtained by calculating the linear least square fit of duplicate data for times > 125 hours.

2.3.3. Desorption and rapid isotopic exchange

Sorption reversibility was studied in desorption and rapid isotopic exchange (RIE) experiments. In desorption experiments, the suspensions in the 100 ml vessels were transferred to teflon (FEP) centrifuge tubes and centrifuged for 20 minutes at 20215 *g*. The supernatant was then replaced with an equal amount of electrolyte without tracer and carrier. The new suspensions were transferred back from the centrifuge tubes into the reaction vessels. Desorption was followed in time by withdrawing subsamples as described under sorption.

RIE experiments were carried out in 40 ml FEP centrifuge tubes with duplicates for each solution composition and each sampling time. Forty ml of solution were pre-equilibrated with 200 mg $CaCO_3$ for > 48 hours. At the start of the experiment both tracer and carrier were added to one tube (A), while only carrier was added to the other tube (B).

At the sampling time, both tubes were centrifuged for 10 minutes at 20215 g and 10 ml of the supernatant of tube (B) was replaced with 10 ml of the supernatant of tube A. A subsample of tube (A) was taken for counting the tracer activity in solution.

The subsequent procedures were different for phosphate and cadmium, because Cd sorption continues in time, whereas phosphate sorption remains at a certain plateau, which is reached very rapidly. For phosphate, tube B was shaken in the shakerbath for 15 minutes, centrifuged for 10 minutes at 20215 g and a subsample was taken for counting the tracer activity in solution. For Cd, tube B was shaken by hand for 5 minutes and subsamples were withdrawn with a syringe, filtered through a 0.22 μm screw-on micropore filter, and counted. No sorption of Cd onto the filter was detected. The exchangeable percentage Cd (or PO_4) was calculated according to eq (1):

$$E = \left[\frac{(^{109}Cd_{aq})^*}{(^{109}Cd_T)^*} \Big/ \frac{(Cd_{aq})}{(Cd_T)} \right] \times 100\% \tag{1}$$

where Cd_{aq} denotes the Cd activity in solution after sorption, Cd_T denotes the activity of Cd before sorption, $^{109}Cd_{aq}$ is the activity of the tracer in solution after rapid isotopic exchange, and $^{109}Cd_T$ is the activity of the tracer in solution before rapid isotopic exchange.

2.4. Results and discussion

2.4.1. Sorption

In Fig. 1 the percentage of Cd sorption versus time is plotted for pH = 7.4, 8.0, 8.37, 9.04, and 9.53. Sorption percentages are equal for Cd concentrations of 1.25×10^{-9} M and 4.5×10^{-8} M. Sorption of Cd consists of fast initial sorption (< 48 hours), by integration into kinks/steps followed by a much slower burial process resulting from Ostwald ripening (Van der Weijden et al., 1994). The initial sorption % is independent of the Cd concentration, implying linearity of the isotherm in the range 1.2×10^{-9} - 4.5×10^{-8}M Cd. Sorption increases from pH = 7.4 to pH = 9, because (Ca^{2+}) decreases and therefore competes less with Cd. However, at pH = 9 and pH = 9.5, the sorption maxima are 99% and 94% respectively, despite the fact that (Ca^{2+}) is ten times lower at pH = 9.5 than at pH = 9. This may be explained by a lower (Cd^{2+}), e.g. as a result of the formation of a $Cd(CO_3)_3^{4-}$ complex (Sillén and Martell, 1971) at pH = 9.5.

Initial sorption of Cd can be described with a cation exchange model (Davis et al., 1987; Zachara et al., 1991; Van der Weijden et al., 1994):

$$Ca^{2+}_s + Cd^{2+}_{aq} = Cd^{2+}_s + Ca^{2+}_{aq} \tag{2}$$

with the exchange constant:

$$K_{ex} = \{(Ca^{2+})_{aq}/(Cd^{2+})_{aq}\} \times \{(Cd)_s/(Ca)_s\} \tag{3}$$

where $(Ca^{2+})_{aq}$ and $(Cd^{2+})_{aq}$ represent the free Ca^{2+} and Cd^{2+} activities in solution as calculated with MINTEQA2 and $(Cd)_s$ and $(Ca)_s$ denote the surface activities of Cd and Ca.
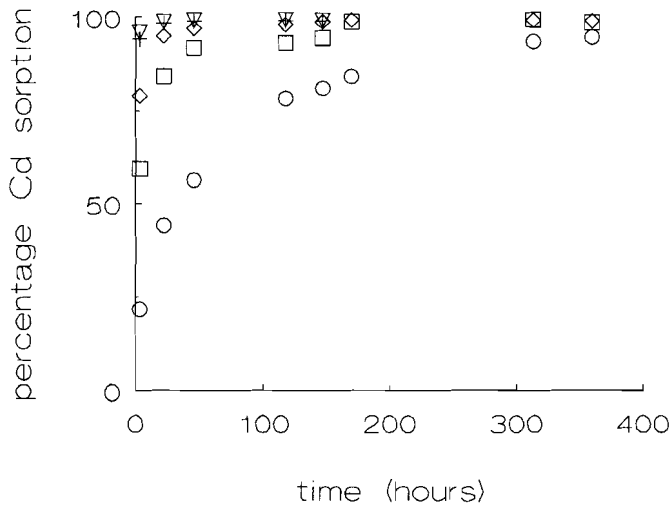
Fig. 1. Cd sorption on calcite versus time for [Cd] = 1.25×10^{-9} M and 4.5×10^{-8} M at pH = 7.4 (O), 8.0 (□), 8.37 (◊), 9.04 (∇) and 9.53 (+).
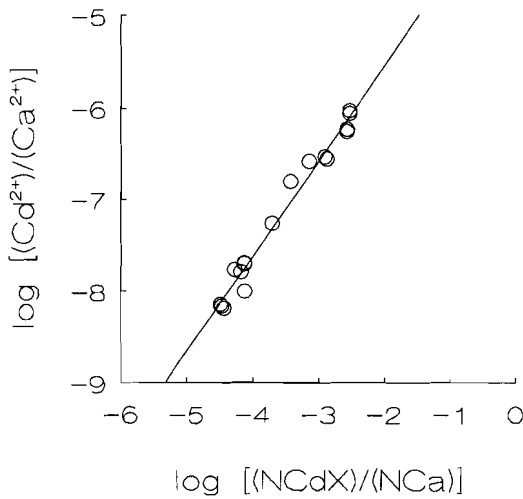

Fig. 2. Cadmium-calcium exchange plot based on eq (4) for Cd sorption (t = 48 hours), at pH = 7.4, 8.0 and 8.37 and [Cd] = 1.2×10^{-9} M, 8.93×10^{-9} M and 4.5×10^{-8} M.

Using a value of 3.6×10^{-3} mole/kg for the total amount of sorption sites (X_t) as estimated with ^{45}Ca exchange (after 4 hours), assuming a value of 1 for the activities of Ca and Cd in the solid, and rewriting (3) as:

$$\log \frac{(Cd^{2+})_{aq}}{(Ca^{2+})_{aq}} = -\log K_{ex} + n \log \frac{(NCdX)}{(NCaX)} \tag{4}$$

a plot as shown in Fig. 2 can be made, in which $NCdX$ denotes (Cd_s/X_t), $NCaX$ denotes (1-(Cd_s/X_t)) and n is an empirical constant. Data for pH > 8.4 are not included, since Cd was nearly completely removed from solution after fast initial sorption. For sorption in the range pH = 7.4 - 8.4, data plot on a line with slope (n) = 1.03 and intercept ($-\log K_{ex}$) = 3.4. The slope of nearly 1 indicates almost ideal behavior. The value 3.4 is lower than for $\log(K_{sp}CdCO_3/K_{sp}CaCO_3)$ = 3.7, which seemingly suggests that besides Ca/Cd exchange, other exchange reactions may take place. An alternative explanation for the lower K_{ex}, however, is that the estimate for X_t is too high. By setting $-\log K_{ex}$ = 3.7 and n = 1, nonlinear regression with the Levenberg-Marquardt method yielded X_t = (2.48 ± 0.21)$\times 10^{-3}$ mol Ca sites/kg. This X_t value deviates 30% from the value used in plot 2, but is very close to a value of 2.41×10^{-3} mol Ca sites/kg calculated from the surface area and the estimate of 5×10^{14} atoms Ca/cm^2 at pH = 8.3 by Möller and Sastri (1974).

Fig. 3 shows the percentage of phosphate (1.25×10^{-7}M) sorption at various pH values versus time. Phosphate sorption is fast and is completed within 48 hours. The decrease in sorption at higher pH probably results from the increase in competition of phosphate with carbonate ions. From pH = 7.4 to pH = 9, the free PO_4^{3-} activity increases by a factor of 1000, but the phosphate/carbonate ratio decreases by a factor 10. The change in surface charge towards negative values at higher pH can also contribute to the decrease in sorption, but as phosphate is generally believed to be chemisorbed it is expected to be less susceptible to electrostatic forces.

In Fig. 4 the phosphate sorption percentage is plotted as a function of pH at various total PO_4 concentrations after 24 hours of sorption. Sorption percentages and K_d values ([PO_4]$_s$/[PO_4]$_{aq}$) (Fig. 5) are almost equal in the range from 1×10^{-9} M to 1×10^{-7} M phosphate, but decrease from 1.25×10^{-7} M to 1.25×10^{-5} M phosphate. This can be explained from a decrease of the most favorable sorption sites as the surface coverage increases. At high phosphate concentrations (1.25×10^{-4} M) and pH = 7.4, K_d increases since the [PO_4]$_s$ increases from 13% sorption after 3 hours, to 74% after 24 hours. The increase in K_d together with the rapid phosphate removal kinetics, suggest precipitation of an unknown amorphous calciumphosphate phase. Such an increase is observed above [PO_4]$_s$ = 10^{-3} mol/kg (Fig. 5), a number that is close to the number of sorption sites.
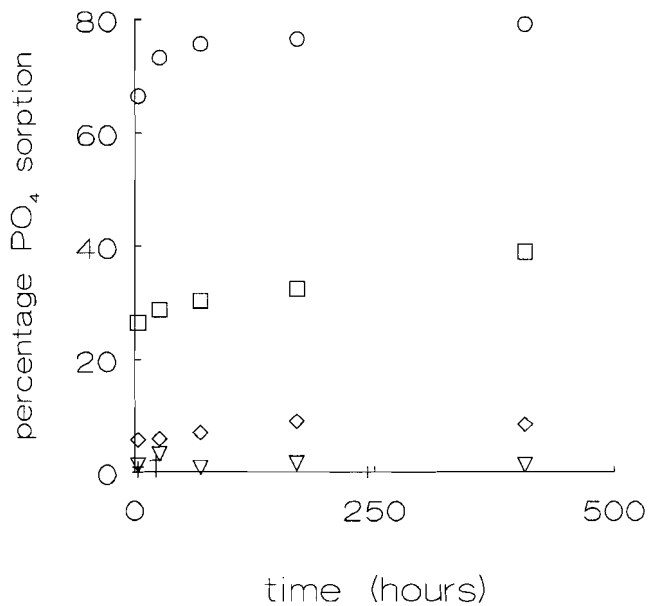
Fig. 3. Percentage phosphate (1.25×10^{-7} M) sorption on calcite versus time at pH = 7.4 (O), 8.0 (□), 8.37 (◊), 9.04 (∇) and 9.53 (+).
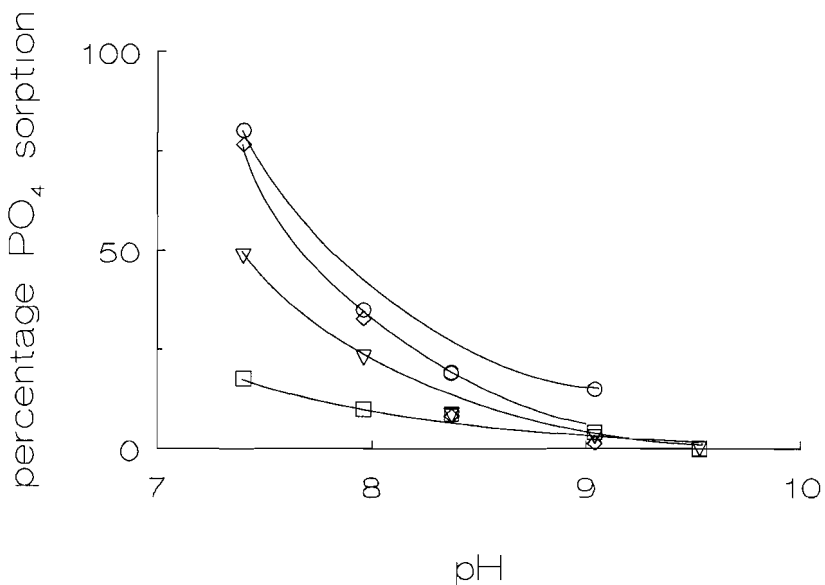

Fig. 4. Percentage phosphate sorption on calcite as a function of pH and phosphate concentration 1.25×10^{-8}M (O), 1.25×10^{-7}M (◊), 1.25×10^{-6}M (∇), 1.25×10^{-5}M (□) phosphate.
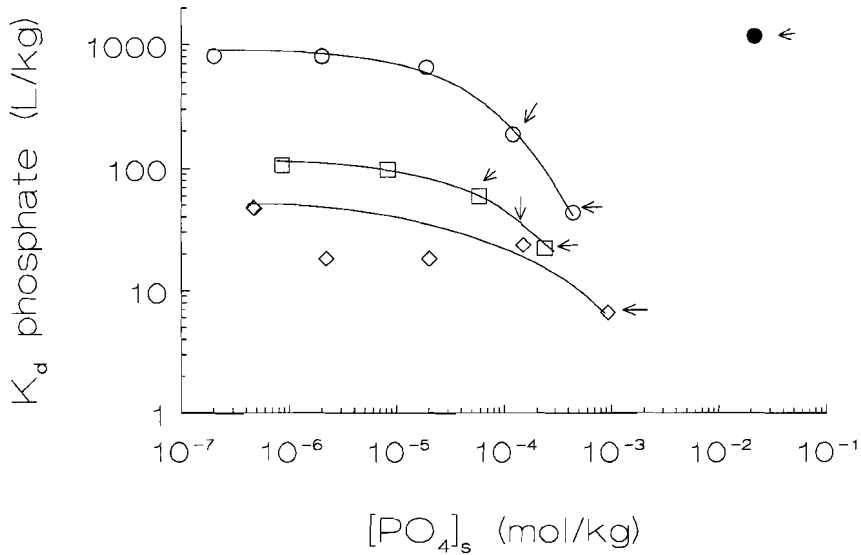
Fig. 5. K_d ([PO$_4$]$_s$/[PO$_4$]$_{aq}$) versus [PO$_4$]$_s$ at pH = 7.4 (O), 8.0 ($\square$), 8.37 ($\lozenge$). Arrows indicate supersaturated solutions with respect to a calciumphosphate solid phase. ($\bullet$) = increase in K_d at pH = 7.4 at [PO$_4$] = 1.25 $\times 10^4$ M.
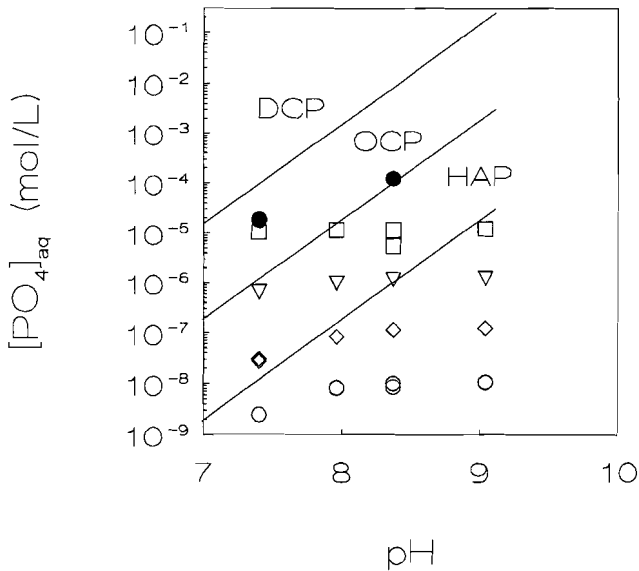

Fig. 6. Solubility diagram of DCP = dicalciumphosphate (CaHPO$_4$.2H$_2$O), OCP = octacalciumphosphate (Ca$_4$H(PO$_4$)$_3$.3H$_2$O) and HAP = hydroxyapatite (Ca$_5$(PO$_4$)$_3$(OH)). Aqueous concentrations after sorption are plotted for 1.25×10^{-8} M (O), 1.25 ×10^{-7} M ($\lozenge$), 1.25×10^{-6} M (∇), 1.25×10^{-5} M ($\square$) and 1.25×10^{-4} M ($\bullet$) total phosphate.

The aqueous phosphate concentrations do not seem to be limited by the saturation concentrations of the crystalline octacalciumphosphate (OCP, $Ca_4H(PO_4)_3.3H_2O$) or hydroxyapatite (HAP, $Ca_{10}(PO_4)_6(OH)_2$) phases. A supersaturated state with respect to these phases is apparent in the solubility diagram in Fig 6. If the suspected precipitated phase was a HAP precipitate, 25 layers of HAP would have formed, as calculated from the number of moles that may precipitate and the number of sorption sites. The aqueous PO_4 concentrations would definitely reflect the presence of such a surface precipitate. Of course, the possible formation of an amorphous precipitate with a higher K_{sp} still remains open, since precipitation of HAP is thought to proceed along various amorphous and metastable crystalline phases (Eanes et al., 1965) and OCP or HAP have slow kinetics of formation (Cole et al., 1953; Griffin and Jurinak, 1973; House and Donaldson, 1986).

Several models have been applied to describe sorption of phosphate on calcite, such as a Langmuir isotherm at constant pH involving the adsorbing species PO_4^{3-} and HPO_4^{2-} (House and Donaldson, 1986), a heterogeneous isotherm model consisting of two linear parts (DeKanel and Morse, 1978), a singular Langmuir isotherm involving only PO_4^{3-} (Reddy, 1977), a heterogeneous surface model (Holford and Mattingly, 1975) and an anion-exchange model (Ishikawa and Ichikuni, 1981).

For the phosphate concentrations below 1.25×10^{-7} M, where a genuine sorption process occurs, we applied the anion exchange model to describe our sorption data because this model seems to reflect best the competition between phosphate and carbonate ions. Firstly, we assume the exchange to be:

$$3CO_3^{2-}{}_{(s)} + 2PO_4^{3-}{}_{(aq)} = 3CO_3^{2-}{}_{(aq)} + 2PO_4^{3-}{}_{(s)} \tag{5}$$
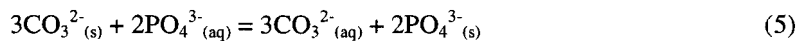
with the exchange constant:

$$K_{ex} = \{(CO_3^{2-})^3_{aq}/(PO_4^{3-})^2_{aq}\} \times \{(PO_4^{3-})_s^2/(CO_3^{2-})_s^3\} \tag{6}$$

where $(CO_3^{2-})_{aq}$ and $(PO_4^{3-})_{aq}$ denote the free CO_3^{2-} and PO_4^{3-} activities in solution and $(CO_3^{2-})_s$ and $(PO_4^{3-})_s$ are the surface activities of CO_3^{2-} and PO_4^{3-}. Using $X_t = 2.48 \times 10^{-3}$ mole Ca sites/kg calcite as calculated above, assuming the activities of the surface species to be 1, eq. (6) transforms into:

$$\log \frac{(PO_4^{3-})_s}{(PO_4^{3-})_{aq}} = 0.5 \ \log K_{ex} \ -1.5 \ \log \frac{(CO_3^{2-})_{aq}}{X_t \ - \ 1.5 \ (PO_4^{3-})_s} \tag{7}$$

A plot as shown in Fig. 7 can be drawn for $[PO_4]_T$ values $< 1 \times 10^{-6}$ M, concentrations where K_d is more or less constant. Such a plot yields an intercept of 6.7 and a slope of -1.34. The value of the slope should be close to -1.5, if reaction (5) were the only occurring reaction. Probably the reaction:

$$HPO_4^{2-}{}_{(aq)} + CO_3^{2-}{}_{(s)} = HPO_4^{2-}{}_{(s)} + CO_3^{2-}{}_{(aq)} \tag{8}$$
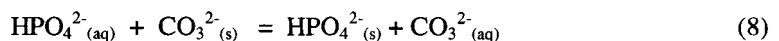
which in a similar plot as shown in Fig. 7 would lead to a slope of -1, is also involved in the sorption process. Based on the found slope of -1.34, we assume that at low phosphate concentrations, reaction (8) contributes for about 30% and reaction (5) for about 70% to the sorption process. In any case, the results indicate that PO_4^{3-} and HPO_4^{2-} are the sorbing species, of which PO_4^{3-} dominates. Studies of phosphate inhibition of calcite and aragonite
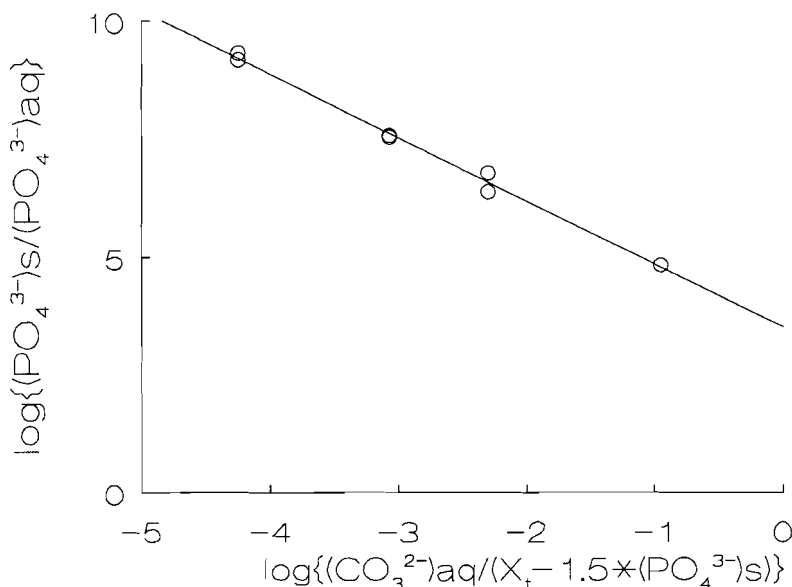
Fig. 7. Phosphate - carbonate exchange plot based on eq (7) for phosphate sorption (t = 24 hours) on calcite at pH values 7.4-9.5 and phosphate concentrations of 1.25×10^{-9}M to 1.25×10^{-7} M.

precipitation rates in seawater point out the relative importance of PO_4^{3-} and HPO_4^{2-} adsorption on $CaCO_3$ and support the conclusions of this study (Mucci, 1986; Burton and Walter, 1990).

For concentrations of $[PO_4]_T \geq 1.25 \times 10^{-5}$ M, when K_d decreases, a similar plot is made and a slope of -1 is obtained, suggesting a one on one exchange of HPO_4 and CO_3 and yielding a K_{ex} of 4. The lower exchange ratio of CO_3/PO_4 and the lower K_{ex} at higher PO_4, indicate that the number of surface sites with low sorption energies decreases as the degree of surface occupation increases, rendering exchange more difficult.

Since PO_4^{3-} and HPO_4^{2-} appear to be the sorbing species, we also tested the model of House and Donaldson (1986), who found that the sorption isotherms could be described with a two-component Langmuir model, with the constants K_1 and K_2 in the pH range 7 - 9 (eq 9):

$$\frac{Pads}{Xt} = \frac{K_1(PO_4^{3-}) + K_2(HPO_4^{2-})}{1 + K_1(PO_4^{3-}) + K_2(HPO_4^{2-})} \tag{9}$$

where *Pads* denotes the number of moles of PO_4 at the surface. From 5 different $[PO_4]_T$ for each pH value, and from a plot of:

$$\frac{1}{(PO_4^{3-})} \frac{Pads}{X_t} = K_1 + K_2 \frac{(HPO_4^{2-})}{(PO_4^{3-})} \tag{10}$$

for $[PO_4]_T < 10^{-6}$M, log K_1 was estimated to vary between 12.2 and 10.7 and log K_2 between -6.5 and -7 in the pH range of 7.5 to 9. Donaldson and House were probably able to model their data with single K_1 and K_2 values, because the (CO_3^{2-}) in their experiments varied by a factor 4 only, as the pH was varied by varying PCO_2, whereas in the present study the
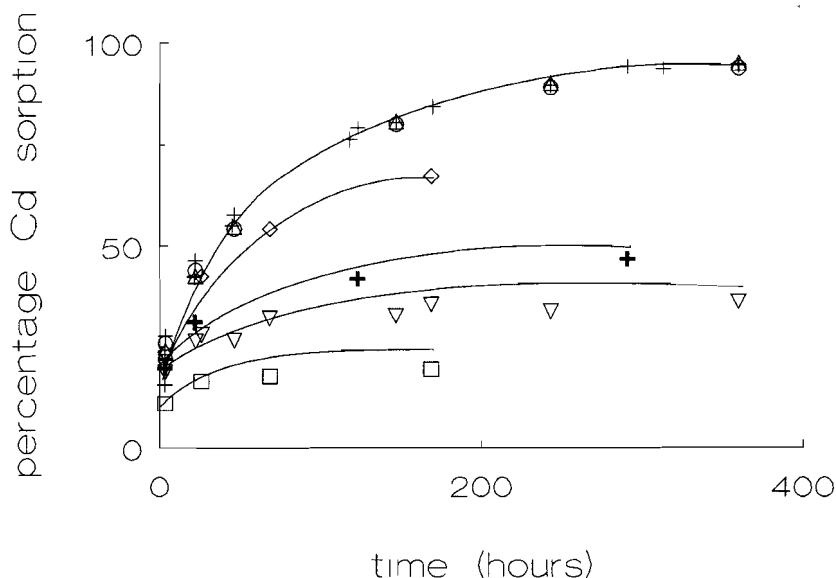
Fig. 8. Cd sorption on calcite versus time at pH = 7.4 and no (+), 1.25×10^{-9} M (Δ), 1.25×10^{-8} M (O), 1.25×10^{-7} M ($\Diamond$), 5×10^{-7} M (+), 1.25×10^{-6} M (∇), 1.25×10^{-5} M ($\square$) phosphate.

(CO_3^{2-}) varied by a factor of 1800 and therefore competition was greater. At $[PO_4]_T >$ 10^{-6} M, the K_1 and K_2 values obtained for our data deviate from those at lower$[PO_4]_T$, which would be supportive of a heterogeneous isotherm model consisting of two linear parts (DeKanel and Morse, 1978). In summarizing, eq 7 seems to describe the sorption data best.

In Fig. 8 and Fig. 9 the influence of various phosphate concentrations on the sorption of Cd on calcite is shown for pH = 7.4 and pH = 8.37 respectively. Phosphate reduces the percentage of initial fast (< 48 hours) Cd sorption. At lower pH this effect is more pronounced, which, when calculating the K_d values for Cd and PO_4 after 48 hours sorption (250 and 600 (l/kg) at pH = 7.4, and 6500 and 55 (l/kg) at pH = 8.37 respectively), could be expected.

The reduction of Cd sorption is likely the result of competition of phosphate and cadmium for similar sites at the surface, like kink sites. Substitution of carbonate by phosphate may alter the characteristics of a kink site and therefore reduce Cd sorption. This can be concluded from the fact that at pH = 7.4 and $[PO_4]_T = 5 \times 10^{-7}$ M, phosphate sorption is 1.9×10^{-8} mole/gram (1% surface coverage), and Cd sorption ($[Cd]_T = 1.25 \times 10^{-9}$ M) is reduced by 50% to 5.54×10^{-11} mole/gram, whereas the estimated total number of sorption sites equals 2.48×10^{-6} mole/gram.

A high surface coverage (21%) of phosphate at $[PO_4]_T = 1 \times 10^{-5}$ M and pH = 7.4, still allows for 12% of Cd sorption. This could indicate i) formation of ternary complexes of Cd with phosphate (Morel, 1983), also because Cd displays a great affinity for the surface of HAP (Middelburg and Comans, 1991), ii) faster integration into kink sites of Cd as compared to phosphate, iii) sorption of phosphate or cadmium at surface sites with higher sorption energies. The latter option seems the most plausible one, because: ad i): the formation constants for Cd and Ca complexes with phosphate are almost equal (Apx. 1) and
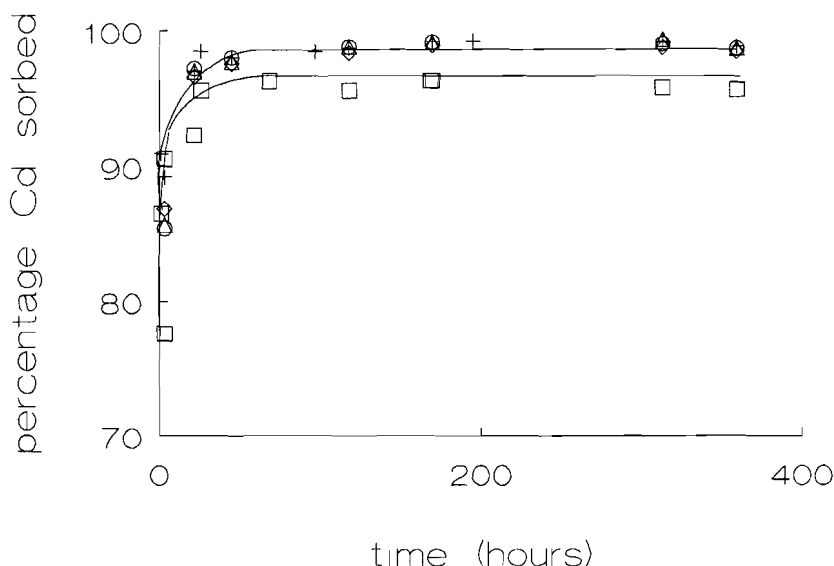
Fig. 9. Cd sorption on calcite versus time at pH = 8.37 and no (+), 1.25×10^{-9} M (Δ), 1.25×10^{-8} M (O), 1.25×10^{-7} M ($\Diamond$), 5×10^{-7} M (+), 1.25×10^{-6} M (∇), 1.25×10^{-5} M ($\square$) phosphate.

only a tiny fraction of Ca and Cd (0.1%) is bound as such in solution. Therefore, we assume that similar (ternary) complexes at the surface play a minor role. Ad ii): in an experiment in which the Cd tracer and carrier were added three hours after the addition of the phosphate tracer and carrier the same sorption percentage for Cd was found. Kinetics of surface integration obviously do not determine the final sorption percentage. Ad iii): as will be discussed in the section on reversibility, phosphate sorption is much more reversible than Cd sorption. Cd could therefore force phosphate to sorb on energetically less favorable sites, while Cd occupies the energetically more favorable sites.

In Fig. 10 and Fig. 11, Cd sorption versus time in the presence of various sulfate concentrations is shown at pH = 7.8 and 8.37 respectively. The initial fast sorption of Cd is retarded in the presence of sulfate as a result of the competition at the surface between Cd and SO_4, and at the highest $[SO_4^{2-}]$ of 0.1 M also by complexation (45%) as $CdSO_4^\circ$ and $Cd(SO_4)_2^{2-}$.

The reduction in Cd sorption in the presence of sulfate is greater at lower pH (Fig. 12), because the reduced carbonate concentration increases the sorption of sulfate. Sorption of sulfate was not studied separately, but like phosphate, sulfate probably replaces carbonate at the surface (anion-exchange). In travertine, for instance, SO_4 was found to replace the CO_3 in the crystal lattice, and replacement was highly dependent on pH (Takano, 1985). Regarding the concentrations of SO_4 needed to substantially affect Cd sorption, we can conclude that the interaction of sulfate with the calcite surface is small, as compared to PO_4. Phosphate at a surface concentration of 1.9×10^{-5} mol/kg already reduces the Cd sorption by 19%. Since the radius and tetrahedral form of both anionic groups are very similar, the difference in affinity for the calcite surface is probably related to the solubility of $CaSO_4.2H_2O$, which is much higher than the solubility of $CaHPO_4.2H_2O$.
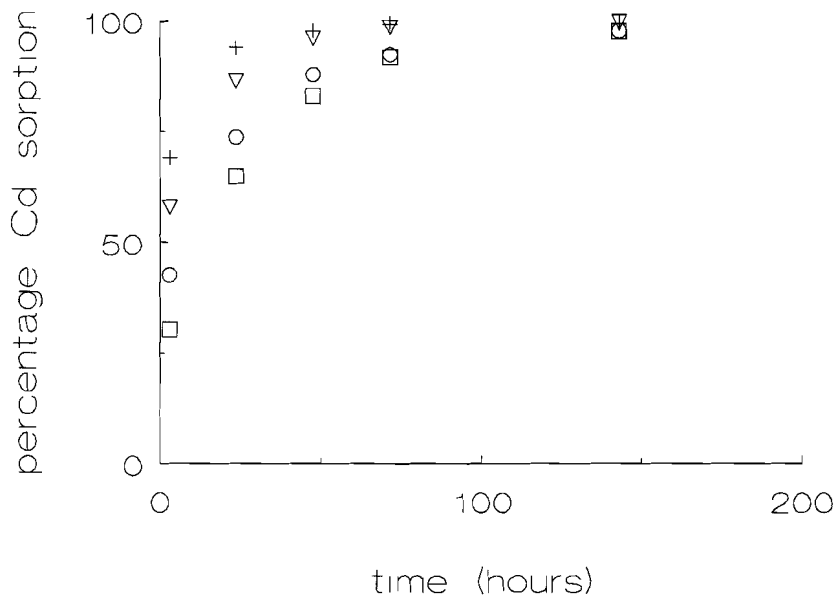
Fig. 10. Cd sorption on calcite versus time at pH = 7.82 and no (+), 3×10^{-5} M (∇), and 1×10^{-3} M (O) and 0.1 M ($\square$) sulfate.
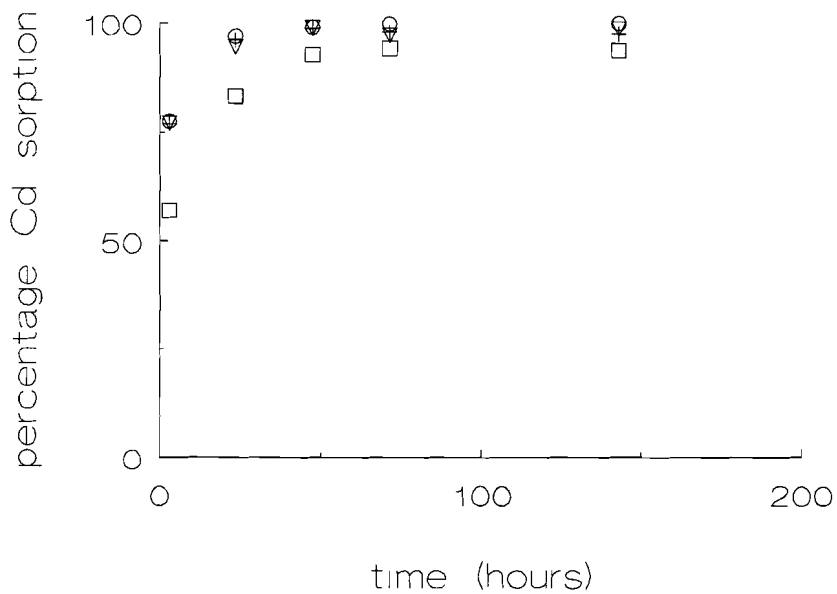
Fig. 11. Cd sorption versus time at pH = 8.37 and no (+), 3×10^{-5} M (∇), and 1×10^{-3} M (O) and 0.1 M ($\square$) sulfate.
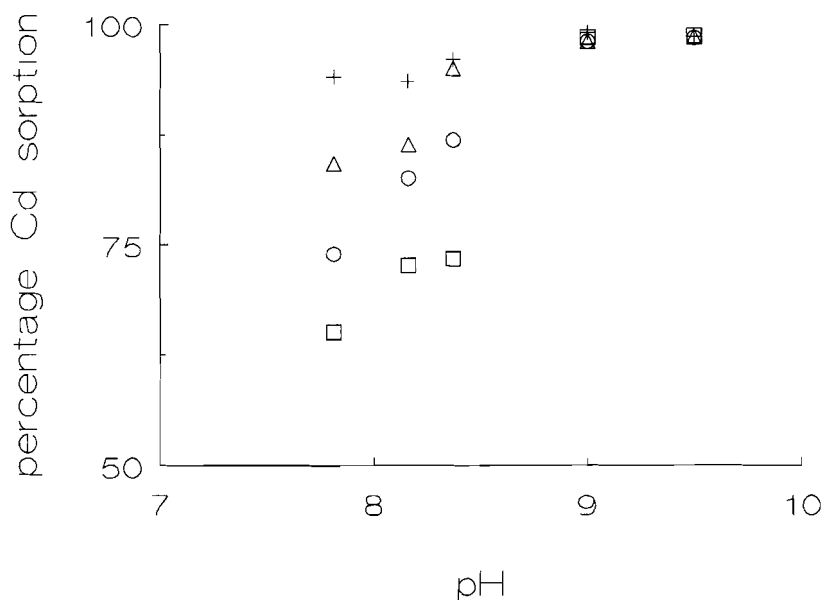
Figure 12. Percentage cadmium sorption on calcite as a function of pH and no (+), 3×10^{-5} M ($\triangle$), and 1×10^{-3} M (O) and 0.1 M ($\square$) sulfate.

2.4.2 . ^{45}Ca isotopic exchange

In addition to fast initial sorption, the slow Cd uptake resulting from Ostwald ripening (Fig.1) contributes significantly to Cd removal from solution. This is especially clear for sorption at pH = 7.4, where fast initial sorption removes 20% Cd, but the slow removal raises this percentage to 95% after 300 hours. The Ostwald ripening rate increases below and above pH = 8.37 (see Table 2), because total concentrations of Ca and CO_3 ions in solution increase, i.e., the fluxes to and from the surface increase. The easier dehydration of carbonate as compared to Ca may cause the ripening rate to increase relatively more above than below pH = 8.37 (Lahann, 1978).

In solution with varying phosphate (1-5) and sulfate (7-10) concentrations (see Table 1), STE and LTER were calculated as described under "methods". Calcite "ca" had a specific surface area of 0.29 m^2/g and calcite "cb" had a specific surface area of 0.4 m^2/g.

In the presence of phosphate and sulfate, the slow Cd uptake after fast initial sorption is reduced. In Fig. 8 this is very clear for times above 100 hours. The decrease is a direct result from a reduction in the Ostwald ripening rate in the presence of PO_4 and SO_4 (Figs. 13 and 14 and Table 2). This is not surprising, regarding the fact that low PO_4 concentrations (10^{-7}-10^{-6} M) and to a lesser extent SO_4 (10^{-4} M) are known to reduce calcite precipitation rates, by blocking growth (kink) sites at the surface (e.g. Meyer, 1981; Busenberg and Plummer, 1985; Mucci et al., 1989).

Table 2. Short term exchange (STE) of [45]Ca and long term exchange rate (LTER) of [45]Ca.

Solution	STE (ca)/ STE (cb) Ca (μmol / gram)	LTER (ca)/ LTER (cb) Ca (nmol / (gram$\times$hour))	pH
1		180	7.40
1(+1$\times$10^{-7}M PO$_4$)		53	
1(+1$\times$10^{-6}M PO$_4$)		3.8	
2	1.7	246	8.01
3	1.2	141	8.37
3(+1$\times$10^{-7}M PO$_4$)		123	
3(+1$\times$10^{-6} M PO$_4$)		2.23	
4		97	9.02
5	0.7	484	9.48
5(+1$\times$10^{-7} M PO$_4$)		356	
5(+1$\times$10^{-6} M PO$_4$)			
7a	2.7 / 17.5	23.5 / 500	8.01
7c		8.7 / 34	
7d		8.6 / < 0.1	
8a	0.6 / 0.6	5 / 28	8.37
8c		/ 23	
8d		/ 11	
9a	1.9 / 2.5	32 / 762	9.03
9c		/ 669	
9d		/ 700	
10a	2.7 / 3.6	55 / 2600	9.54
10c		/ 700	
10d		/ 1880	

In addition to the lower Cd removal rate, these lower Ostwald ripening rates also yield lower partition coefficients for Cd, as calculated from [45]Ca exchange, the low Cd removal rate (SCRR, calculated from Fig. 8), and the Ca and Cd activities in solution (activities of Ca and Cd in the solid are assumed to equal one) (Table 3). Another effect of lower ripening rates in the presence of phosphate is that the trend of the precipitation rates versus the partition coefficients is reversed, compared to the experimental results of Lorens (1981).

2.4.3. Sorption reversibility

Sorption reversibility was investigated with rapid isotopic exchange (RIE) and desorption experiments. In the case of RIE, sorption is considered to be 100% reversible if the ratios aqueous/sorbed of the carrier are equal to the ratios aqueous/sorbed of the radioactive tracer. In desorption experiments, a sorption reaction is considered to be 100% reversible, if the ratios of the sorbed and aqueous species before and after desorption in a solution of the same composition, plot on a single sorption isotherm.
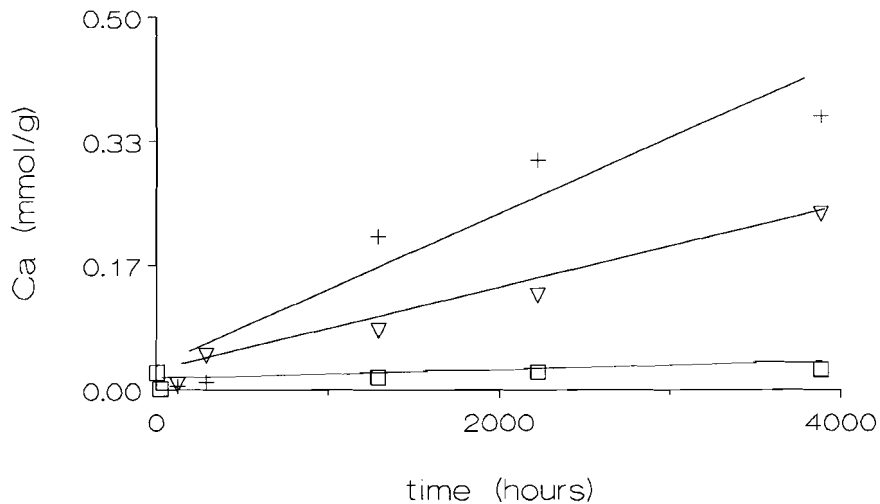
Fig. 13. Influence of phosphate on the ^{45}Ca exchange versus time at pH = 7.4 and no (+), 1.25×10^{-6} M (∇), 1.25×10^{-5} M (□) phosphate.
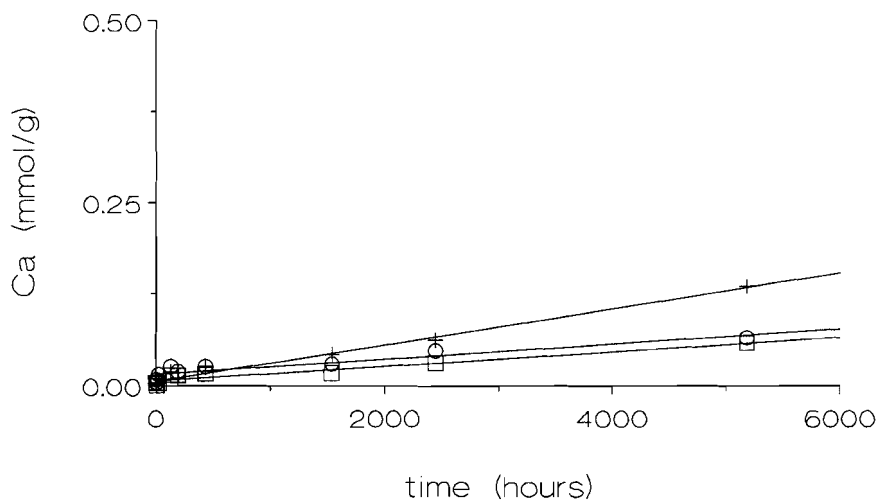

Fig. 14. Influence of sulfate on the ^{45}Ca exchange of calcite versus time at pH = 7.8 and no (+), 1×10^{-3} M (O) and 0.1 M (□) sulfate.

Table 3. Partition coefficients (D) of Cd with calcite, as calculated from ^{45}Ca exchange rate (LTER), the slow Cd removal rate (SCRR) and the Ca and Cd concentrations in solution.

[PO$_4$]	LTER (nmol/(g×hr))	SCRR (pmol/(g×hr))	D (Cd)
< 10^{-8} M	180	9.8	960
10^{-7} M	53	4.4	550
10^{-6} M	3.8	0.45	490

Short term sorption reversibility of phosphate, investigated with RIE experiments, revealed a slightly lower reversibility at pH = 7.4 as compared to pH = 8.37 (Table 4). At higher pH, and smaller [PO$_4$]$_s$, more PO$_4$ could be located at energetically favorable sites. E is nearly constant in time for both phosphate concentrations. Should a solid phase with slow kinetics of formation (see above) precipitate on the calcite surface, one would expect E to decrease over time. Therefore, within the run time of the experiments in this study, slow surface precipitation does not seem to occur. The smaller reversibility at 1.25×10^{-5} M PO$_4$ in solution (20%) as compared to 1.25×10^{-8} M (70%), however, does suggest the presence of more irreversibly bound PO$_4$ at high concentrations after 1 hour sorption. As E remains constant in time and with regard to the kinetics of PO$_4$ removal/precipitation at 1.25×10^{-4} M (see above), formation of a precipitate within an hour is unlikely. Therefore, slow kinetics of isotopic exchange may give rise to the different values found for E at low and high [PO$_4$]$_T$, although two hours exchange instead of fifteen minutes, yielded similar results. Further investigation to clarify this phenomenon is needed.

Long term sorption reversibility of phosphate after sorption for 360 hours at 1.25×10^{-8} M PO$_4$ and at pH = 7.4, was investigated by desorption at the same pH. A K_d (l/kg) of 1050 after desorption compared to a K_d value of 900 after sorption, suggests that sorption is almost completely reversible. In contrast to Cd, phosphate is not incorporated to a great extent during Ostwald ripening, which explains the absence of a slow PO$_4$ removal process (Fig. 3). In fact, Ostwald ripening is slowed as a result of the presence of phosphate, as was shown above.

Table 4. Results of rapid isotopic exchange experiments with phosphate (1.25×10^{-5} M and 1.25×10^{-8} M) at pH = 7.4 and 8.37. "E" was calculated according to eq (1).

pH	time (hours)	1.25×10^{-5} M PO$_4$		1.25×10^{-8} M PO$_4$	
		sorption %	E	sorption %	E
7.4	1	23.4	25.5		
7.4	3	23.8	22	70.9	73
7.4	24	25.4	19	75.2	
7.4	144	28.1			
8.37	1	16.5	19.5		
8.37	3	19	13	14.5	
8.37	24	17.8	11	7.9	68.5
8.37	144	15.3	24	6.1	66

Table 5. Results of rapid isotopic exchange experiments with cadmium (1.2×10^{-9} M) at pH $= 7.4$ and 8.37 in presence and absence of phosphate (1.25×10^{-5} M). "E" was calculated according to eq (1).

pH	time (hours)	1.2×10^{-9} M Cd		1.2×10^{-9} M Cd + 1.25×10^{-5} M PO$_4$	
		sorption%	E	sorption%	E
7.4	1			4.4	81
7.4	3	23.1	83	3.4	
7.4	24	41.5	26.5	10.0	27.5
7.4	144	60.1	10	12.1	21
8.37	1	89.3	95	85.7	70.5
8.37	3	92.5	91	87.3	46.5

RIE experiments with Cd (Table 5) indicate that the short term reversibility ($t < 24$ hours) at pH = 7.4 is smaller than at pH = 8.37. In a previous paper (Van der Weijden et al., 1994) it was demonstrated that the difference in short term reversibility can result from competition for sorption sites. At a high competition with Ca (pH = 7.4), Cd may be sorbed onto the energetically most favorable sites only. After longer sorption times the reversibility of Cd decreases as a result of integration into kink sites at the surface, and (after 144 hours) also as a result of Ostwald ripening. The influence of ripening can also be observed in desorption experiments. As a result of the higher Ostwald ripening rates at pH values below and above pH = 8.3 - 8.4, desorption at these pH values results in relatively higher K_d (Cd) values increase (Table 6). This means that sorption reversibility is highest at pH = 8.3 - 8.4, which is in agreement with the RIE results.

Table 6. K_d ([Cd]$_s$/[Cd]$_{aq}$) after sorption and desorption.

pH	sorption time (hours)	K_d ads (l/kg)	K_d des (l/kg) 22 hours
7.9 [*)	121 [*)	2047 [*)	3569 [*)
8.3 [*)	121 [*)	10100 [*)	675 [*)
8.37	360	14900	1600
9.04	360	54700	86300

[*): data from chapter 1: after sorption in 0.665 M NaNO$_3$ (pH = 7.9) and 0.7 M NaNO$_3$ (pH = 8.3) and desorption in 0.665 M NaCl at pH = 7.9 and 8.3 respectively. Other data are from the present study and represent adsorption in solutions **3** and **4** (Table 1) and desorption in 0.5 M NaCl, adjusted with NaNO$_3$ to $I = 0.7$, at pH = 8.37 and 9.04 respectively.
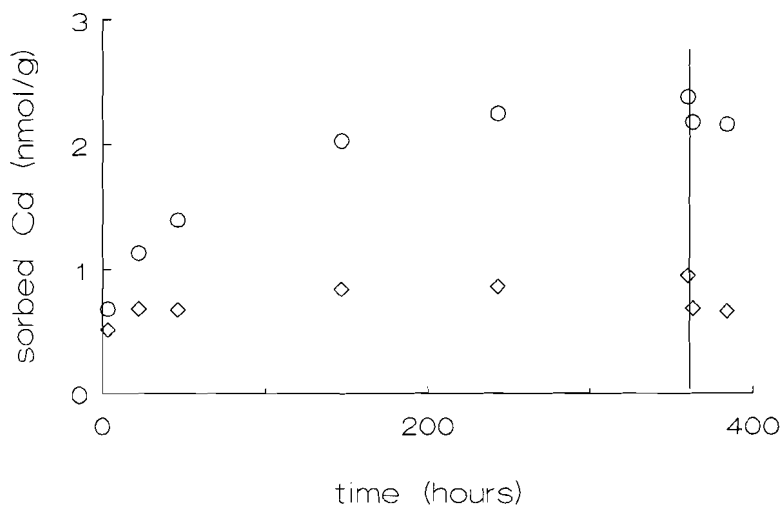
Fig. 15. Desorption of Cd after 360 hours sorption at pH = 7.4 and 1.25×10^{-6} M (O) and 1.25×10^{-8} M (◊) phosphate. Total phosphate concentrations after desorption are 5.7×10^{-7} M and 1.2×10^{-8} M respectively.

RIE experiments of Cd in the presence of phosphate suggest equal short term reversibility (Table 6) at pH = 7.4, whereas the reversibility is reduced at pH = 8.3. At pH = 8.3, Cd is probably forced to sorb onto the more favorable sites, due to the higher competition, whereas competition at pH = 7.4 was already high. After longer sorption times (144 hours sorption at pH = 7.4, Table 5), the reversibility in the presence of phosphate is greater than in the absence of phosphate. This is directly related to the Ostwald ripening rate, which is lower when phosphate is present, therefore, less Cd is buried. It can also be seen in Fig. 15, where the % of desorption of Cd after 360 hours sorption, increases with increasing phosphate concentration.

5. Concluding remarks

The results presented here show that in the pH range 7.4 - 8.4 in our experiments, phosphate and sulfate reduce both the fast and slow Cd sorption on calcite, increase the long term sorption reversibility, and reduce the partition coefficient of Cd with calcite.

The conditions in deep ocean water (like PCO_2, T and P) are, of course, different from laboratory conditions. Possibly, the effect of phosphate on Cd sorption in the deep ocean, where carbonate concentrations are about 75 μM (Broecker and Peng, 1982) compares best with conditions at pH = 8.37 in our study. The reduction of Cd sorption at high phosphate concentrations is 8% at pH = 8.37, yet corresponds with lower Cd/Ca ratios at the calcite surface and in the recrystallized calcite (Ostwald ripening). This relationship between Cd/Ca ratios and aqueous phosphate concentrations in our study is therefore the opposite of the trend that exists between Cd/Ca ratios in foraminifera and aqueous phosphate in deep ocean waters. In ocean deep water, a higher phosphate concentration corresponds with a

higher Cd/Ca ratio. Therefore, the Cd/Ca ratio in foraminifera is probably biochemically rather than chemically controlled. In order to fully understand the partition coefficient (D) of Cd between foraminifera and seawater, further study of the effects of biochemical parameters is required. Finally, direct translation of Cd/Ca ratios of calcite precipitated in the laboratory into growth rates of foraminifera does not seem warranted, regarding the biochemical rather than chemical nature of foraminiferal growth.

Acknowledgements

References

Allison, J.D., Brown, D.S. and Novo-Gradac, K.J., 1991. MINTEQA2/PRODEFA2, a geochemical assessment model for environmental systems: version 3.11.

Boyle, E.A., 1988. Cadmium: Chemical tracer of deepwater paleoceanography. Paleoceanography, 3: 471-489.

Broecker, W.S. and Peng, T.H., 1982. Tracers in the Sea. Lamont-Doherty geological observatory, 690 pp.

Busenberg, E. and Plummer, I.N., 1985. Kinetic and thermodynamic factors controlling distribution of SO_4^{2-} and Na^+ in calcites and selected aragonites. Geochim. Cosmochim. Acta, 49: 713-725.

Cole, C.V., Olsen, S.R. and Scott C.O., 1953. The nature of phosphate sorption by calcium carbonate. Soil Sci.Soc. Amer. Proc., 17: 352-356.

Comans, R.N.J., 1987. Adsorption, desorption and isotopic exchange of cadmium on illite: evidence for complete reversibility. Water Res., 21: 1573-1576.

Davis, J.A., Fuller, C.C. and Cook, A.D., 1987. A model for trace metal sorption processes at the calcite surface: Adsorption of Cd^{2+} and subsequent solid-solution formation. Geochim. Cosmochim. Acta, 51: 1477-1490.

De Baar, J.W., Saager, P.M., Nolting, R.F., and van der Meer, J. 1994. Cadmium versus phosphate in the world ocean. Mar. Chem., 46 : 261-283.

DeKanel, J. and Morse, J.W., 1978. The chemistry of orthophosphate uptake from seawater onto calcite and aragonite. Geochim. Cosmochim. Acta, 42: 1335-1340.

Eanes, E.D., Gilessen, I.H., and Posner, A.S., 1965. Intermediate states in the precipitation of hydroxyapatite. Nature, 208: 365-367.

Frèche, M. and Heughebaert, J.C., 1989. Calcium phosphate precipitation in the 60-80 °C range. J. Cryst. Growth, 94: 947-954.

Griffin, R.A. and Jurinak J.J., 1973. The interaction of phosphate with calcite. Soil Sci. Amer. Proc., 37: 847- 850.

Hietanen, S., Sillén, L.G. and Hegfeldt, E., 1975. Some phosphate equilibria. Chimica Scripta, 3, 65-72.

Holford, I.C.R. and Matingly, G.E.G., 1975. Phosphate sorption by Jurassic oolitic limestones. Geoderma, 13: 257-264.

House, W.A. and Donaldson, L., 1986. Adsorption and coprecipitation of phosphate on calcite. J. of Coll. Interf. Sci., 112: 309-324.

Ishikawa, M. and Ichikuni, M., 1981. Coprecipitation of phosphate with calcite. Geochemical Journal, 15: 283-288.

Lahann, R.W., 1978. A chemical model for calcite crystal growth and morphology control. J. Sed. Petrol., 48: 337-344.

Lorens, R.W., 1981. Sr, Cd, Mn and Co distribution coefficients in calcite as a function of calcite precipitation rate. Geochim. Cosmochim. Acta, 45:553-561.

Meyer, H.J., 1984. The influence of impurities on the growth rate of calcite. J. Cryst. Growth, 66: 639-646.

Middelburg, J.J. and Comans, R.N.J., 1991. Sorption of cadmium on hydroxyapatite. Chem. Geol., 90: 45-53.

Möller, P. and Sastri, C.S., 1974. Estimation of the number of surface layers of calcite involved in Ca-^{45}Ca isotopic exchange with solution. Z. Phys. Chem. N.F., 89: 80 - 87.

Morel, F.M.M., 1983. Principles of Aquatic Chemistry. Wiley, Chichester, 446 pp.

Morse, J.W. and Bender, M.L., 1990. Partition coefficients in calcite: examination of factors influencing the validity of experimental results and their application to natural systems. Chem. Geol., 82:265-277.

Mucci, A., 1986. Growth kinetics and composition of magnesian calcite overgrowths precipitated from seawater: Quantitative influence of orthophosphate ions. Geochim. Cosmochim. Acta, 50: 2255-2265.

Reddy, M.M., 1977. Crystallization of calcium carbonate in the presence of trace concentrations of phosphorus containing anions. I. Inhibition by phosphate and glycerophosphate ions at pH 8.8 and 25° C. J. Cryst. Growth, 41: 287 - 295.

Saager, P.M., 1994. On the relationships between dissolved trace metals and nutrients in seawater. Dissertation Free University of Amsterdam, 240 pp.

Saager, P.M. and De Baar, H.J.W., 1993. Limitations to the quantitative application of Cd as a paleoceanographic tracer, based on results of a multi-box model (MENU) and statistical considerations. Global and Planetary Change, 9: 69-92.

Sigg, L. and Stumm, W., 1991. Aquatische Chemie. Teubner Verlag, Stuttgart, Germany, 388 pp.

Sillèn, L.G. and Martell, A.E., 1971. Stability constants of metal ion complexes, suppl. no 1. The Chemical Society, London. 865 pp.

Stumm, W. and Leckie, J.O., 1970. Phosphate exchange with sediments: its role in the productivity of surface waters. In Advances in Water Pollution Research Vol. 2. III, Pergamon Press, 1-16.

Takano, B., 1985. Geochemical implications of sulfate in sedimentary carbonates. Chem.Geol., 49: 393-403.

Van Gaans, P.F.M., 1989. WATEQX-A restructured, generalized and extended FORTAN 77 computer code and database format for the WATEQ aqueous chemical model for element speciation and mineral saturation, for use on personal computers or mainframes, Computer and Geosciences, 15: 843-887.

Van der Weijden, R.D., Van der Weijden, C.H. and Comans, R.N.J., 1994. Sorption and sorption reversibility of Cd on calcite under simulated riverine, estuarine and marine conditions. Mar. Chem., 47: 65-79.

Zachara, J.W., Cowan, C.E. and Resch, C.T., 1991. Sorption of divalent metals on calcite. Geochim. Cosmochim. Acta, 55: 1549-1562.

Appendix 1

Aqueous speciation reactions and equilibrium constants

reaction					logK	source
CO_3^{2-}	$+$	H^+	$=$	HCO_3^-	10.33	1
CO_3^{2-}	$+$	$2H^+$	$=$	$H_2CO_3^{\,o}$	16.68	1
PO_4^{3-}	$+$	H^+	$=$	HPO_4^{2-}	12.35	1
PO_4^{3-}	$+$	$2H^+$	$=$	$H_2PO_4^-$	19.55	1
PO_4^{3-}	$+$	$3H^+$	$=$	H_3PO_4	21.70	1
SO_4^{2-}	$+$	H^+	$=$	HSO_4^-	1.99	1
Ca^{2+}	$+$	OH^-	$=$	$CaOH^+$	1.4	1
Ca^{2+}	$+$	CO_3^{2-}	$=$	$CaCO_3^{\,o}$	3.15	1
Ca^{2+}	$+$	$H^+ + CO_3^{2-}$	$=$	$CaHCO_3^+$	11.46	3
Ca^{2+}	$+$	PO_4^{3-}	$=$	$CaPO_4^-$	6.5	1
Ca^{2+}	$+$	$H^+ + PO_4^{3-}$	$=$	$CaHPO4^{\,o}$	15.1	1
Ca^{2+}	$+$	$2H^+ + PO_4^{3-}$	$=$	$CaH_2PO_4^+$	21.0	1
Ca^{2+}	$+$	SO_4^{2-}	$=$	$CaSO4^{\,o}$	2.31	1
Na^+	$+$	CO_3^{2-}	$=$	$NaCO_3^-$	1.27	1
Na^+	$+$	$H^+ + CO_3^{2-}$	$=$	$NaHCO_3^{\,o}$	10.08	1
Na^+	$+$	$H^+ + PO_4^{3-}$	$=$	$NaHPO_4^-$	12.64	1
Na^+	$+$	SO_4^{2-}	$=$	$NaSO_4^-$	0.70	1
Cd^{2+}	$+$	OH^-	$=$	$CdOH^+$	3.90	1
Cd^{2+}	$+$	$2OH^-$	$=$	$Cd(OH)_2^{\,o}$	7.60	1
Cd^{2+}	$+$	NO_3^-	$=$	$CdNO_3^+$	0.40	1
Cd^{2+}	$+$	SO_4^{2-}	$=$	$CdSO_4^{\,o}$	2.47	1
Cd^{2+}	$+$	$2SO_4^{2-}$	$=$	$Cd(SO_4)_2^{2-}$	0.50	1
Cd^{2+}	$+$	CO_3^{2-}	$=$	$CdCO_3^{\,o}$	4.00	3
Cd^{2+}	$+$	$H^+ + CO_3^{2-}$	$=$	$CdHCO_3^+$	12.30	2
Cd^{2+}	$+$	$3CO_3^{2-}$	$=$	$Cd(CO_3)_3^{4-}$	6.24	4
Cd^{2+}	$+$	$H^+ + PO_4^{3-}$	$=$	$CdHPO_4^{\,o}$	15.03	7
Cd^{2+}	$+$	$2H^+ + PO_4^{3-}$	$=$	CdH_2PO_4+	19.40	7
Ca^{2+}	$+$	CO_3^{2-}	$=$	$CaCO_3(s)$	8.43	5
Cd^{2+}	$+$	CO_3^{2-}	$=$	$CdCO_3(s)$	12.10	2
$5Ca^{2+}$	$+$	$PO_4^{3-} + OH^-$	$=$	$Ca_5(PO_4)_3OH(s)$	55.60	1
$4Ca^{2+}$	$+$	$H^+ + 3PO_4^{3-} + 3H_2O$	$=$	$Ca_4H(PO_4)_3 \cdot 3H_2O(s)$	49.60	6
Ca^{2+}	$+$	$HPO_4^{2-} + 2H_2O$	$=$	$CaHPO_4 \cdot 2H_2O(s)$	6.69	6

Sources:
1) Morel (1983)
2) Zachara et al. (1991)
3) Davies et al. (1987)
4) Sillén and Martell (1971)
5) Sigg and Stumm (1991)
6) Frèche and Heughehaert (1989)
7) Hietanen et al. (1975)

Chapter 3

The seeded-precipitation of calcite in solutions composed
of various $[Ca]_T$ and $[C]_T$ in a chemo-stat system

Abstract— The growth of calcite was studied with a chemo-stat system, in which total carbonate, total calcium and PCO_2 were systematically varied. Results confirmed that calcite grows via a spiral growth mechanism, which is controlled by surface reactions. The linear growth rate was practically constant up to an outgrowth of 3, indicating size-independent growth. The linear growth rate increased with increasing supersaturation ($[Ca]_T$) and with increasing total carbonate at a constant supersaturation. The latter can be understood if a contribution of bicarbonate to crystal growth is taken into account. Macrosteps formed during growth, as observed with SEM and AFM, indicated the presence of impurities. Investigation of the influence of the most likely contaminants (Zn and PO_4) revealed that an effect on the growth rates in our system can be excluded.

3.1. Introduction

The crystal growth of calcite has been studied extensively. Calcite is an important (by)product in the industry and 7% of the surface of the earth is composed of $CaCO_3$. Investigation of the parameters which influence growth, composition and morphology, can give insight into the formation conditions and the formation rates of (naturally occurring) calcite. Furthermore, incorporation in, solid solution formation with, and adsorption on calcite, influence the mobility and the concentration in solution of trace elements.

Many papers have contributed to the understanding of calcite growth (e.g. Reddy and Nancollas, 1971; Nancollas and Reddy, 1971; Folk, 1978; Lahann, 1978; Christoffersen and Christoffersen, 1990), dissolution (e.g. Plummer et al., 1978/1979; Reddy et al., 1981; Busenberg and Plummer, 1986; Mucci et al., 1989; MacInnis and Brantley, 1992), the effect of additives on growth rates (e.g. Reddy and Nancollas, 1976; Reddy, 1977; Reddy and Wang, 1980; Giannimaras and Koutsoukos, 1987; Xyla et al., 1991), the effect of the seed size on growth rates (e.g. Tai et al., 1993), and the effect of the seed mass/solution ratio on growth (De Boer, 1977; Reddy and Gaillard, 1981). The general findings are that calcite growth can be explained by a spiral growth mechanism, in which the rate controlling step is a combination of surface reactions. The rate of crystal growth depends on the density of kink sites (or steps), which is a function of the supersaturation, and on the step velocity, which depends on the flux and the effectiveness of the molecular jump of ions into kink sites (Christoffersen and Christoffersen, 1990). The crystal growth rate in turn, influences the partitioning of foreign elements with calcite.

Though many of the questions concerning the growth of calcite have been answered, some phenomena have not been addressed. For instance, in growth experiments no rate dependence on total concentrations and pH has been observed (Christoffersen and Christofferson, 1990), although Sigg and Stumm (1990) did indicate that such a dependence can exist. Furthermore, in Ostwald ripening experiments, the ripening rate appears to increase with total concentrations of carbonate and calcium (Zachara et al., 1991; Van der Weijden et al., 1994). Therefore, calcite growth experiments were carried out to further investigate the (in)dependence on total concentrations. While in most other studies the growth rate was varied by changing the amount of total carbonate or the amount of seeds, in this study the total calcium concentration $[Ca]_T$ was varied systematically at a constant total carbonate concentration $[C]_T$. Furthermore, since the electrolyte solution contained about 4.6×10^{-8}M Zn and since phosphate in small concentrations can affect carbonate crystal growth, a possible effect of Zn or phosphate in the experiments was investigated. The appearance of the crystals at different stages of outgrowth after addition of Zn or phosphate was checked by means of SEM and AFM.

3.2. Materials and Methods

3.2.1. Materials

Solutions were prepared from reagent grade chemicals KCl, $CaCl_2.2H_2O$ (Merck), K_2CO_3, $KHCO_3$, KH_2PO_4 (Baker) and doubly distilled (IKADEST) water containing 4.6×10^{-8} M Zn. In some experiments, small amounts of phosphate and zinc were added as a solution of 0.001M KH_2PO_4 in 0.7 M KCl and a Zn-standard solution (Merck) respectively. Suprapure calcite (Merck) served as seeds with grain sizes of 10-100 μm of intergrown rhombohedrons
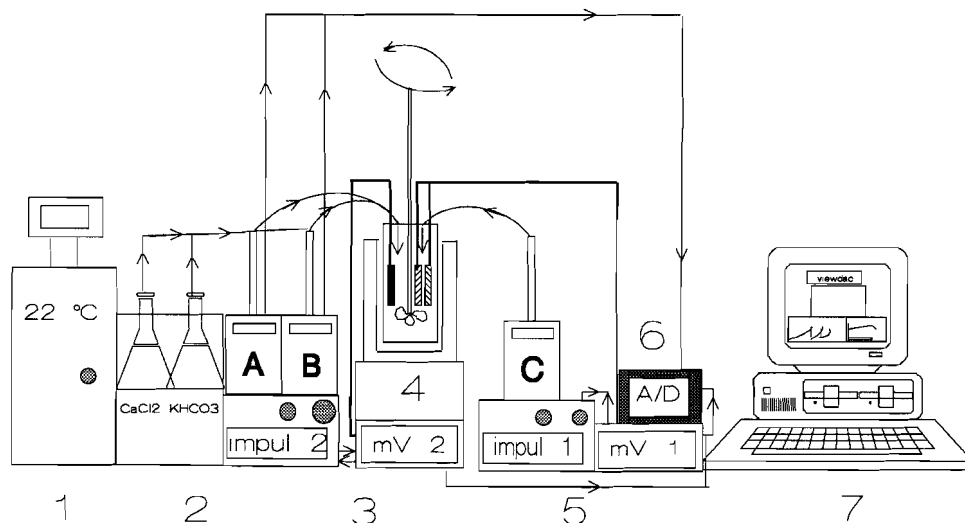
Fig. 1 A chemo-stat system.
1 = thermostat, 2 = thermostated bath with storage vessels for reactants, 3 = Ca (mV) signal, connected to an impulsomat which activates burettes A and B filled with reactants, 4 = thermostated teflon reactor vessel with 4-bladed teflon stirrer, Ca, pH, and calomel electrodes, 5 = pH (mV) signal, connected to an impulsomat, which sends pulses to burette C, whenever the pH signal drops below a setpoint value, 6 = A/D converter receiving mV values from mV meters and volume values from burettes A and B, 7 = Viewdac software package "Keithley Assist" was used for data recording and analysis.

and a specific surface area of 0.29 m^2/gram as determined with a micromeritics type PulseChemiSorb 2700. Gases (Airproducts) contained 1.5 and 5 mol% CO_2 in nitrogen. In Fig. 1 a schematic presentation of the chemo-stat system is shown. As these experiments were also used to investigate Cd incorporation during growth (see chapter 4), the 1 l reaction vessel, the four-bladed stirrer, a home-made copy of a type 665 Metrohm buret setup and the buret supply vessels were all made of teflon (PFA) to minimize Cd sorption onto container walls. Other supply vessels and buret setups used for storage of solutions were made out of glass. Solutions were kept at a constant temperature of 22.0 ± 0.1°C, by pumping water through a double walled glass mantle surrounding the reactor vessel, with a Braun thermomix bath/pump.

The composition of the supersaturated solution in the reactor vessel was measured with several electrodes. The Ca^{2+} activity was measured with a Ca-membrane electrode (Radiometer). The H^+ activity was measured with a combination of a glass and calomel electrode (both Radiometer), with microtips of 2.5 mm to minimize Zn (or Cd) adsorption. The signals of all electrodes and of burettes A and B were fed to a Keithley 575 measurement and control system.

3.2.2. Chemo-stat system

Calculations for the preparation of supersaturated solutions were made with the chemical speciation programmes MINTEQA2 and WATEQX, using Pitzer equations. Formation constants of the aqueous components are given in Apx.1. A background electrolyte of 0.7 M KCl was chosen based on the ionic strength of seawater and to keep the ion activity

products of Cd^{2+} or Zn^{2+} with CO_3^{2-} below K_{sp}(otavite) and K_{sp}(smithsonite). KCl rather than NaCl was chosen, because K^+ is not incorporated into the calcite lattice as easily as Na^+ (White, 1977; Ishiwaka and Ichikuni, 1984), and because the Ca-membrane electrode is more sensitive to the presence of Na^+ ions. Since precipitation of calcite was studied with a chemo-stat technique (constant K^+, Cl^-, Ca^{2+} and CO_3^{2-} concentrations), the solutions in the burettes (A, B, and C, Fig. 1) produced the exact composition of the precipitating solution plus an excess in calcium and carbonate to compensate for calcite growth. Zn and phosphate concentrations in the burettes were chosen, as to prevent dilution.

Prior to each experiment, the solutions for the reactor vessel and the burettes were filtered through a 0.22 μm micropore filter. The pH electrodes were calibrated with Ingold standardized buffers of pH = 7.00 and 9.21. The supersaturated solution (500 ml) was transferred to the reaction vessel and equilibrated by bubbling with a H_2O saturated CO_2/N_2 stream (200 ml/min) under continuous stirring (530 rpm) for 2-3 hours, until the signals of the electrodes stabilized. The pH was set to the desired value with a 0.3 M K_2CO_3/0.7 M KCl solution (burette C, Fig. 1). After stabilization, a 50 ml subsample was withdrawn with a syringe and stored in a teflon vessel for further analysis.

Precipitation was started by adding a certain mass of a calcite seed suspension to the solution in the reactor vessel with a pycnometer (Witkamp, 1989). During precipitation, pH, $[Ca]_T$ and $[C]_T$ all decreased, resulting in a change in the mV signals of the electrodes. Impulsomat 1 (Metrohm) then triggered burettes A and B to add equal volumes of burette solutions to the reactor vessel. Burette A contained a solution of $CaCl_2$ in 0.7 M KCl and burette B contained a solution of $KHCO_3/K_2CO_3$ in 0.7 M KCl. In experiments where the influence of additives on the growth of calcite was studied, phosphate and Zn were added to the $CaCl_2$ solution in burette A. The pH was kept constant within 0.005 pH-unit by correction with the solution in burette C. Since the Ca- signal reacted to a change in pH-signal while $[Ca]_T$ was constant, the maintenance of a constant pH was essential in this experimental setup. During the experimental run, subsamples (5 ml) were withdrawn and filtered through a 0.22 μm membrane filter. After a certain outgrowth, the supersaturated solution was filtered through a 0.22 μm membrane filter to obtain a final sample and the calcite precipitate. During filtration, the same CO_2/N_2 mixture as applied during precipitation was bubbled through the solution. All subsamples and the filtered end-solution were stored in teflon vessels for determination of $[Ca]_T$ by EDTA titration and $[C]_T$ by Gran potentiometric titration. Analysis by means of ICP for some samples, produced Ca values within 5% of the values found by titration. The precipitate on the filter was washed three times with a $CaCO_3$ saturated 0.7M KCl solution and subsequently with a $CaCO_3$ saturated solution. The filter was oven-dried at 35 °C and the precipitate was checked with XRD, to confirm crystallization of calcite.The appearance of the crystals was investigated by means of SEM and AFM (Topometrix-2000).

Zn was measured with GFAAS. Determination of Zn was complicated, as the sensitivity for contamination was extremely high. Preparation of the samples in a clean-lab, and measurement in a clean-room was necessary. We found the following conditions best for measuring Zn: samples were acidified with suprapure HCl, diluted ten times to yield a 0.07M KCl matrix (30 μl), modified with 0.1% $NH_4.H_2PO_4$ (5 μl), and measured at incineration and atomization temperatures of 720 °C and 1700 °C, respectively.
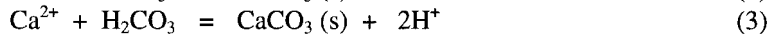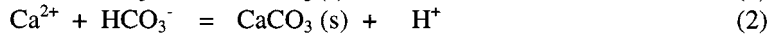
3.2.3. ^{45}Ca isotopic exchange

Electrolyte solutions for studying ^{45}Ca exchange at various pH values were prepared from reagent grade chemicals $NaNO_3$ and Na_2CO_3 and suprapure chemicals HCl and $CaCO_3$

(Merck). Duplicate samples were prepared by equilibrating 60 ml solution with 2.1 gram calcite in a 100 ml teflon (PFA) vessel for > 48 hours in a shakerbath at 25 °C. After centrifugation for 20 minutes at 20215 *g*, 1 ml of the supernatant and 9 ml Instagel scintillation fluid were transferred to polythene scintillation vials. The vials were counted on a Philips β-scintillation counter. The Ostwald ripening rate (nmol Ca/(g×hour)) was calculated by least square analysis for times > 125 hours.

3.3. Data Analysis

Calcite precipitation can result from (a combination of) the following reactions:

$$Ca^{2+} + CO_3^{2-} = CaCO_3(s) \qquad\qquad (1)$$
$$Ca^{2+} + HCO_3^- = CaCO_3(s) + H^+ \qquad\qquad (2)$$
$$Ca^{2+} + H_2CO_3 = CaCO_3(s) + 2H^+ \qquad\qquad (3)$$

The amount of calcite (M_t) at time = *t* during an experimental run follows from:

$$M_t = M_o + [V_{burette} \times ((Ca_{burette}/2) - Ca_{reactor})] \times M_{calcite} \text{ (g)} \qquad (4)$$

where M_o is the mass of the seed crystals, $V_{burette}$ denotes the volume added by the burette containing $CaCl_2$ at time = *t*, $Ca_{burette}$ denotes the calcium concentration in the burette, $Ca_{reactor}$ denotes the concentration of calcium in the supersaturated solution, and $M_{calcite}$ is the molecular weight of calcite. The outgrowth factor is defined as:

$$outgrowth\ factor = (M_t/M_o) \qquad\qquad (5)$$

The supersaturation, σ, is defined as:

$$\sigma = (IAP/K_{sp})^{1/2} - 1 \qquad\qquad (6)$$

where *IAP* is the ion activity product and K_{sp} the thermodynamic solubility product. The overall growth rate during an experiment, without correction for the increase in surface areas is given as:

$$R = d(M_t/M_o)/dt \sim (M_t/M_o)^\alpha \qquad (s^{-1}) \qquad\qquad (7)$$

In a plot of log *R* versus log (M_t/M_o), the slope of the curve, α, is indicative for the number of directions in which the crystals grow. For needle growth $\alpha = 0$, for platelets $\alpha = 0.5$ and if $\alpha = 2/3$, the original geometry is retained. The linear growth rate, *Rlin*, is calculated based on the addition rate and the measured initial surface area of 0.29 m²/gram:

$$Rlin = \frac{dL}{dt} = \frac{dV_c}{dt} \frac{1}{3(NV_c^2)^{1/3}} \qquad (m\ s^{-1}) \qquad\qquad (8)$$

where *N* is the number of particles based on an estimated (SEM) mean rib length (8 μm) of the seed crystals and L and V_c are the mean rib length and the volume of the calcite crystals at time = *t*, respectively. The linear growth rate can also be expressed as:

$$Rlin = k\sigma^n \qquad (\text{m s}^{-1}) \tag{9}$$

where k is the growth rate constant and n the reaction order. For bulk diffusion controlled crystallization n equals 1, for combined mechanisms such as adsorption and surface diffusion, volume diffusion and integration etc. $1 < n < 2$, for spiral growth n equals 2, for polynuclear growth (in combination with spiral growth) $n > 2$ (Zhang and Nancollas, 1990).

3.4. Results and discussion

In Table 1 the conditions for growth for all experiments are summarized. In these experiments, activities of Ca^{2+} and CO_3^{2-} were of the same order of magnitude. Bubbling with air combined with stirring did not have any effect on the growth rate of calcite as compared to stirring only (530 rpm) at pH = 8.9. Therefore a contribution of heterogeneous precipitation on bubbles can be excluded. Experiments in which the effect of ripening of the seeds was studied, showed that there was no difference between the growth rates for seeds that had ripened for 24 hours or for two months. Furthermore, the use of ultrapure water instead of IKADEST water did not result in a different growth rate.

3.4.1. Habit and outgrowth

The supersaturations at which calcite growth was studied varied from $\sigma = 0.3$ to 2.3. Below $\sigma = 0.3$ no growth was observed. This effect is common whenever the growth of crystals is stopped and subsequently resumed, and most likely results from the contamination of spiral centers (Jetten et al., 1983). Above $\sigma = 2.3$ the maximum addition rate of the burettes was too low to maintain a constant supersaturation.

In most experiments an initial growth surge was observed (Fig. 2). The surge can result from the healing of e.g. the rounded corners of the seed crystals and the disappearance of {111} forms present on the seeds, as observed by means of SEM (Fig. 3a,b). The surge, up to stages of outgrowth of $(M_t/M_o) - 1 = 0.08$ at lower σ, was camouflaged at higher supersaturations ($\sigma > 2$), because of the relatively high growth rates. After the surge, growth proceeds in three dimensions, retaining the geometry of the crystals, which is concluded from a value of 0.7 for α at both low and high σ, in a log R versus M_t/M_o plot (Fig. 4). This is also confirmed by SEM photographs (Fig. 5a,b), which show that the rhombohedral faces at the different outgrowth stages are preserved. At outgrowths up to 1.7, macrosteps with a mean width of 180 nm (AFM) have developed near the ribs and corners of the rhombohedrons, at all supersaturations. The bunching of monolayer steps results from sorption of contaminants at growth sites and is a very common feature regarding calcite growth (Reddy and Wang, 1980; Woensdregt, personal communication). Near the corners of the rhombohedrons the effect is more pronounced as compared to the ribs, because at corners steps converge and the contaminant is thus accumulated. At a higher outgrowth of $M_t/M_o = 3 - 4$, the major part of the contaminant(s) may have been built into the crystal lattice, since the ribs and corners of the rhombohedrons have healed. Still, macrosteps with a mean width of 600 nm and a mean height of 400 nm could be observed with AFM, suggesting that the influence of the contaminants is still present.

Table 1. Total calcium and carbonate concentrations ([Ca]$_T$, [C]$_T$), free aqueous activities, volume in the reactor and duration of the experiment A: $PCO_2 = 10^{-3.5}$ atm, burette concentrations were 0.04 M $CaCl_2$ and 0.04 M $KHCO_3/K_2CO_3$. B: $PCO_2 = 10^{-3.5}$ atm, burette concentrations were 0.01 M $CaCl_2$ and 0.015 M $KHCO_3/K_2CO_3$. C: $PCO_2 = 0.015$ atm. burette concentrations were 0.01 M $CaCl_2$ l and 0.083 M $KHCO_3/K_2CO_3$. E: $PCO_2 = 0.015$ atm, burette concentrations were 0.004 M $CaCl_2$ and 0.083 M $KHCO_3/K_2CO_3$. F: $PCO_2 = 0.05$ atm, burette concentrations were 0.004 M $CaCl_2$ and 0.12 M $KHCO_3/K_2CO_3$.

pH	Ca_T $(10^{-4}M)$	C_T $(10^{-3}M)$	Ca^{2+} $(10^{-4}M)$	CO_3^{2-} $(10^{-4}M)$	Vend (ml)	time (min)	seeds (mg/l)	σ $(10^{-10}ms^{-1})$	Rlin
A									
8.925	6.18	8.3	1.50	1.59	1000	392	351	1.52	2.79
8.923	6.80	8.3	1.66	1.58	860	289	379	1.65	2.26
8.839	3.89	7.4	0.97	1.20	N.D.	1125	478	0.77	0.70
8.829	4.25	7.5	1.06	1.19	765	788	584	0.84	0.93
8.798	3.26	6.8	0.82	1.07	866	2062	517	0.53	0.37
8.789	3.00	6.8	0.99	0.76	774	2666	361	0.42	0.24
8.878	4.10	8.2	1.07	1.43	950	598	494	0.96	1.15
8.870	5.60	8.2	1.38	1.40	740	303	479	1.27	2.14
8.780	2.51	6.8	0.63	0.97	718	6816	281	0.28	0.39
8.847	4.72	8.1	1.16	1.33	834	755	267	1.03	1.61
8.890	5.56	8.1	1.36	1.45	927	535	186	1.31	1.83
8.780	3.10	6.8	0.78	0.97	N.D.	3526	261	0.43	0.19
B									
8.898	4.50	7.3	1.11	1.30	995	1471	172	0.92	1.16
8.898	5.22	7.7	1.28	1.39	N.D.	563	205	1.20	1.32
8.896	3.60	6.9	0.89	1.24	849	1678	173	0.77	0.40
8.899	6.80	7.3	1.67	1.31	989	407	183	1.46	1.90
C									
7.976	6.00	39	1.42	0.98	806	106	155	0.94	2.25
7.965	7.80	37.4	1.87	0.91	784	61	163	1.14	4.40
D									
8.898	3.63	6.8	0.91	1.24	750	705	172.0	0.74	0.43
8.893	5.95	7.3	1.48	1.31	756	136	174.5	1.29	1.74
8.898	6.42	7.6	1.59	1.37	791	116	183.3	1.44	2.12
8.893	4.56	6.4	1.14	1.15	774	443	187.2	0.89	0.62
8.898	3.48	6.4	0.87	1.16	714	667	158.2	0.66	0.39
8.898	6.48	7.8	1.62	1.41	759	125	172.0	1.50	1.80
8.898	5.77	7.7	1.43	1.40	748	195	155.6	1.33	1.34
8.892	5.19	7.7	1.28	1.38	798	179	202.6	1.19	1.73
8.890	10.6	6.8	2.65	1.20	749	38	159.1	1.94	6.81
8.898	12.2	7.1	3.03	1.28	756	29	149.6	2.24	7.49
8.898	11.7	6.9	2.91	1.25	820	44	147.8	2.14	6.57
8.898	12.2	6.6	3.05	1.19	821	33	161.9	2.14	8.58
8.898	11.7	6.6	2.93	1.18	795	35	154.5	2.67	7.47
8.900	5.90	8.0	1.45	1.46	760	94	166.8	1.38	2.70
8.897	3.90	7.1	0.97	1.28	748	403	172.4	0.84	0.85
8.900	11.8	6.6	2.95	1.20	790	30	154.0	2.10	8.86
8.893	10.0	6.6	2.49	1.18	750	39	142.5	1.83	5.31
8.900	9.80	6.5	2.43	1.18	750	60	145.3	1.79	4.08
8.900	9.80	6.8	2.44	1.17	750	53	162.2	1.84	4.65
8.898	3.70	6.8	0.92	1.23	725	515	149.9	0.75	0.62
8.897	3.90	6.4	0.97	1.14	734	627	175.4	0.3	0.52
8.898	8.78	6.5	2.18	1.16	776	84	171.4	1.67	3.47
8.898	11.7	7.3	2.88	1.30	823	35	162.9	2.20	7.24
8.899	6.01	7.1	1.34	1.26	738	288	152.5	1.14	1.33

pH	Ca_T $(10^{-4}M)$	C_T $(10^{-3}M)$	Ca^{2+} $(10^{-4}M)$	CO_3^{2-} $(10^{-4}M)$	Vend (ml)	time (min)	seeds (mg/l)	σ $(10^{-10}ms^{-1})$	Rlin
8.895	5.80	7.6	1.43	1.16	750	162	165.6	1.30	2.07
8.902	9.73	7.5	2.39	1.36	796	46	167.8	1.98	6.11
8.900	5.85	6.7	1.45	1.21	742	145	161.9	1.19	1.76
8.898	5.04	7.1	1.25	1.28	706	175	170.7	1.08	1.44
8.898	5.53	6.9	1.37	1.14	748	127	168.2	1.15	2.28
E									
7.965	6.18	39	1.47	0.95	792	131	177.7	0.97	2.11
7.975	5.80	41	1.38	1.02	806	106	155.2	0.96	2.47
7.985	5.75	40	1.37	1.01	773	144	166.4	0.95	1.63
7.970	8.48	40	2.11	0.97	780	63	159.4	1.37	3.86
7.985	7.72	41	1.83	1.03	766	75	178.7	1.28	2.98
8.059	6.49	44	1.48	1.33	750	68	153.3	1.33	3.84
8.055	8.13	43	1.88	1.28	762	44	162.6	1.56	5.06
8.049	8.09	43	1.87	1.26	762	45	148.2	1.55	5.73
8.051	2.73	45	0.63	1.33	802	1339	153.4	0.51	0.40
F									
7.555	9.70	50	2.34	0.47	769	29	164.3	0.74	1.75
7.555	9.10	49	2.17	0.46	770	267	163.6	0.64	1.12
7.565	11.0	50	2.69	0.48	768	78	164.3	0.90	2.73
7.657	8.02	60	1.87	0.72	801	89	175.5	0.93	2.72
7.649	6.00	60	1.40	0.71	770	212	177.6	0.65	0.99
7.653	4.94	57	1.16	0.68	744	729	162.6	0.47	0.50
7.650	8.48	64	1.97	0.76	790	66	180.1	1.01	3.23
7.654	8.09	59	1.89	0.71	774	100	151.0	0.91	2.45
7.650	5.52	61	1.48	0.68	750	244	162.2	0.60	0.96
7.660	10.8	60	2.53	0.71	816	30	175.6	1.21	7.00
7.655	5.10	59	1.19	0.70	850	652	174.5	0.51	0.78
7.653	5.48	60	1.27	0.71	751	327	162.9	0.55	0.75
7.657	9.88	61	2.30	0.72	750	52	169.2	1.12	4.08
7.656	6.10	60	1.41	0.72	750	268	165.4	0.67	0.88
7.672	5.85	63	1.29	0.78	754	280	151.0	0.66	0.90
7.666	4.80	64	1.10	0.78	710	630	159.4	0.53	0.60
7.672	10.05	64	2.30	0.78	769	61	155.2	1.19	4.01
7.673	6.44	68	1.48	0.83	776	197	175.2	0.79	1.36
7.670	5.72	68	1.31	0.83	748	352	166.7	0.71	0.86

3.4.2. Growth rate and outgrowth

In Fig. 6 the overall growth rate is plotted versus the supersaturation at pH = 8.9 (data in Table 1 A-B). In these experiments the different supersaturations were created by varying $[Ca]_T$, while maintaining a constant $[C]_T$ and pH. R increases with σ, which almost completely results from an increase in surface area, which can be concluded from a plot of *Rlin* versus σ (Fig. 7). Size-dependent growth as seen in other studies (Tai et al., 1993), is therefore not supported by the results in this study.
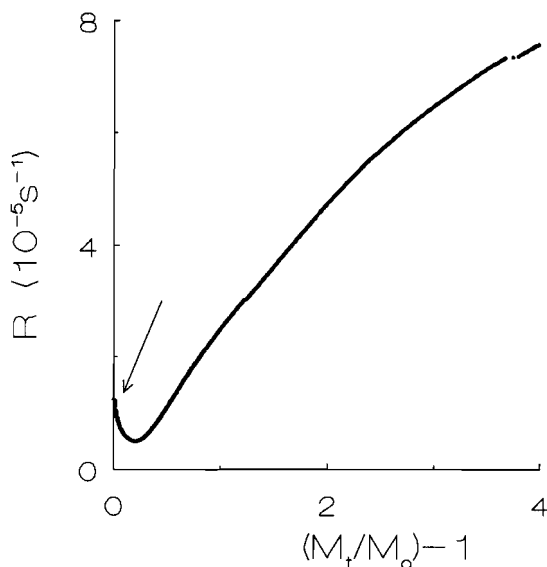
Fig. 2 Initial surge (at arrow) during the first stages of outgrowth for $\sigma = 0.42$.

From Fig. 7 a value for the reaction rate constant, k, of 1.1×10^{-10} ms^{-1} can be derived, which agrees with values of 2 to 20×10^{-10} ms^{-1} reported in other studies (Christoffersen and Christoffersen, 1990; Tai et al., 1993; Nielsen and Toft, 1984). A reaction order of 1.7-2 can be estimated from the slope of the curves. This indicates a spiral growth mechanism, where the rate is controlled by surface reactions. When the growth rate is expressed in terms of these processes (e.g. dehydration, adsorption) another equation for $Rlin$ is obtained (Christoffersen and Christoffersen, 1990). Here a plot of log $Rlin$ versus log $(S-1)\ln(S)S^{\frac{1}{2}}$, where $S = (\sigma + 1)$, should yield a curve with a slope of 1. Such a plot for the data in Fig. 7, produces a slope of 0.9, indeed suggesting a surface integration controlled growth (Fig. 8). Of these surface processes, surface diffusion over great distances is believed to be unimportant in controlling the growth rate, because during calcite crystal growth an absence of step- step interaction was observed (Gratz et al., 1993).

3.4.3. Total concentrations and growth rate

In Fig. 9 $Rlin$ versus σ is plotted for pH = 8.9, 8.0 and 7.6 (data in Table B-F). In all these experiments calcite was grown in the presence of 70 ppb Cd, as these same experiments were also used to study Cd incorporation (chapter 4). Cd did not affect the reaction rate and mechanism, because the data in Table B and C plot within the error range in Fig 9. This is not surprising, because the ionic radii of Ca and Cd are very similar. The same observation for the growth of gypsum in the presence of Cd has been made (Witkamp, 1989).
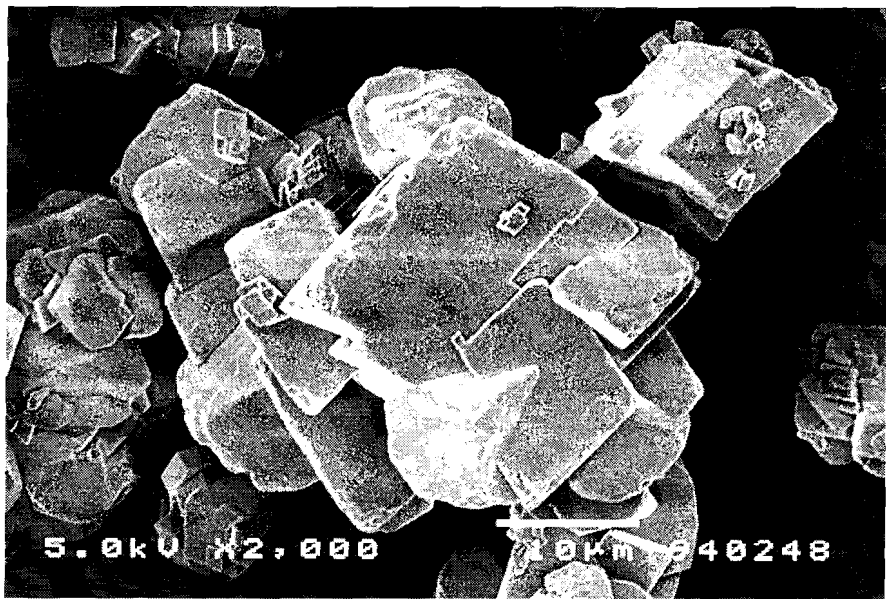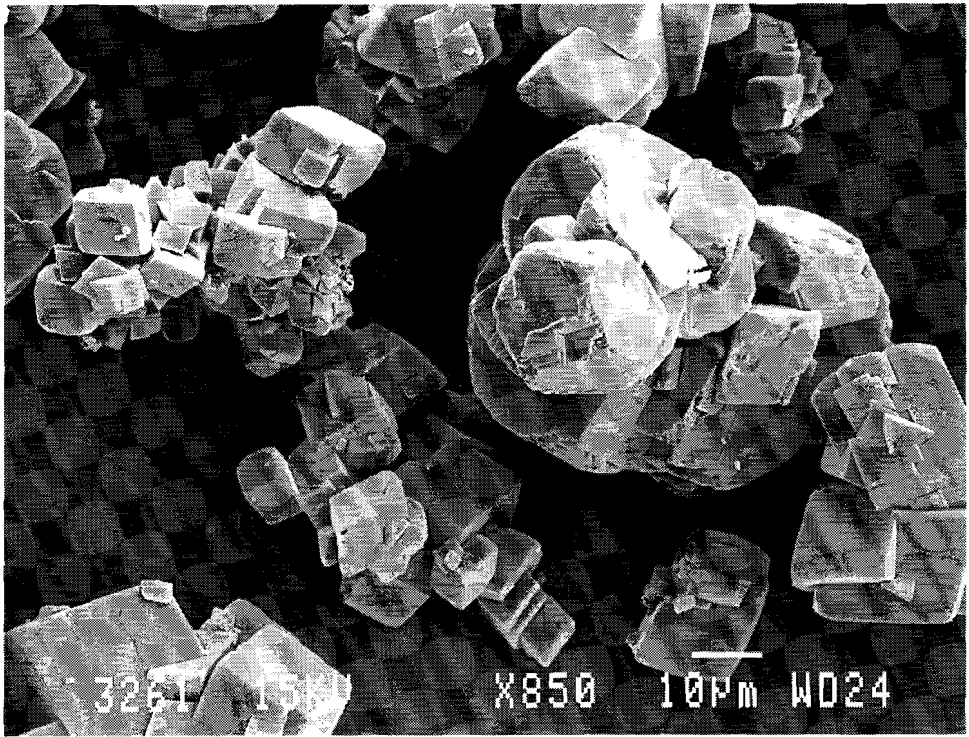
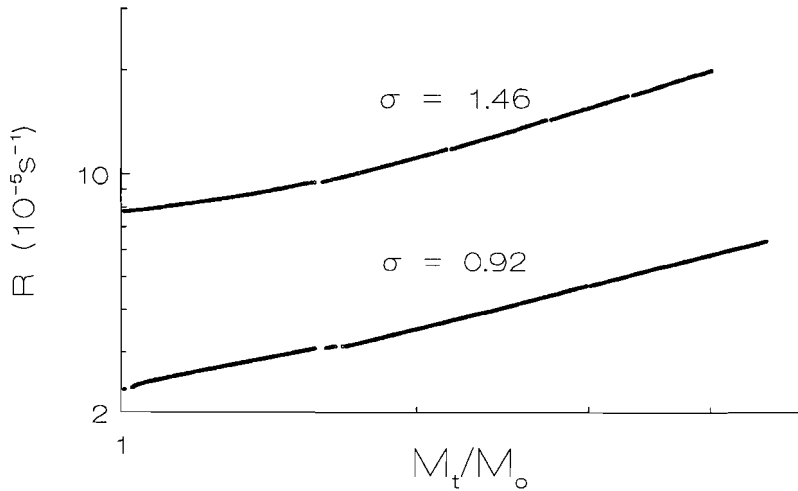Fig. 3 SEM photograph of dry suprapure calcite (a) and after two months ripening (b).

Fig. 4 Overall growth rate versus outgrowth (log scales), slope $\alpha \approx 0.7$.

Rlin increases at equal σ in a vertical direction with higher $[C]_T$ and lower pH. This can be understood if the reaction with bicarbonate (eq 2) also contributes to calcite growth, since the activity of carbonate does not change significantly. The reaction rate constant with bicarbonate is probably small compared to the rate constant for the reaction with carbonate, but at high concentrations, the contribution of bicarbonate to growth may become considerable. Therefore, the total concentration of carbonate, and not merely the free activity of carbonate, seems to affect the crystal growth rate.

A similar observation is made for Ostwald ripening of calcite, where the ripening rate is also influenced by species of calcium and carbonate other than their free ions. Table 2 demonstrates that the ripening rate is minimal at pH = 8.4, where the sum of $[Ca]_T$ and $[C]_T$ is lowest. Considering that growth proceeds via adsorption, HCO_3^- can be regarded as an additional sorbing species of which the sorption constant is small as compared to carbonate. Christoffersen and Christoffersen (1990) reported that calcite growth is independent of pH and total concentrations of calcium or carbonate and only depends on the free activities of Ca^{2+} and CO_3^{2-}. However, the ratio $[HCO_3^-]/[CO_3^{2-}]$ in their experiments did not exceed a value of 48, whereas in our experiments the ratio increased from 27 to 488 at pH values of 8.9 and 7.6 respectively. In addition, the low pH of 7.6 and 8.0 in our study as compared to the pH range of 8.5 to 10.0 in their study, may have resulted in positive surface charges, facilitating the sorption of carbonate species. Since *Rlin* depends on step velocity, density and height, HCO_3^- probably causes an increase in *Rlin* by accelerating the step velocity as fluxes increase.
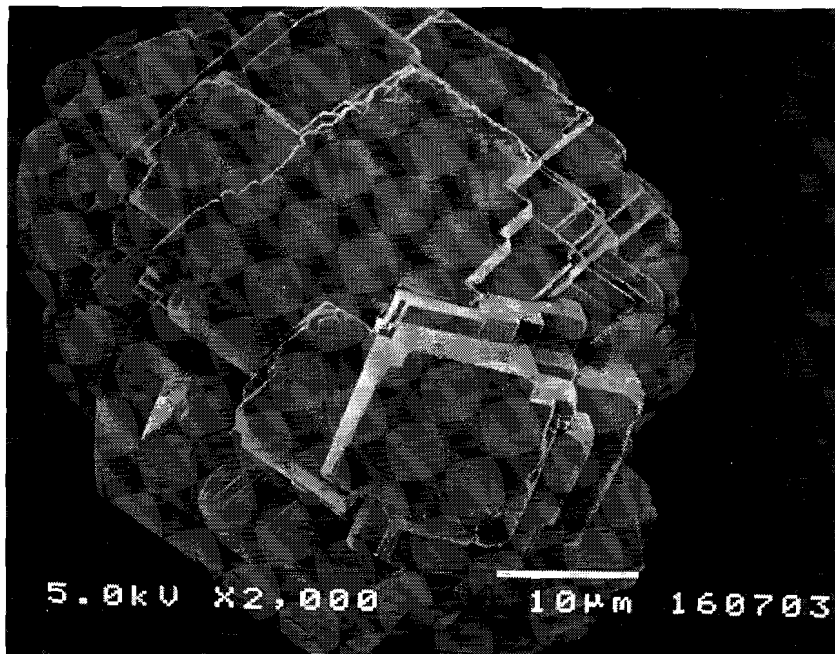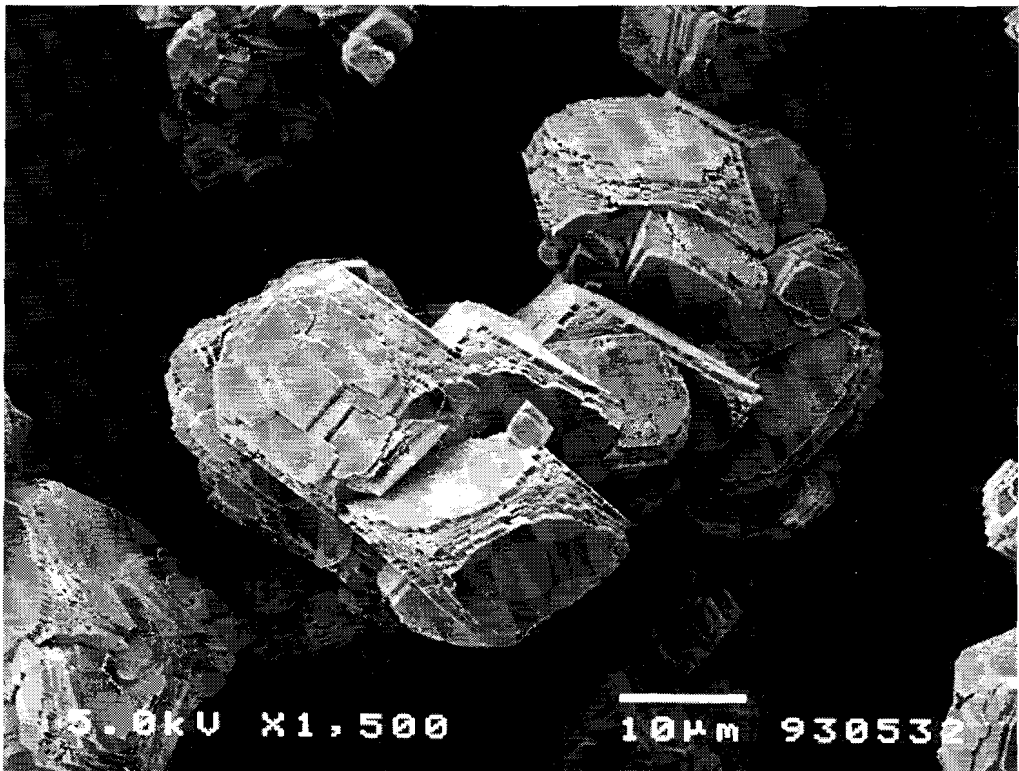
Fig. 5 SEM photographs of calcite crystals at outgrowth stages of 1.7 (a) and 4 (b).
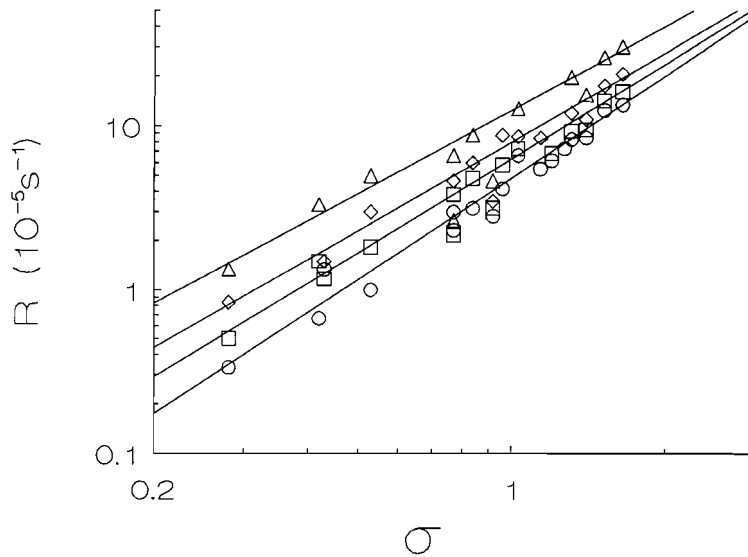
Fig. 6 Overall growth rate versus supersaturation for various stages of outgrowth.
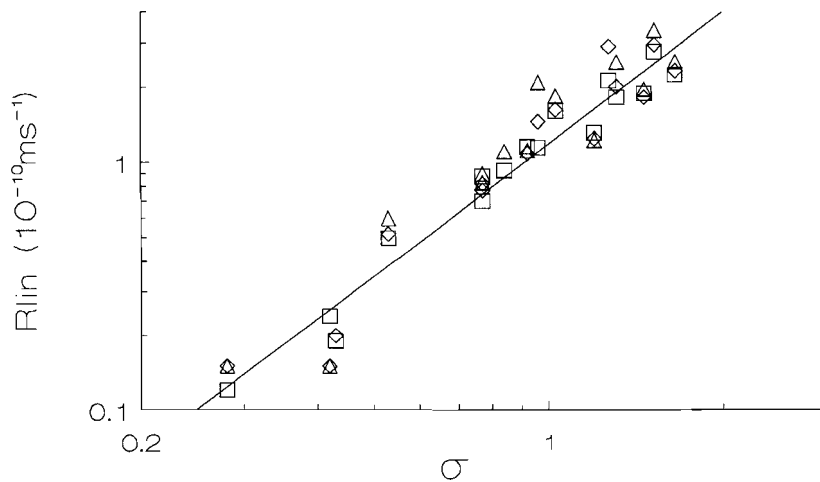O, □ ,◊,Δ: outgrowth = 0.3, 0.6, 1 and 2 resp. for the data in Table 1A- B.

Fig. 7 Linear growth rates versus supersaturation at various stages of outgrowth.
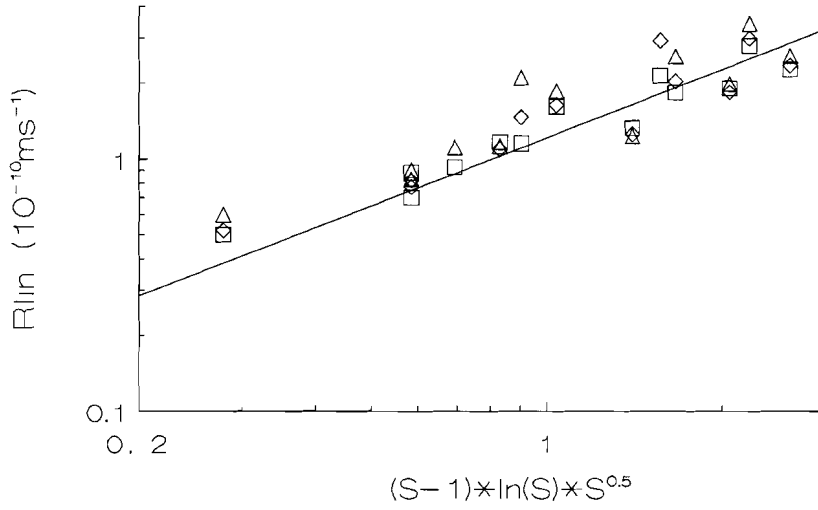□ ,◊,Δ: outgrowth = 0.6, 1 and 2 resp. for the data in Table 1A-B.

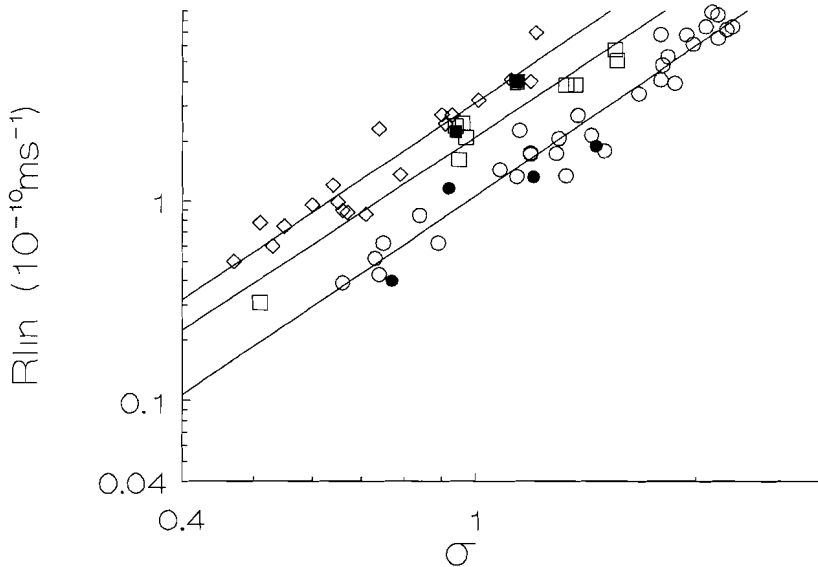Fig. 8 Linear growth rate versus $(S-1)\ln(S)S^{0.5}$ for the data in Table 1A-B.

Fig. 9 Linear growth rate versus supersaturation for the data in Table 1B-F. $O,\square,\Diamond$, represent pH = 8.9, 8 and 7.6 respectively. Closed symbols data Table 1B-C.

Table 2. Ostwald ripening rates of calcite at various pH values as determined with ^{45}Ca experiments

pH	Ostwald rate Ca[nm/(g×h)]	$[Ca^{2+}]$ mM	$[HCO_3^-]$ mM	$[CO_3^{2-}]$ mM	$[Ca]_T$ mM	$[C]_T$ mM
8.01	23.5	6.280	0.62	0.008	8.700	0.73
8.37	5	1.130	1.76	.054	1.130	2.10
9.04	32	0.050	8.95	1.060	0.080	12.46
9.53	55	0.003	32.9	13.70	0.009	63.40

The same values for the slopes in Fig. 9 indicate that the reaction mechanism is the same at the various $[C]_T$ concentrations. The increase in the reaction rate constant k for pH = 8 and 7.6 as compared to k at pH = 8.9, is 100% and 330% respectively, for an estimated value of $k = 1.1 \times 10^{-10}$ ms^{-1} at pH = 8.9. A simple quantitative relationship between $[C]_T$ and the increase in k was not found, but the increase could be related to the ratio of $[HCO_3^-]/[CO_3^{2-}]$ as is shown in Fig. 10.

3.4.4. Effect of contaminants

Nearly every crystallization experiment is subject to influences of contamination. An impurity can either retard or completely stop crystal growth. The effect of impurities not only depends on their concentration, but also on their sorptive behavior (kinetics, affinity and sorption reversibility) and the supersaturation of the solution, which determines the step density, the critical distance between impurities (Cabrera and Vermilyea, 1958; Van der Eerden and Müller-Krumbaar, 1986) and the competition of the impurity with building species. Furthermore, different impurities may influence the step movement in different ways. The reason for this is a difference in crystal properties in the various crystallographic directions. Therefore, one impurity may influence the morphology in a completely different way than another impurity.

For calcite, chloride at seawater concentrations was found to selectively disrupt positive steps (oriented towards c-axis), while it left the negative steps (oriented away from the c-axis) unchanged (Hillner et al., 1993). Hence, at the levels of 0.7 M KCl in our experiments, this may also be the case. In Table 3 the conditions for growth experiments with (initial) concentrations of 3×10^{-7}M Zn and with phosphate concentrations of 1×10^{-6} M and 1×10^{-5} M are listed. Zinc at levels of 1×10^{-6} M and at $\sigma = 1.5$ completely stopped calcite crystal growth, while zinc at a level of 3×10^{-7}M retards the growth rate by 10, 15 and 24% at supersaturations of 1.51, 1.14 and 0.97 respectively, considering outgrowths up to 1.3. At lower supersaturations, zinc has a greater effect, which may be caused by a lower number of growth sites and/or a greater surface coverage. From the added burette volume versus time curves (Fig. 11) of experiments with and without Zn ($\sigma = 1.14$) it can be seen that the retardation is most pronounced at the beginning of the experiment, when Zn concentrations are high (3×10^{-7} M). After an outgrowth of about 1.1, calcite growth proceeds as growth
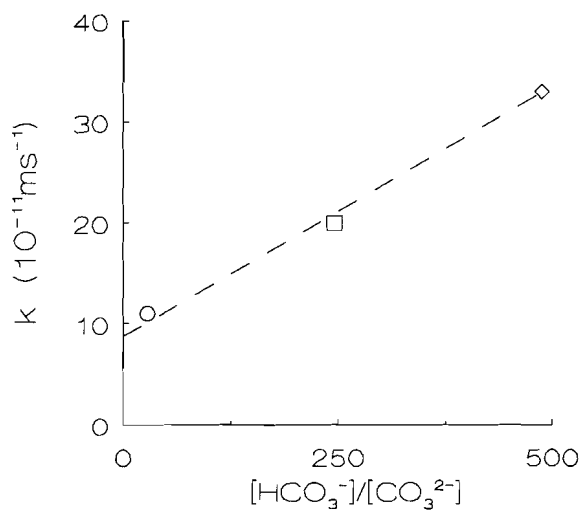
Fig. 10 The growth rate constant versus the ratio of bicarbonate and carbonate. °,Δ,◊, represent pH values of 8.9, 8 and 7.6 respectively.
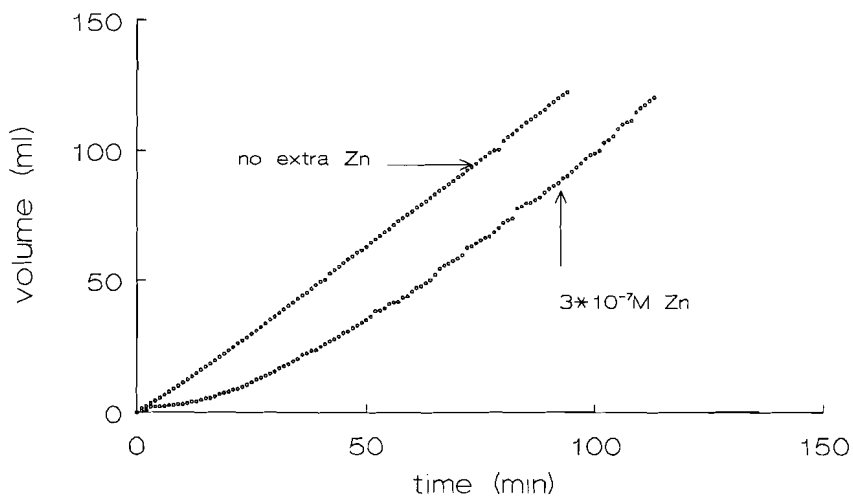

Fig. 11 Added volume of burette A versus time for an experiment at $\sigma = 1.14$ with and without 3×10^{-7} M Zn.

Table 3. Total calcium and carbonate concentrations ($[Ca]_T$, $[C]_T$), free aqueous activities, volume in the reactor and duration of experiments to which extra Zn or phosphate was added. For experiments with Zn, burette concentrations were 0.004 M $CaCl_2$ and 0.083 M $KHCO_3/K_2CO_3$, PCO_2 = 0.015 atm. For phosphate, burette concentrations were 0.004 M $CaCl_2$ and 0.015 M $KHCO_3/K_2CO_3$, PCO_2 = $10^{-3.5}$ atm.

pH	Ca_T $(10^{-4}M)$	C_T $(10^{-3}M)$	Ca^{2+} $(10^{-4}M)$	CO_3^{2-} $(10^{-4}M)$	Vend (ml)	time (min)	seeds (mg/l)	σ	$Rlin$ $(10^{-10}ms^{-1})$
3×10^{-7} M Zn									
8.050	7.82	43.6	1.85	1.10	738	51	145.1	1.51	5.03
8.052	5.73	42.8	1.32	1.08	758	135	170.0	1.14	2.78
8.053	4.8	43.6	1.10	1.10	*568*	*93*	159.4	0.97	1.92
10^{-5} M phosphate									
8.898	9.58	7.2	2..37	1.26	764	60	152.7	1.80	3.92

without Zn, when the Zn concentration has dropped below 2×10^{-8} M. Zn apparently is built into the calcite crystal lattice. Therefore, the low levels of Zn contamination in our system (4.6×10^{-8} M) are assumed to have a negligable influence on growth rates. The appearance of the crystal surface at an outgrowth of 1.7 is similar for experiments with and without Zn, as can be observed with SEM and AFM (Fig. 12a, b).

Phosphate is known to inhibit calcite crystal growth (e.g. Reddy, 1977; House, 1986; Giannimaras and Koutsoukos, 1987) and retard the Ostwald ripening rate of calcite (chapter 2). In our experiments, 1×10^{-6} M phosphate had no effect on the growth rate, whereas 1×10^{-5} M reduced the growth rate by 17% (Fig. 13). In contrast with Zn, phosphate influences the growth rate throughout the entire experimental run, since phosphate is not built into the calcite crystal lattice as easily as Zn, because the similarity in charge and radius between Zn and Ca is greater than between phosphate and carbonate. Furthermore, the sorption reversibility of phosphate is high and sorption experiments under similar conditions show that only 3-4% is adsorbed due to the competition with carbonate (chapter 2). Therefore, in experiments with higher $[C]_T$ concentrations (Table 1E-F), contamination with phosphate will influence growth even less. Despite the small amounts of phosphate present at the surface, the effect on macrostep formation is pronounced (Fig. 14a, b). Steps are no longer parallel and the open ribs and corners show a roughened step pattern. For the experiments in Table 1, no such observations were made with SEM or AFM. We can therefore safely conclude that phosphate contamination did not influence our experiments.

Fig. 12 SEM (a) and AFM, 1800 nm by 1800 nm (b) images of calcite grown in the presence of 3×10^{-7} M Zn at an outgrowth of 1.7 and $\sigma = 1.14$.

Fig. 13 Added volume of burette A versus time for an experiment at $\sigma = 1.82$ with and without 1×10^{-5} M phosphate.
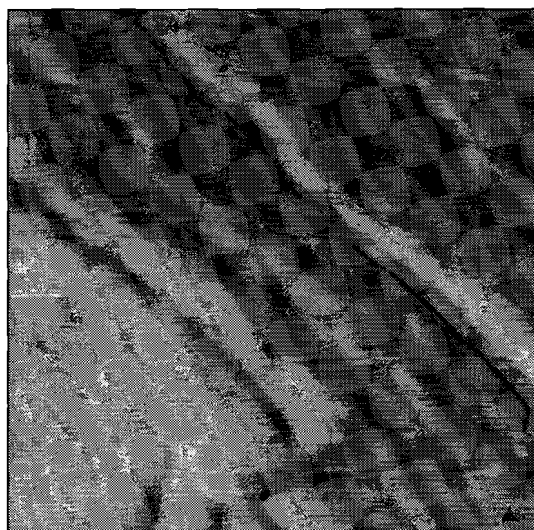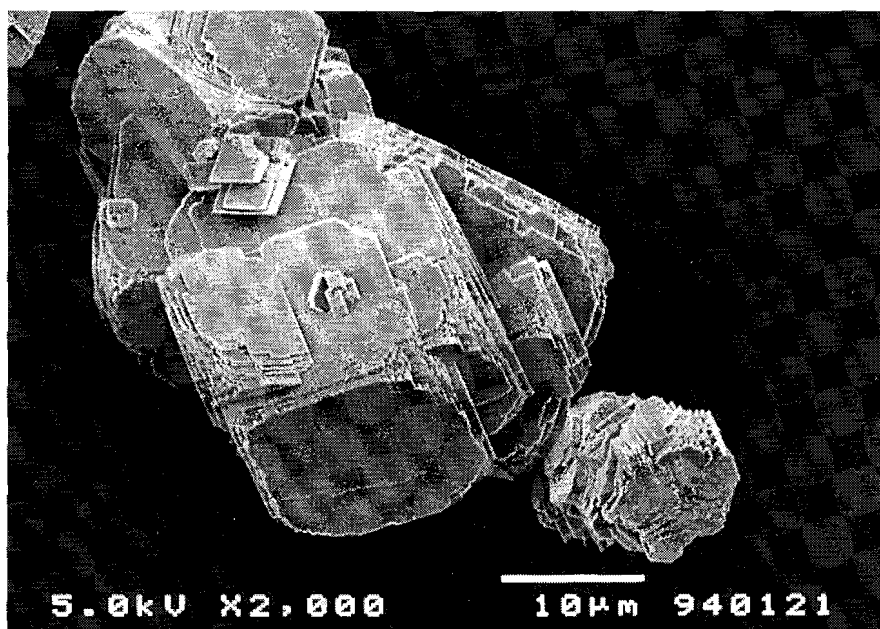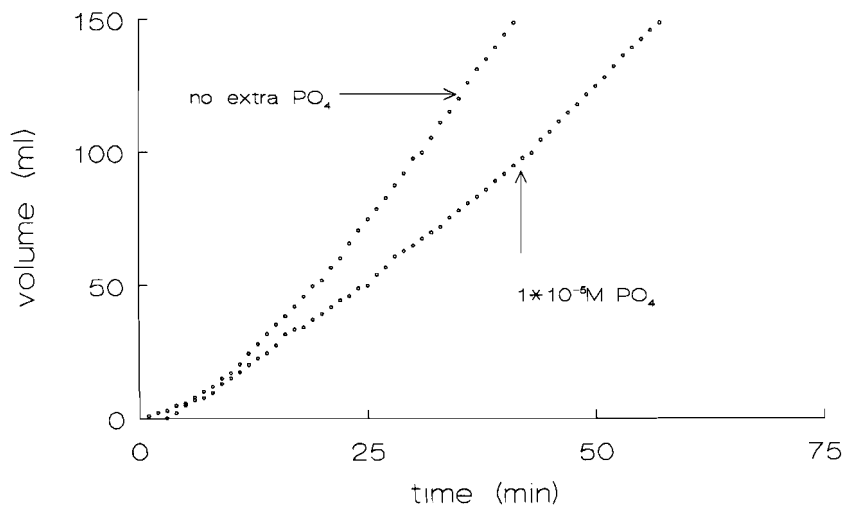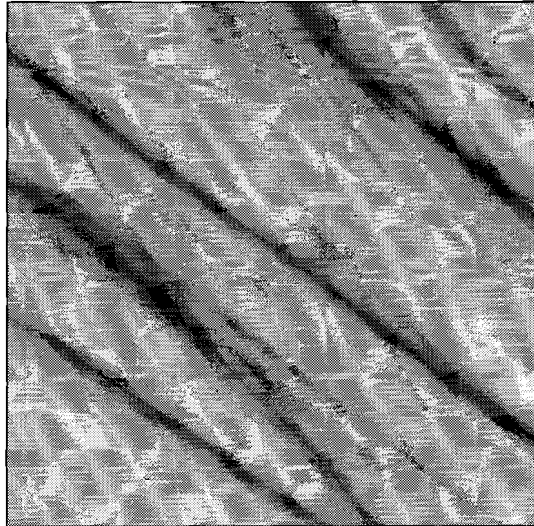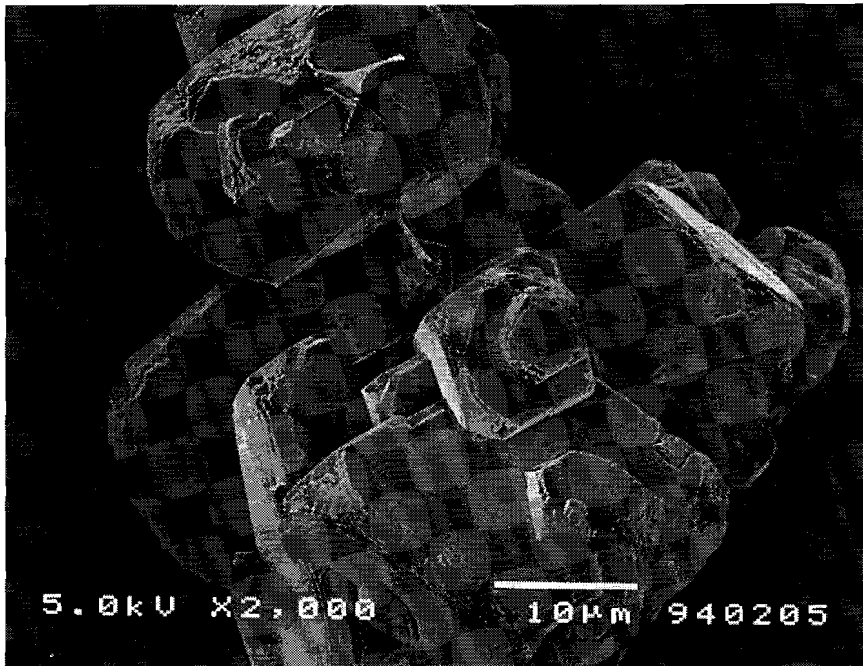
Fig. 14 SEM (a) and AFM, 1500 nm by 1500 nm (b) images of calcite grown in the presence of 1×10^{-5} M phosphate at an outgrowth of 1.7 and $\sigma = 1.82$.

Acknowledgements

References

Allison, J.D., Brown, D.S. and Novo-Gradac, K.J., 1991. MINTEQA2/PRODEFA2, a geochemical assessment model for environmental systems: version 3.11.

Busenberg, E. and Plummer, L.N., 1986. Kinetic and thermodynamic factors controlling the distribution of SO_4^{2-} and Na^+ in calcite and selected aragonites. Geochim. Cosmochim. Acta 49: 713-725.

Cabrera, N. and Vermilyea, D., 1958. Growth and perfection of crystals. Doremus, R.H., Roberts, B.W. and Turnbull, D. eds., Wiley: 393-410.

Christoffersen, J. and Christoffersen, M.R., 1990. Kinetics of spiral growth of crystals and determination of the absolute rate constant. J. Crystal Growth 100: 203- 211.

Davies, J.A., Fuller, C.C. and Cook, A.D., 1978. A model for trace metal sorption processes at the calcite surface: Adsorption of Cd^{2+} and subsequent solid solution formation. Geochim. Cosmochim. Acta, 51: 1477-1490.

DeBoer, R.B.,1977. Influence of seed crystals on the precipitation of calcite and aragonite. Am J. Sci. 277: 38-60.

Folk, R.L., 1978. A chemical model for calcite crystal growth and morphology control. J. Sed. Petrology 48: 345-347.

Frèche, M. and Heughebaert, J.C., 1989. Calcium phosphate precipitation in the 60-80° C range. J. Cryst. Growth, 94: 947-954.

Giannimaras, E.K. and Koutsoukos, P.G., 1987. The crystallization of calcite in the presence of orthophosphate. J. Colloid Interface Sci. 116: 423-430.

Gratz, A.J., Hillner, P.E., and Hansma, P.K., 1993. Step dynamics and spiral growth on calcite. Geochim. Cosmochim. Acta 57: 491-495.

Hillner, P.E., Manne, S., Gratz, A.J. and Hansma, P.K., 1993. The AFM: A new tool for imaging crystal growth processes. Presented at: The Royal Society of Chemistry. Faraday Division, General Disc. 95.

House, W.A., 1987. Inhibition of calcite crystal growth by inorganic phosphate. J. Colloid Interface Sci., 2: 505-511.

Ichikawa, M. and Ichikuni, M. 1984. Uptake of sodium and potassium by calcite. Chem. Geol. 42: 137-146.

Jetten, L.A.M.J., Van der Hoek, B., Van Enckevort W.P.J., 1983. In situ observations of the growth behaviour of the {010} face of potassium hydrogen phtalate. J. Cryst. Growth 62: 603-611.

Lahann, R.W., 1987. A chemical model for calcite crystal growth and morphology control. J. of Sed. Petr. 48: 337-344.

MacInnis, I.N. and Brantley, S.L., 1992. The role of dislocations and surface morphology in calcite dissolution. Geochim. Cosmochim. Acta 56 : 1113- 1126.

Morel, F.M.M., 1983. Principles of Aquatic Chemistry, Wiley, Chichester, 446 pp.

Mucci, A., Canuel, R. and Zhong, S., 1989. The solubility of calcite and aragonite in sulfate-free seawater and the seeded growth kinetics and the composition of the precipitates. Chem. Geol., 74: 309-320.

Nancollas, G.H. and Reddy, M.M., 1971. The crystallization of calcium carbonate. II calcite growth mechanism. J. Colloid Interface Sci. 37: 824- 830.

Nielsen, A.E. and Toft, J.M., 1984. Electrolyte crystal growth kinetics. J. Cryst. Growth 67: 278-288.

Plummer, L.N., Wigley, T.M.L. and Parkhurst, D.L., 1978. The kinetics of calcite dissolution in CO2-water systems at 5 ° to 60 °C and 0.0 to 1.0 atm CO_2: Am. J. Sci. 278: 179- 216.

Plummer, L.N., Wigley, T.M.L. and Parkhurst, D.L., 1979. Critical review of the kinetics of calcite dissolution and precipitation, in E.A. Jenne, ed., Chemical modelling in aqueous systems: American Chemical Society Symposium Series 93: 537-573.

Reddy, M.M. and Nancollas, G.H., 1971. The crystallization of calcium carbonate. I. Isotopic exchange and kinetics. J. Colloid Interface Sci. 36: 166- 172.

Reddy, M.M. and Nancollas, G.H., 1976. The crystallization of calcium carbonate IV: the effect of magnesium, strontium and sulfate ions. J. Cryst. Growth 35: 33- 38.

Reddy, M.M., 1977. Crystallization of calcium carbonate in the presence of trace concentrations of phosphorus-containing anions. I. Inhibition by phosphate and glycerophosphate ions at pH 8.8 and 25 °C. J. Cryst. Growth 41: 287-295.

Reddy, M.M. and Gaillard, W.D., 1981. Kinetics of calcium carbonate seeded crystallization: Influence of Solid/Solution ratio on the reaction rate constant. J. Colloid Interface Sci. 80: 171-178.

Reddy, M.M., Plummer, L.N. and Busenberg, E. 1981. Crystal growth of calcite from calcium bicarbonate solutions at constant PCO_2 and 25 °C: a test of a calcite dissolution model. Geochim. Cosmochim. Acta 45:1281-1289.

Reddy, M.M. and Wang, K.K., 1980. Crystallization of calcium carbonate in the presence of metal ions. J. Cryst. Growth 50: 470-480.

Sigg, L. and Stumm, W.,1990. Aquatische Chemie. Verlag der Fachvereine Zürich, 388 pp.

Stumm, W. and Morgan, J.J., 1981. Aquatic chemistry. John Wiley & Sons, 780 pp.

Tai, C.Y., Chen, P. and Shih, S., 1993. Size dependent growth and contact nucleation of calcite crystals. AIChE J. 39 : 1472- 1481.

Van der Eerden, J.P. and Müller-Krumbhaar, H., 1986. Formation of macrosteps due to time dependent impurity adsorption. Electrochim. Acta, 31: 1007-1012.

Van Gaans, P.F.M., 1989. Wateqx-A restructured, generalized and extended FORTAN 77 computer code and database format for the WATEQ aqueous chemical model for element speciation and mineral saturation, for use on personal computers or mainframes, Computer and Geosciences, 15: 843-887.

Van der Weijden R.D., Van der Weijden C.H. and Comans R.N.J.,1994. Sorption and sorption reversibility of Cd on calcite under simulated riverine, estuarine and marine conditions. Mar. Chem. 47: 65-79.

Van der Weijden, R.D., Meima, J. A. and Comans, R.N.J., 1995. Sorption and sorption reversibility of Cd on calcite in the presence of phosphate and sulphate. Submitted to Mar. Chem.

White, A.F., 1977. Sodium and potassium coprecipitation in aragonite. Geochim. Cosmochim. Acta 41: 613-625.

Witkamp, G.J., 1989. Crystallization of calcium sulfate and the uptake of impurities. Dissertation Delft University of Technology, 219 pp.

Xyla, A.G., Efthimios, E.K. and Koutsoukos, P.G. 1991. The precipitation of calcium carbonate in aqueous solutions. Colloids and Surfaces 53: 241- 255.

Zachara J.M., Cowan C.E. and Resch C.T., 1991. Sorption of divalent metals on calcite. Geochim. Cosmochim. Acta, 55: 1549-396.

Zhong, J.W. and Nancollas, F.H., 1990. Mechanism of growth and dissolution of sparingly soluble salts. Reviews in Mineralogy 23: 365-396.

Appendix Aqueous speciation reactions and equilibrium constants

reaction		log$K$	source [*]
$CO_3^{2-} + H^+ = HCO_3^-$		10.33	1
$CO_3^{2-} + 2H^+ = H_2CO_3^{\,\circ}$		16.68	1
$PO_4^{3-} + H^+ = HPO_4^{2-}$		12.35	1
$PO_4^{3-} + 2H^+ = H_2PO_4^-$		19.55	1
$PO_4^{3-} + 3H^+ = H_3PO_4$		21.70	1
$Ca^{2+} + CO_3^{2-} = CaCO_3^{\,\circ}$		3.15	1
$Ca^{2+} + H^+ + CO_3^{2-} = CaHCO_3^+$		11.46	2
$Ca^{2+} + PO_4^{3-} = CaPO_4^-$		6.5	1
$Ca^{2+} + H^+ + PO_4^{3-} = CaHPO4^{\,\circ}$		15.1	1
$Ca^{2+} + 2H^+ + PO_4^{3-} = CaH_2PO_4^+$		21.0	1
$Zn^{2+} + CO_3^{2-} = ZnCO_3^{\,\circ}$		5.43	1
$Zn^{2+} + 2CO_3^{2-} = Zn(CO_3)^{2-}$		9.63	1
$Zn^{2+} + H^+ + CO_3^{2-} = ZnHCO_3^+$		12.4	1
$Ca^{2+} + CO_3^{2-} = CaCO_3(s)$		8.43	3
$Zn^{2+} + CO_3^{2-} = ZnCO_3(s)$		10.0	1
$5Ca^{2+} + 3PO_4^3 + OH^- = Ca_5(PO_4)_3OH(s)$		55.60	1
$4Ca^{2+} + H^+ + 3PO_4^{3-} +3H_2O = Ca_4H(PO_4)_3.3H_2O(s)$		49.60	4
$Ca^{2+} + HPO_4^{2-} + 2H_2O = CaHPO_4.2H_2O(s)$		6.69	4

Sources:
1) Morel (1983)   3) Sigg and Stumm (1991)
2) Davies et al. (1987)   4) Frèche and Heughehaert (1989)

Chapter 4

Partitioning of Cd between calcite and supersaturated
solutions composed of various $[Ca]_T$ and $[C]_T$ in a
chemo-stat system

Abstract— Partitioning of cadmium between calcite and supersaturated solutions was investigated by performing seeded-growth experiments. The composition of the super-saturated solutions with various total calcium and total carbonate concentrations, was held constant by means of a chemo-stat system. Calcite growth proceeds with an order 2.0 ± 0.3 in relative supersaturation, indicating spiral growth. The growth rate increased with increasing calcium concentration and also with increasing bicarbonate concentration, i.e. decreasing pH, at equal supersaturation. Although in previous studies expressions were derived that relate a partition coefficient directly to the growth rate, this study indicates that not merely the growth rate, but also the solution composition determines the degree of partitioning. Furthermore, the ripening of the seeds and the stoichiometry and supersaturation of a solution, can bring about changes in the surface features of calcite, a factor which is considered in few other partitioning studies. It is made plausible in this study that the Cd partitioning, in turn, is influenced by the calcite surface structure.

R.D. van der Weijden, A.E.D.M. van der Heijden, G.J. Witkamp and G.M. van Rosmalen

4.1. Introduction

Trace element partitioning between minerals and solutions can provide a geochemical tool to broaden our understanding of the geochemical fate of certain elements, their occurrence in mineral deposits, paleoenvironments, paleoceanic circulation patterns, redox conditions, lithification, and diagenesis. Its use extends into the industrial field, as the presence of trace amounts of "foreign" elements can greatly reduce or accelerate a crystallization process and can influence the shape, size and properties of a product. Furthermore, knowledge of the various aspects of partitioning, can aid in predicting the influence on the environment of waste products after exposure, and can be implemented in waste-treatment procedures, to yield a less harmful product. Because of the broad applicability, many studies concerning the effects of thermodynamic and kinetic parameters on partitioning have been carried out.

Of these parameters, the effect of the rate of crystal growth has received by far the most attention. It is generally expected that with increasing growth rate, the partition coefficients converge towards unity (Burton et al., 1953). More recently the influences of crystal morphology and surface microtopography on the uptake of trace elements have been investigated. It was found that the different faces of the crystal and of the growth hillocks on a certain crystal face can display differential partitioning, referred to as sectoral and intrasectoral zoning respectively (Reeder and Grams, 1987; Paquette and Reeder, 1995). Since the crystal morphology and microtopography can be affected by the growth rate, we may conclude that the value of the partition coefficient at a certain growth rate actually represents the net effect of the thermodynamic (interaction affinity) plus the structural (the interacting surface) and the kinetic (such as the interaction time) parameters. These parameters are, however, not always independent. For instance, the surface structure is strongly influenced by the supersaturation and the growth process.

Bearing this in mind, we investigated Cd partitioning between calcite and a supersaturated solution as a function of total calcium (Ca_T) and total carbonate (C_T) with seeded growth experiments in a chemo-stat. The influence of the seed type and seed quantity was inspected as well. Furthermore, the significance of these laboratory experiments for simulation of real-life processes will be discussed. Such real-life processes are, for instance, the Cd incorporation in benthic foraminifera (calcite) (Boyle, 1988), and the uptake of Cd in calcite during carbonation of municipal incinerated waste bottom-ash (Comans et al., 1993, chapter 5).

4.2. Materials and Methods

A chemo-stat (Van der Weijden et al., 1995) was utilized for the seeded crystal growth experiments. All chemical components, except Cd, were kept at a constant concentration. In addition to monitoring the pH and the volume of the solution in the reactor, the Ca concentration was monitored by a Ca-membrane electrode (Radiometer). Instead of a system where the growth rate was set by a certain rate of addition of a reagent volume (Zhong and Mucci, 1993), the addition of the burette solutions was controlled by the growth of calcite, and therefore growth rates could be accurately measured even after prolonged outgrowth (Weijnen, 1986). During growth, a minute change in the Ca signal on a mV meter caused an impulsomat (Metrohm) to trigger two burettes containing $CaCl_2$ with $CdCl_2$ (Aldrich, 99+) in 0.7 M KCl and $K_2CO_3/KHCO_3$ in 0.7 M KCl respectively, to add equal volumes

producing the exact composition of the precipitating solution plus an excess in calcium and carbonate to compensate for calcite growth. A concentration of Cd twice as high as in the initial solution, was added to one burette solution ($CaCl_2$) in order to prevent its dilution in the reactor. The pH was maintained at a constant value by an impulsomat which triggered a burette containing a solution of 0.3 M K_2CO_3 in 0.7 M KCl. The pH electrodes were calibrated against standard Ingold buffers of 7.00 and 9.21. Reaction and storage vessels for solutions containing Cd, as well as the four-bladed stirrer (530 rpm), were made of teflon to avoid Cd loss by sorption onto container walls. Cd sorption onto the Ca-membrane electrode, was less than 3% after 3 days.

Solutions were prepared from doubly distilled water (IKADEST) and the reagent grade chemicals KCl, $CaCl_2.2H_2O$ (Merck), K_2CO_3 and $KHCO_3$ (Baker). Supersaturations, σ, ranged from 0.5 to 2.3. The PCO_2, total carbonate $[C]_T$ and total calcium $[Ca]_T$ were chosen in such a manner that the activities of calcium and carbonate in the supersaturated solutions were of an equal order of magnitude (10^{-4} M). The solution speciations for the different pH values were calculated with WATEQX (Van Gaans, 1989) using Pitzer equations, and are listed in Apx 1. A background electrolyte of 0.7 M KCl was chosen based on the ionic strength of seawater. KCl rather than NaCl was used, because Na^+ is more easily incorporated into the calcite crystal lattice than K^+ (Ichiwaka and Ichikuni, 1984; White, 1977), and because the Ca-membrane electrode is more sensitive to Na^+. Since Cd forms complexes with chloride (Apx. 2), an easily measurable (GFAAS) Cd concentration of 6.25×10^{-7} M could be added, without exceeding the solubility product of otavite.

For each experiment 450 ml of a filtered (0.22 µm) supersaturated solution was equilibrated by bubbling a H_2O-saturated CO_2/N_2 gas mixture (Airproducts) for at least two hours (300 ml/min) through the solution (22°C) (Romanek et al., 1992; Zhong and Mucci, 1993). An aliquot of the solution was withdrawn and stored for comparison of the initial and final $[Ca]_T$, $[C]_T$ and Cd concentrations. Crystal growth was started by adding about 75 mg of calcite seeds as a suspension with a pycnometer. A suspension instead of dry crystals was applied to minimize crystal surface damaging. By using a pycnometer the actually added seed amount could be determined accurately. Seeds were suprapure calcite seeds (Merck) with a specific surface area of 0.29 m^2/gram, equilibrated in a $CaCO_3$ saturated solution for 3 months in a teflon vessel (batch A) and 1-1.5 year in a polythene vessel (batch B).

During an experimental run, subsamples (5 ml) were withdrawn with a syringe, filtered, and stored in teflon vessels for analysis. After an outgrowth of about 50 mg, the experiment was stopped, a final subsample was withdrawn, and the precipitate was washed three times with a $CaCO_3$ saturated 0.7 M KCl solution and subsequently three times with a $CaCO_3$ saturated solution. The seeds were oven-dried at 40 °C and inspected by means of SEM. The $[Ca]_T$ in the solutions was determined with EDTA titration and $[C]_T$ was determined with GRAN plot titration. Cd in both, solids and solutions, was determined at least twice by means of GFAAS (triplicates). Zn, an unavoidable contaminant, maybe originating from the IKADEST apparatus, was also measured with GFAAS. Quite a number of the solution samples were also analyzed for Cd with a Trace Lab (Radiometer). The mean deviation between values determined by these different methods was only 3.8%.

Cd adsorption was investigated using the radiotracer [109]Cd (Amersham) at similar L/S ratios and Cd concentrations (6.25×10^{-7} M). The same suprapure calcite was used and pre-equilibrated in a 0.7 M KCl solution for 24 hours. The experiment was started by adding Cd tracer and carrier. After 30 hours, two subsamples of the solution were centrifuged (4000 *g*) and counted on a Compugamma LKB 1280 gamma-counter with a 3 inch NaI well-type detector.

4.3. Data Analysis

4.3.1. Crystal growth

The calcite supersaturation σ was calculated from $[Ca]_T$, $[C]_T$ and pH, using the association constants in Apx. 2 and the expression:

$$\sigma = (IAP/K_{sp})^{1/2} - 1 \qquad (1)$$

where the ion activity product IAP = $(Ca^{2+})(CO_3^{2-})$ and K_{sp} denotes the thermodynamic solubility product.

The linear growth rate, *Rlin*, was calculated from the calcium mass balance and the initial specific surface area of 0.29 m^2/gram, while assuming retainment of the initial crystal shape during outgrowth. The linear growth rate can be expressed as:

$$Rlin = k\sigma^n \qquad (ms^{-1}) \qquad (2)$$

where k is the growth rate constant and n the reaction order, which is indicative of the reaction mechanism. A value for n of 2.0 ± 0.3 was found in chapter 3, and therefore a spiral growth mechanism apparently dominates the growth.

4.3.2. Partitioning

Partition coefficients, D, are not thermodynamic constants, since they are inevitably strongly influenced by kinetics. The distribution constant, K is defined as the concentration ratio of Cd in the solid and Cd in the solution. The partition coefficient D as defined in this study, takes into account the competition between Ca and Cd, and the activity coefficients of the free Ca^{2+} and Cd^{2+} ions:

$$D = \frac{[Ca_T]_l}{[Ca_T]_s} \times \frac{\gamma_{Cal}}{\gamma_{Cdl}} \qquad (3)$$

in which $[Ca_T]_l$ and $[Ca_T]_s$ denote the total concentrations of Ca in the liquid and the solid respectively, and γ_{Cal} and γ_{Cdl} denote the activity coefficients of Ca^{2+} and Cd^{2+} in the solution respectively, e.g. for cadmium defined as the activity coefficient of the free Cd^{2+} ion times the free Cd^{2+} concentration divided by the total Cd concentration, Cd_T, all in the solution. The ratio of the activity coefficients of Ca and Cd in the solid is assumed to equal one (Van der Weijden et al., 1994). D is only valid for uptake by isomorphous substitution (Angus et al., 1979; Zhong and Mucci, 1995).

The chemo-stat used in this study, can be regarded as a semi-batch system for which the following equation was derived for calculation of K (see Apx 3):

$$\frac{d[Cd]_t}{dlnV_t} = [Cd]_{t=0} - [Cd]_t \ (1 + K[CaCO_3]_{formed,t}) \qquad (4)$$

where V_t denotes the solution volume in the reactor, $[Cd]_{t=0}$ and $[Cd]_t$ denote the initial Cd concentration and the concentration at time = t in solution respectively, and $[CaCO_3]_{formed,t}$

is the weight of the calcite formed at time $= t$ (in kg per kg solution in the reactor). Equation (4) was solved numerically for K, with the Root Bisection method, and D was obtained by combining equations 3 and 4.

4.4. Results and Discussion

4.4.1. Calcite growth

Fig. 1 shows the growth rate versus the supersaturation for four different pH values between 7.56 and 8.90, and for calcite seeds which had ripened for three months (batch A). Further details on the experimental conditions can be found in Apx. 4. From Fig. 1 a value of 2.0 $\pm$ 0.3 for the slope n (eq. 3), indicating a spiral growth mechanism, can be deduced. The linear growth rate constant, k, increases from 1×10^{-10} to 3.3×10^{-10} ms^{-1} for pH = 8.90 to pH = 7.56 (Fig. 1). Values for n and k are in good agreement with values found in the literature (Nielsen and Toft, 1984; Zhong and Mucci, 1989; Christoffersen and Christoffersen, 1990; Tai et al., 1993), and in chapter 3.

From Fig. 1 it is clear that the growth rate not only increases with increasing supersaturation, but also with decreasing pH (i.e. increasing [C]$_T$). This may be caused by i) a direct pH effect, ii) an up to three times higher total and free Ca concentration at lower pH, iii) an up to 1.5 times higher free Ca^{2+}/CO$_3$$^{2-}$ ratio at lower pH, or iv) an up to ten times higher [HCO$_3$$^-$] at lower pH.

Ad i): Since a lower pH is associated with a more positive surface charge of calcite, a direct effect of the change in surface charge on the growth rate would imply that adsorption of negative (bi)carbonate ions is rate limiting, which is unlikely.

Ad ii) In this study the total Ca concentration at equal σ is up to three times higher at lower pH values (see Apx. 4). This is also true for the free [Ca^{2+}], see Fig. 2 where σ is plotted versus the free [Ca^{2+}] for the different pH values. Since data for calcite growth of experiments by Lorens (1981), with a [C]$_T$ concentration similar to the [C]$_T$ in our experiments at pH = 8.90, an up to 100 times lower free carbonate concentration, and an up to 30 times higher free Ca concentration (also a much higher [Ca]$_T$), plot on the same line as the data in this chapter at pH = 8.90 (Fig. 3) it can be concluded that this calcium effect is negligible.

Ad iii): According to Gomez-Morales et al. (1995, subm), a higher free Ca/carbonate ratio of 4:1 compared to 1:4, at equal σ, gives rise to a five-fold increase in growth rate, caused by more stoichiometric ratios of these ions in the sorption layer. Seemingly, there is less adsorption of calcium than of carbonate when these ions are stoichiometrically present in the solution. Qiwei (1991) anticipated an increase at higher [Ca^{2+}] for another reason, namely, the lower dehydration rate of Ca^{2+} as compared to carbonate. In the experiments of this chapter the [Ca^{2+}]/[CO$_3$$^{2-}$] ratio varies at most by a factor of 1.5, which makes a decisive influence of this ratio on the growth rate unlikely. In fact the results of Gomez-Morales are surprising. The change of a factor of 16 in [Ca^{2+}]/[CO$_3$$^{2-}$] is only minor compared to the difference of a few thousand in this ratio between Lorens' experiments and those in this chapter, while his and the data here plot on the same line. An effect of a difference in ratio of 1.5 can therefore not explain the observed increase in the growth rate at lower pH.

Ad iv): It can therefore be concluded that the increase in the bicarbonate activity is the main factor responsible for the increase in growth rate at equal σ in our experiments. In other papers on calcite growth, the bicarbonate contribution was assumed to be negligible,
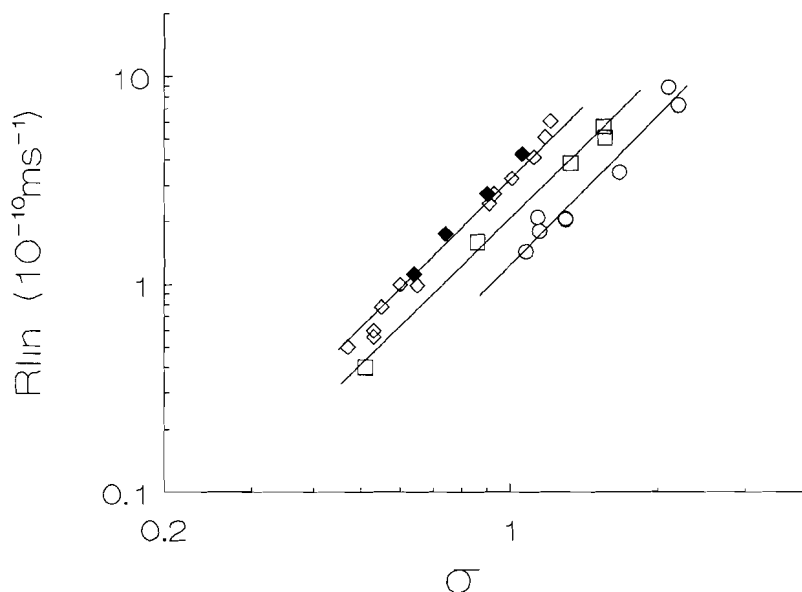
Fig. 1. The linear growth rate of calcite versus the supersaturation. Calcite growth was initiated with calcite seeds that had ripened for three months (batch A). Best linear fits are drawn for pH = 8.90 and C_T = 7.5 mM (O), pH = 8.05 and C_T = 40 mM (□), pH = 7.66 and C_T = 60 mM (◊), pH = 7.56 and C_T = 50 mM (◆). Further details can be found in Apx. 4A.

Fig. 2. Supersaturation versus the free [Ca^{2+}] for data in Apx. 4A. Best linear fits are drawn for pH = 8.90 and C_T = 7.5 mM (O), pH = 8.05 and C_T = 40 mM (□), pH = 7.66 and C_T = 60 mM (◊), pH = 7.56 and C_T = 50 mM (◆).
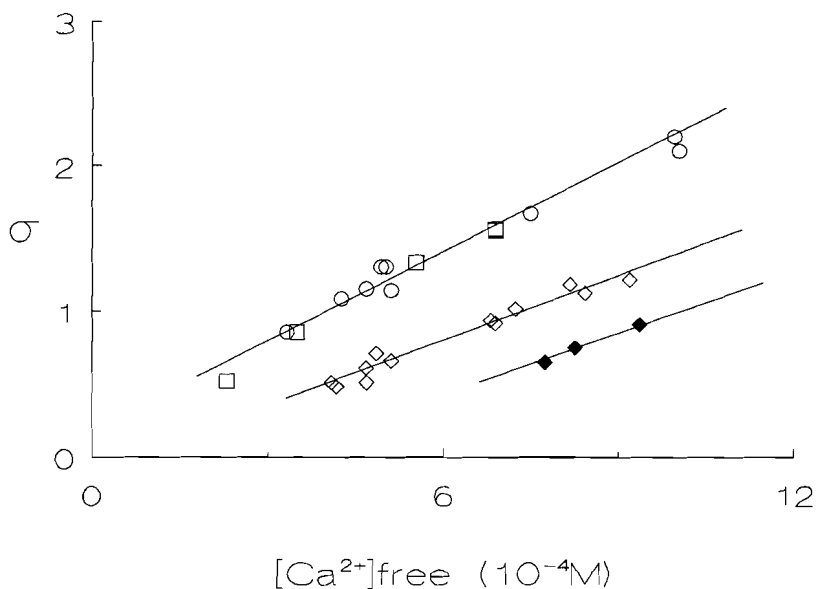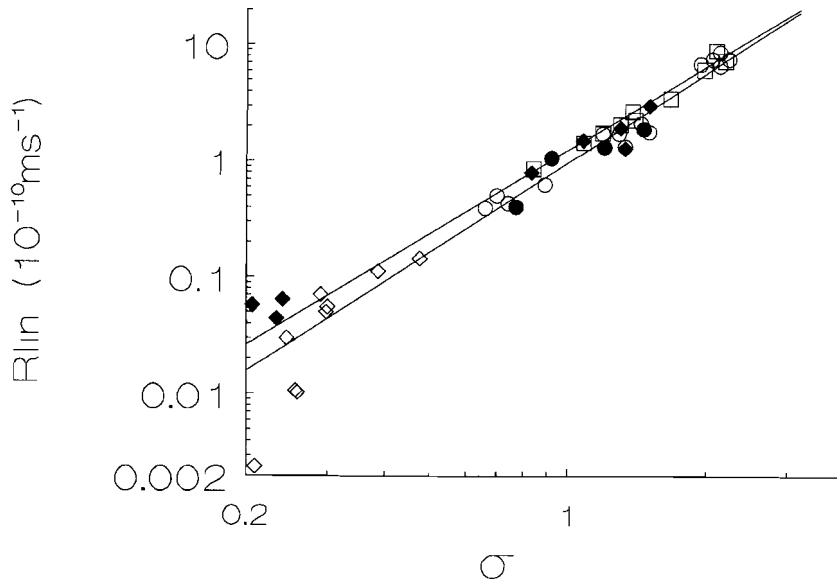
Fig. 3.The linear growth rate of calcite versus the supersaturation at pH = 8.90 and C_T = 7.5 mM with seeds that had ripened for three months (□, batch A) and a year (○, batch B). In four experiments the growth of calcite seeds (batch B) in solutions without Cd was studied (●). Data for calcite growth as presented by Lorens (1981) were recalculated to obtain linear growth rates, and are plotted for experiments at pH = 7.34 and C_T = 4mM (◊) and pH = 7.50 and C_T = 4 -10 mM (◆).

or could not be quantified due to the limited experimental precision (Burton and Walter, 1990; Zhong and Mucci, 1993). Our observations, however, indicate that the contribution of HCO_3^- must be included in kinetic rate equations for calcite at lower pH, i.e. higher CO_2 pressures:

$$CO_3^{2-} + Ca^{2+} = CaCO_3(s) \quad , \text{ and } HCO_3^- + Ca^{2+} = CaCO_3(s) + H^+ \qquad (6)$$
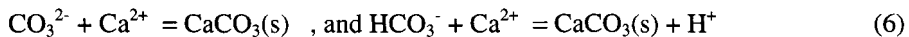
From the data (see also Fig. 3) it can be seen that the growth rates for seeds after ripening for more than a year (batch B, Apx 4B) are about 25% lower at the lower supersaturations, as compared to seeds which had ripened for three months (Batch A, Apx. 4A). This might be caused by a difference in storage vessel materials for batch A (teflon) and B (polythene). Polythene could give rise to a slight poisoning of batch B after long ripening periods. Other factors which may explain the apparently lower growth rate after long ripening times, are a change in crystal morphology or a change in kink site density. SEM photographs, however, show that the main crystal habit of the seeds before and after ripening is the rhombohedron, and no evidence for drastic morphologic changes can be seen (Fig. 4).

Cd does not influence the growth of calcite, as can be concluded from the equal growth rates (Fig. 3) and from the apparently similar crystal surfaces (Fig. 5) in experiments with and without Cd. This is in accordance with findings of Wada et al. (1995).

Summarizing, the observed linear growth rate increases with increasing supersaturation and bicarbonate concentration, and additionally depends on the surface microtopography.
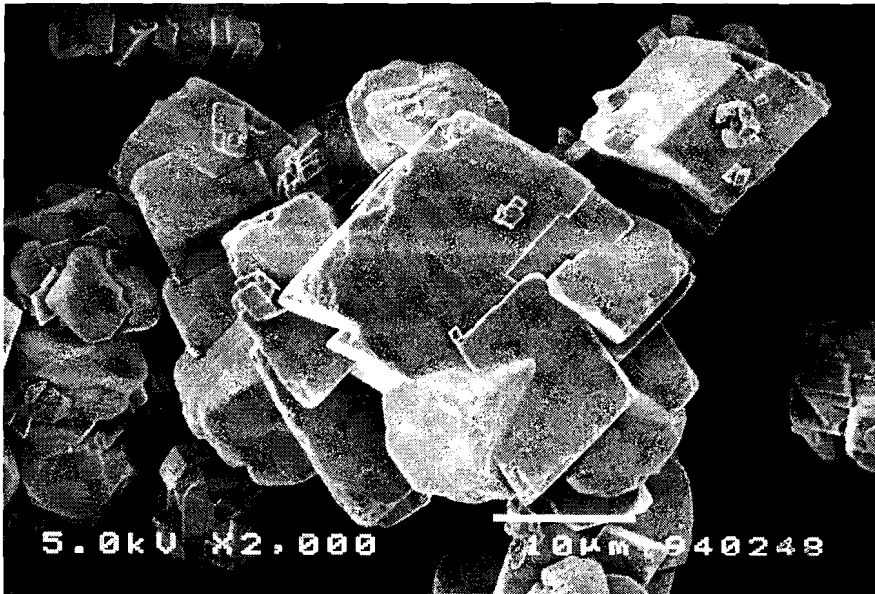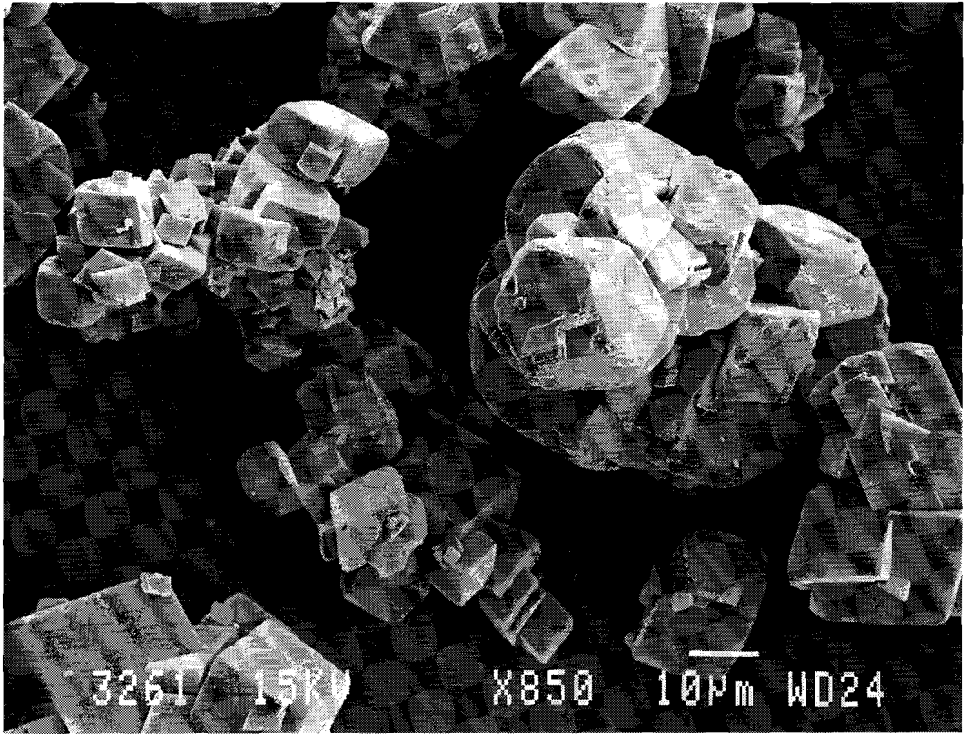
Fig. 4. SEM photographs of dry seeds (a) and after two months ripening in a CaCO₃ saturated solution.

4.4.2. Cd partitioning

4.4.2.1. Effects of cadmium concentration and seed outgrowth

In Fig. 6 the aqueous $[Cd]_T$ values are plotted versus the seed crystal outgrowth factor for experiments 2-6 (a) and 4-7 (b) (Apx. 4). The contribution of Cd adsorption to the decrease in Cd concentration during growth experiments is small, as the adsorption percentage of Cd on calcite in 0.7 M KCl and at a similar L/S ratio was only 4.7% after 30 hours. The decrease in $[Cd]_T$ is therefore virtually exclusively due to incorporation in the grown calcite. By comparing the Cd concentrations in solid and liquid samples the validity of the mass balance could be established. From the curves in Fig. 6, the D values could be fitted with eq 4. A further refinement, namely a reliable determination of the dependency of K on the Cd concentration or the crystal outgrowth, was not feasible. This was concluded from a sensitivity and error analysis which showed that a variation in K of up to 20% during outgrowth would still remain undetected. The values of K and D, calculated from the initial and final values of the [Cd] can thus be considered as averaged values over total outgrowth with a maximal error of 20%.

Sorption reversibility experiments, indicate that some dependency of D on $[Cd]_T$ is expected. These experiments showed that a tenfold increase in $[Ca^{2+}]$ results in a lower surface coverage of Cd and a decrease in the sorption reversibility. This must be caused by sorption site heterogeneity, because the cadmium concentration of at most 10^{-8} M is much lower still than the 1.6×10^{-7} M of available sorption or growth sites (Van der Weijden, 1994). This may explain the concentration dependence of D for partitioning of Zn (Qiwei, 1991), Fe and Mn (Dromgoole and Walter, 1990) and Mg (Mucci and Morse, 1983) during calcite growth. Apart from the effect of the Cd concentration, an influence of the surface microtopography on D is expected. Paquette and Reeder (1995), for instance, demonstrated that $D(Mn)$ varies for the different types of kink sites along the steps at the calcite surface. Also, the number of a particular type of kink, depends on the solution composition. This implies that effects on D can be expected of the type of seed crystals, their degree of outgrowth and the solution composition. In experiments only one of these parameters should thus be varied at the same time. In that respect, experiments where the reagent pump rate is kept constant in combination with a pH-stat (Lorens, 1981), have serious disadvantages for high outgrowth factors of calcite. For instance, σ will decrease during outgrowth due to the increasing surface area, unless very low outgrowth levels are applied, but then other surface structural effects can become dominating, which complicates the interpretation of the results.

In order to investigate the sensitivity of D towards the degree of outgrowth in the chemo-stat system, experiments were performed with outgrowth values between 1 and 30% (compare Appendix 4, series A 4 and D). D was only slightly (< 10%) higher at a lower outgrowth, despite the difference of a factor of 30 in outgrowth. Apparently the surface is already sufficiently adapted to the growing conditions after a few % outgrowth Since in general in all experiments approximately 70% outgrowth was reached, it can be concluded that no effect of this parameter has to be taken into account.
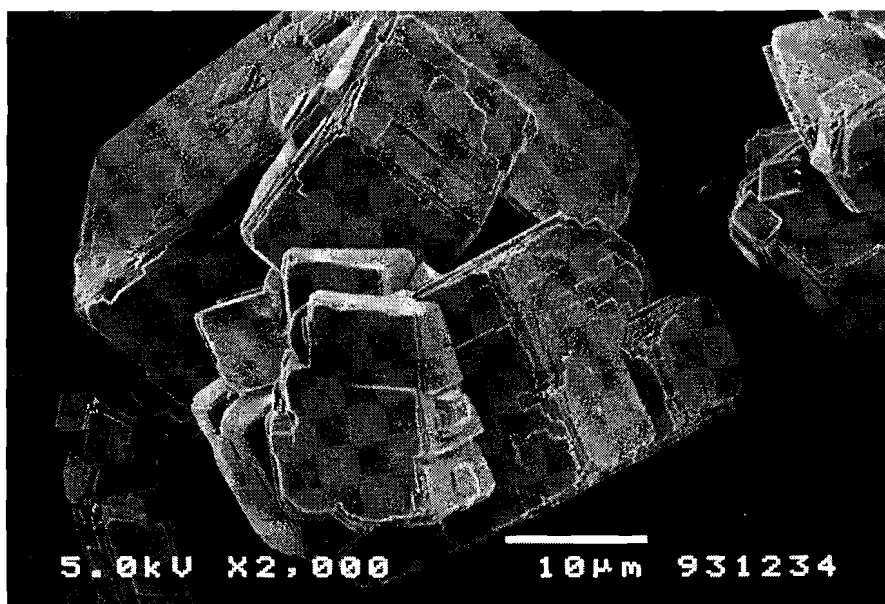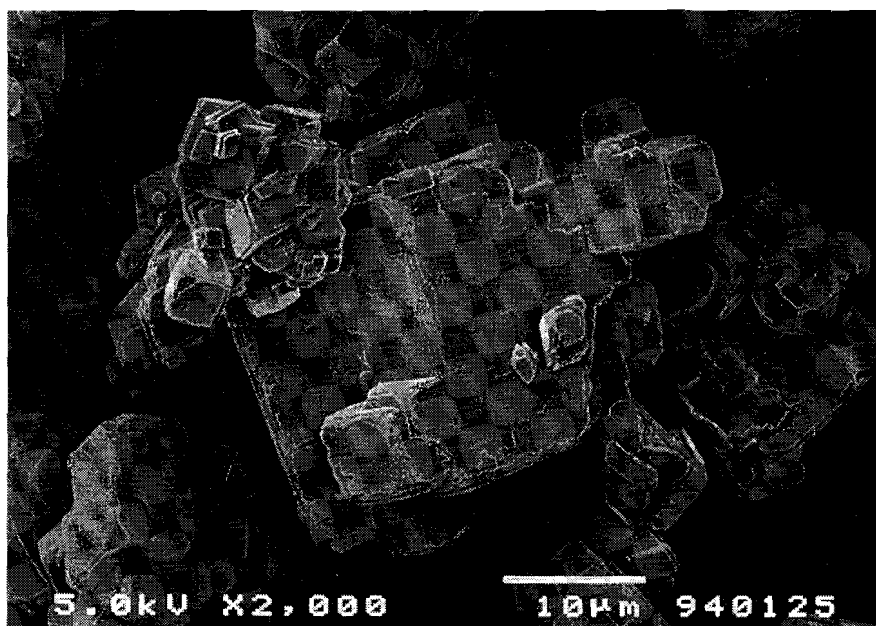
Fig. 5. SEM photographs of calcite seeds with an outgrowth factor of 1.7 grown in solutions with (a) and without (b) cadmium.
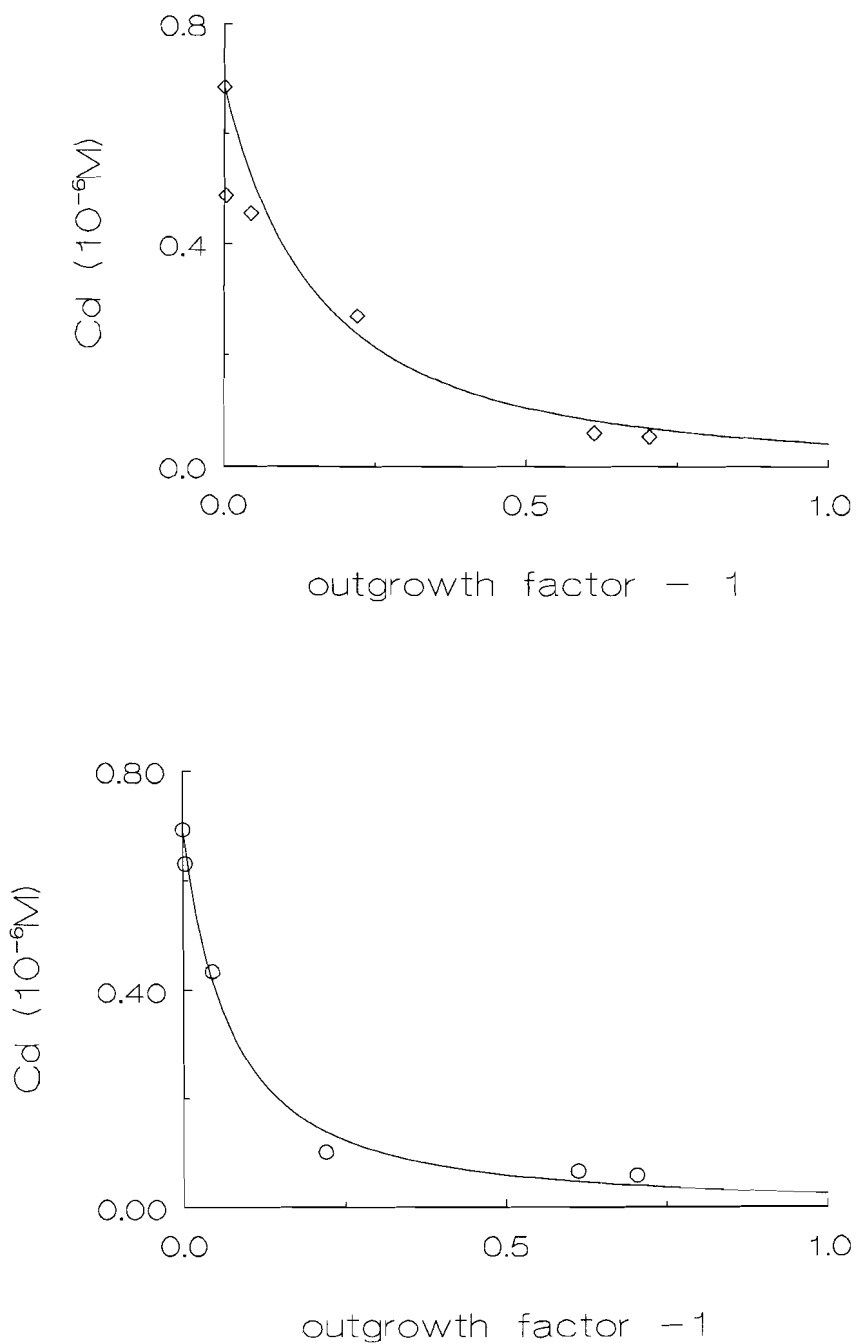
Fig 6. The Cd concentration versus the outgrowth factor during experimental runs 2-6 (a) and 4-7 (b) (Apx. 4).

4.4.2.2. Effect of solution composition (σ and pH).

In Fig. 7a-d the K and D values are plotted versus $Rlin$ and versus σ for calcite batch A (Apx 4A) at different pH values. The supersaturation (σ) was varied by changing the free Ca^{2+} (and total Ca) concentration (see Fig. 2). The growth rates increase with increasing σ and decreasing pH (i.e. increasing bicarbonate concentration at equal σ). The increase in $Rlin$ with increasing $[Ca^{2+}]$ is accompanied by a decrease in K and D. The decrease in D with increasing $Rlin$ is also observed for Zn (Apx 4C) and for Cd when the growth rate is increased by increasing the free carbonate activity or by decreasing the amount of seeds (Lorens, 1981). These changes of D with growth rate must be caused by either surface processes or by effects of the surface microtopography, since bulk diffusion can be excluded as the rate limiting factor during calcite growth in these experiments. Differences in the surface processes such as adsorption at the surface, surface diffusion or integration into kink sites, may cause the decrease in D. However, since surface diffusion is not considered to be a rate controlling step in crystal growth from ionic solution (Chang and Donohue, 1988; Gratz et al., 1993), the most important step for Cd incorporation must be the integration at kink sites. Lorens (1981) explained the decrease in D with growth rate by insufficient time for coordination of Cd with carbonate in a cation site. This would imply that the increase in the kink site density with increasing growth rate, is outweighed by kinetic factors. It remains, however, difficult when the growth conditions (e.g. σ) are varied, to attribute changes in D unambiguously to either the kinetics or to the changes in surface microtopography that can result from the different growth conditions.

For a given pH value D decreases with increasing σ according to the lines in Fig. 7. This decrease is generally expected (Burton, 1953; Lorens, 1981; Morse and Bender, 1990). The fact, however, that the lines do not coincide for the different pH values, or in other words that no unique relationship exists between D and $Rlin$, proves that also the solution composition plays an important role in the Cd incorporation process. At the same $Rlin$ but at different pH values (i.e. solution compositions) the composition and structure of the adsorption layer and/or the surface microtopography are apparently not similar. This also explains why experiments in which only the values of D and $Rlin$ are considered, and not the solution composition (pH), as indicated by the three crosses in Fig. 8 as an arbitrary example, could lead to the conclusion that D increases with $Rlin$. In a similar way, various values for the slope n of the log ($Rlin$) versus log(σ) plot (Fig. 1) can be obtained, when differences in the solution composition are ignored.

Paquette and Reeder (1995) have shown that increasing the calcite crystal growth by increasing either the free calcium or (bi) carbonate concentration, influences the anisotropy of the step velocities and the development of the growth hillocks on the {1014} face in a different way. The growth hillock consists of 4 "faces" with two different kink types each. These eight types of kink sites each have their own size and geometry, resulting in different affinities for foreign element incorporation (Gratz et al., 1993). The Cd^{2+} ion, 5% smaller than Ca^{2+}, would perhaps fit best at some particular sites. Analogously to the findings of Paquette and Reeder (1995) for Mn^{2+}, an increase in growth rate by more Ca^{2+} will result in a relative increase in the size of the hillock faces with kink sites favourable for foreign ions, probably also Cd ions, whereas an increase in carbonate (and likely also in bicarbonate) will cause a relative decrease. At a certain growth rate the degree of Cd incorporation will therefore depend not only on the interaction time at the surface, and the competition with other species, but also on the surface microtopography, which depends on the way in which the growth rate was established. A change in surface and hillock features could therefore explain the higher K and D values found at higher pH (= lower $[C]_T$) values. Such a change
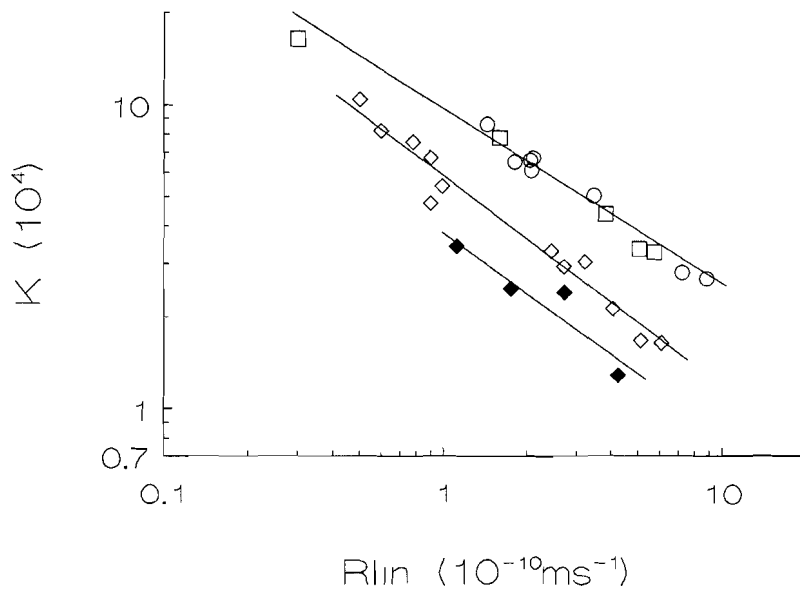
a)
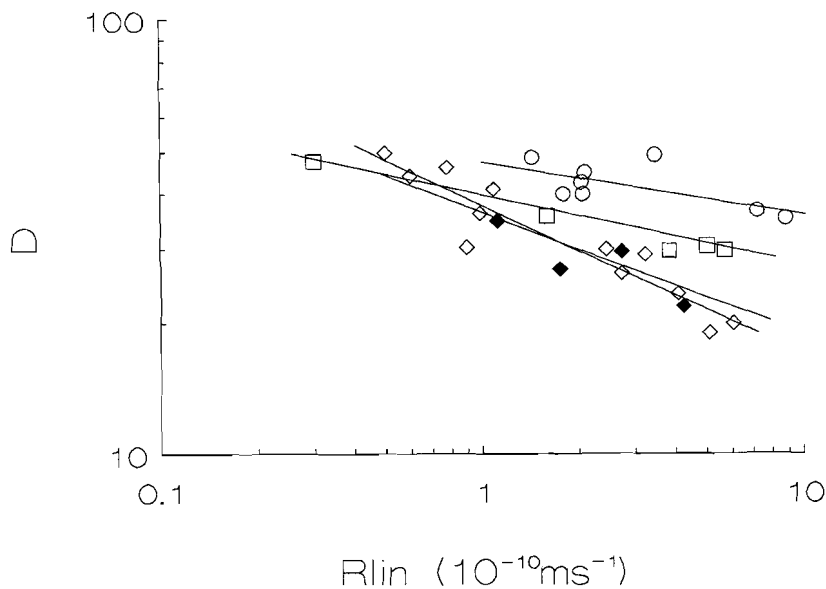
b)

Fig. 7 (a and b). K and D values for Cd partitioning as calculated from equations 5 and 6 versus the linear growth rate (a and b). Calcite seeds were from batch A. Best linear fits are drawn for pH = 8.90 and C_T = 7.5 mM (O), pH = 8.05 and C_T = 40 mM (□), pH = 7.66 and C_T = 60 mM (◊), pH = 7.56 and C_T = 50 mM (♦). Further details can be found in Apx. 4A.
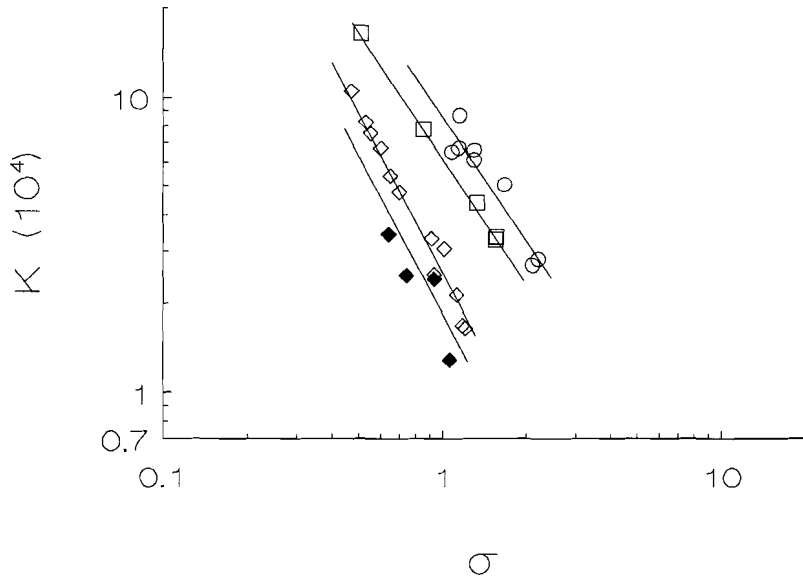
c)
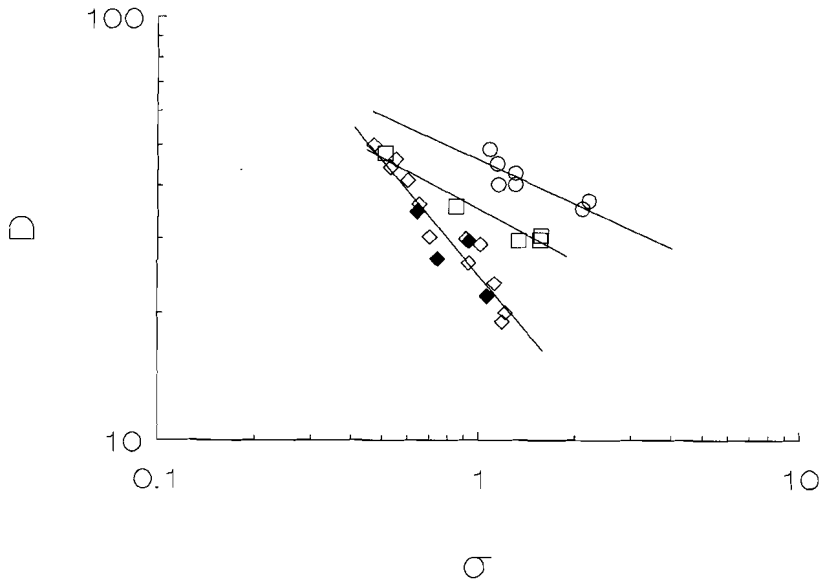
d)

Fig. 7 (c and d). K and D values for Cd partitioning as calculated from equations 5 and 6 versus the supersaturation. Calcite seeds were from batch A. Best linear fits are drawn for pH = 8.90 and C_T = 7.5 mM (O), pH = 8.05 and C_T = 40 mM (□), pH = 7.66 and C_T = 60 mM (◊), pH = 7.56 and C_T = 50 mM (◆). Further details can be found in Apx. 4A.
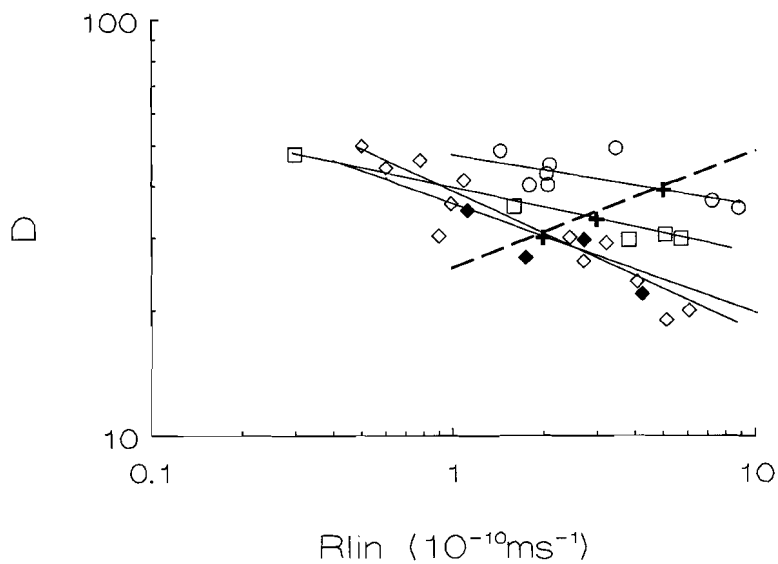
Fig. 8. A choice of solutions conditions (+) from Fig. 7b, which would produce an inverse trend in the *D* versus *Rlin* relationship (dashed line).
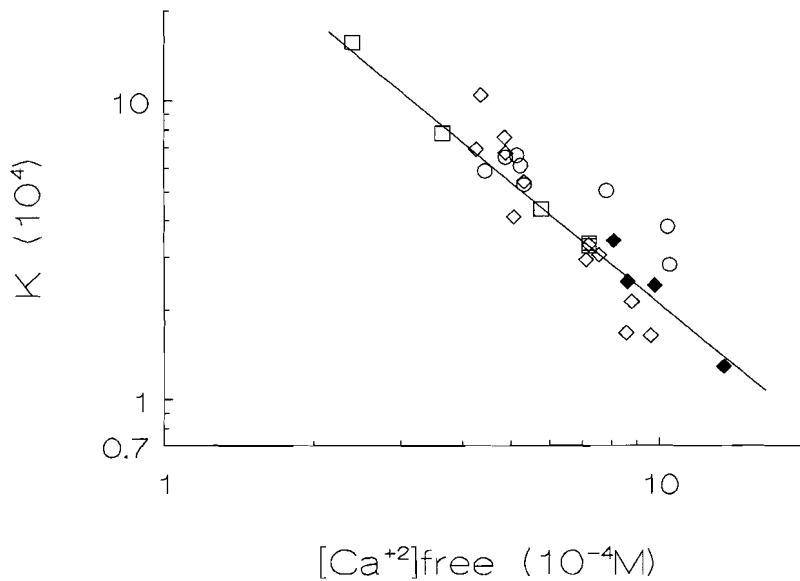
Fig. 9. Best linear fit for the *K* values versus the free $[Ca^{2+}]$ for Cd partitioning in the same experiments as in Fig. 7.

could not be observed with AFM, due to the fact that the scan areas were too small. Still some other possibilities can be thought of, namely, a higher contribution of $CdCO_3^0$ to Cd^{2+} sorption at pH = 8.90 (Apx 1) or the change in the surface charge of calcite towards negative values at pH > 8.2 (Mishra, 1978). This is, however, not likely since the small variation in $[C]_T$ (and therefore in $CdCO_3^0$) at pH = 8.90 does not have a great impact on the D versus *Rlin* curve, and Cd adsorption on calcite was found to be a result of chemical rather than electrostatic factors (Van der Weijden et al., 1994).

In Fig. 9, K is plotted versus the free $[Ca^{2+}]$. The data for the different pH values all seem to conform roughly to a single line. This suggests that the different D values at various pH values (but equal σ) are a result of a similar competition behavior of Cd and Ca for the same adsorption sites at various pH values. In that case the lower K and D values at the lower pH values in Fig. 7 must somehow be related to the higher contribution of bicarbonate to calcite crystal growth. There are, however, probably also effects of the surface microtopography.

4.4.2.3. Comparison with literature data.

In Fig. 10 the data for Cd partitioning between calcite and solutions with a high ionic strength (0.7 M NaCl), as obtained by Lorens (1981) are plotted. Main differences between his experiments and the ones described in this study are the use of Na^+ instead of K^+, the use of a pH-stat instead of a chemo-stat, the lower pH values (7.3-7.4), the lower free carbonate concentrations (10^{-6} M), the higher free calcium concentrations (10^{-2} M), the precipitation of only small amounts of calcite (1 mg) on different amounts of unripened dry seeds (3-200 mg), the variation in growth rate by varying the amount of seeds and/or the concentration of carbonate, and the addition of practically no Cd mass, but only a radiotracer (^{109}Cd). The higher D values are probably caused by the much lower Cd^{2+} concentration, in combination with the sorption site heterogeneity. This agrees with sorption experiments under similar conditions with ^{109}Cd tracer only, where much more (20-40%) sorption was observed than in the case of a Cd tracer in combination with Cd carrier.

4.4.2.4. Effect of seed crystal type.

In Fig. 11a-b the K and D values versus Rlin are plotted for calcite batch B at pH = 8.90 and pH = 8.05 (Apx 4B). Experiments were performed with ripened seeds of one year old (Exp. B 5, B 7) and a year and a half old (Exp.B 6). Instead of the expected decrease with *Rlin* as found for batch A, an increase is seen for both K and D. In general, the K and D values are lower than for batch A, and if D were solely based on the total concentrations of Cd and Ca instead of the activities of the free ions (see eq. 3), some of the values for D would be below unity. The values for D and K are even lower for the longer ripening times of 1.5 year. Another difference with batch A is that the Cd concentrations in the solid also increase with increasing precipitation rate. It is therefore certain that the reversed trend of D versus *Rlin* is not a result of mis-measurement or miscalculation. This trend inversion might be related to the slightly lower growth rate at low σ of batch B compared to batch A (see Fig. 3). The surface morphology is probably changed after longer ripening times, resulting in a different step/kink development. Also the presence of a contaminant, which effect is greatest at the lower supersaturations can play a role. SEM photographs of calcite growth on batch A and B, however, do not give decisive information regarding these two possibilities, and so as of

yet, it can only be assumed that the calcite surface properties are different for the two batches.

4.4.3 Geological relevance of chemo-stat experiments.

Compared to geological time scales, chemo-stat experiments with a maximum duration of 30 hours can not be regarded as a realistic simulation of most geochemical processes. Yet, the experiments are useful for obtaining insight in the effects that several system parameters may have on growth and incorporation processes.

The partition coefficient of Cd in foraminifera is estimated to be approximately 2 (Boyle, 1988), however, the growth rates associated with such a partition coefficient in laboratory experiments can not possibly apply to growth rates for foraminifera. Therefore, one may conclude e.g. that Cd incorporation in foraminifera is a biochemical rather than a chemical process, or that the presence of other species hinders Cd incorporation. In this light, further study on the influence of phosphate on the Cd incorporation in calcite using chemo-stat experiments, may be useful to examine the use of the Cd/Ca ratio in foraminifera as a tracer for paleoceanic nutrient concentrations.

For processes which encompass shorter time scales, chemo-stat experiments can indicate the conditions that are favorable or unfavorable for "foreign" element incorporation. For example, for carbonation processes in municipal waste (chapter 5), a slow CO_2 infiltration rate, resulting in the slow formation of $CaCO_3$, would probably result in a greater amount of heavy metal (e.g. Cd) removal and thereby reduce the mobility of hazardous elements.
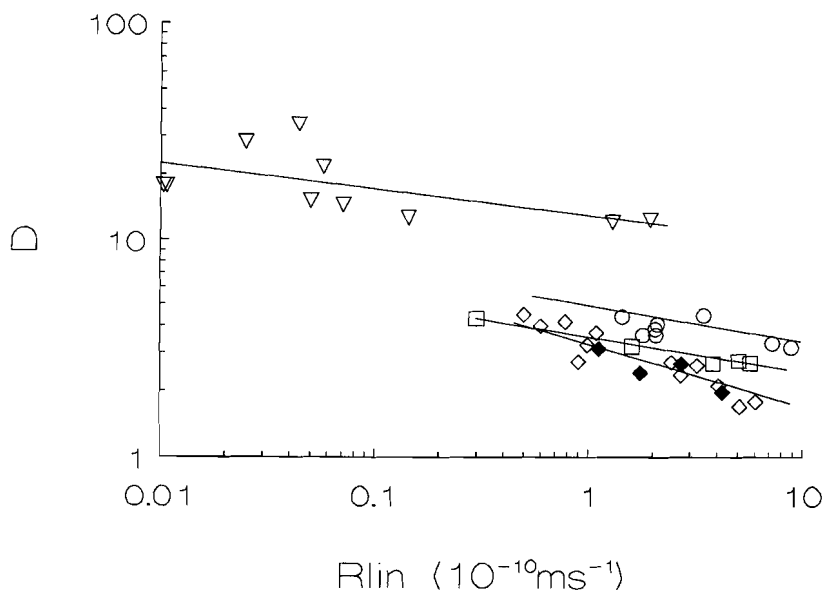
Fig. 10. Values for D based on total concentrations of Cd and Ca without correction for the free activities versus the linear growth rate for the experiments in Fig. 7b and for data presented by Lorens (∇) (1981).
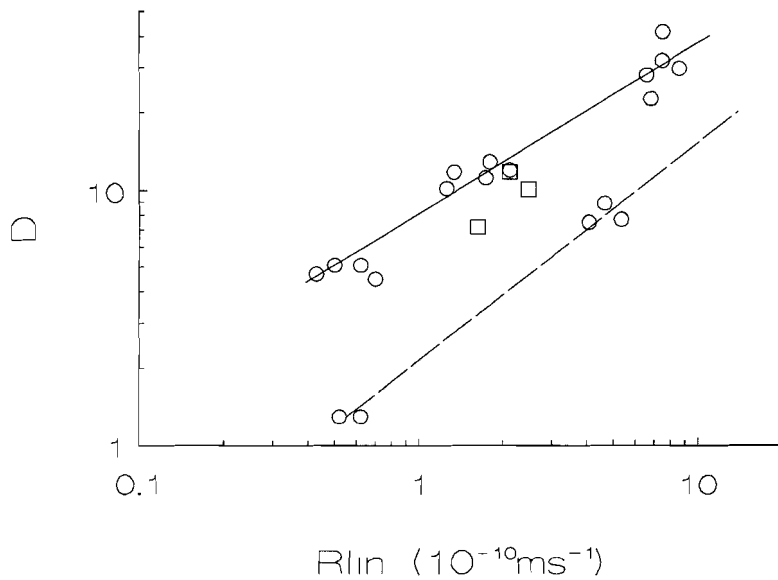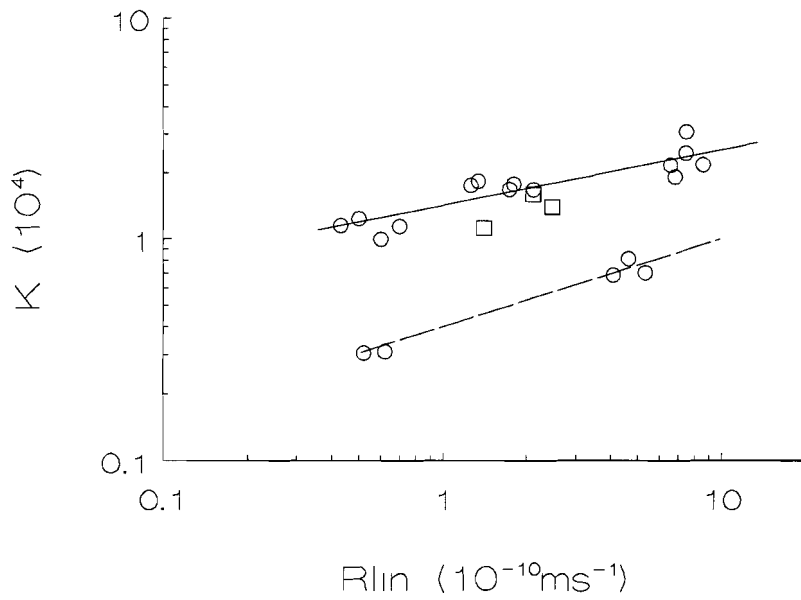
Fig. 11. K and D values for Cd partitioning as calculated from equations 5 and 6 versus the linear growth rate. Best linear fits are drawn for pH = 8.90 and C_T = 7.5 mM (O), pH = 8.05 and C_T = 40 mM (□) for experiments B5, B7 (solid line) and experiments B 6 (dashed line) (Apx. 4).

4.5. Conclusions

Calcite growth proceeds with an order 2.0 ± 0.3 in relative supersaturation, indicating spiral growth. The growth rate is higher at higher bicarbonate concentrations, i.e. lower pH values.

At different solution compositions, but equal growth rates, the value of the partition coefficient was higher at lower pH and for seeds crystals which were ripened shorter. Also, differences in the particular batch of calcite seeds, resulted in different trends: a decrease (with three months ripened seeds) or an increase (with 1 or 1.5 year ripened seeds), of the partition coefficient with increasing growth rates. Values found for $D(Cd)$ in this study are more than a factor three lower than in a study by Lorens (1981), which can be explained from the adsorption site heterogeneity, leading to lower Ds at higher Cd^{2+} concentrations.

Although in previous studies expressions were derived that relate a partition coefficient directly to a certain growth rate, this study indicates that not merely the growth rate, but also the way in which the growth rate is established determines the degree of partitioning. Furthermore, the ripening of the seeds, and the stoichiometry and supersaturation of a solution, can bring about changes in the surface features of calcite, a factor which is considered in few other partitioning studies. Macroscopic observations in this study show that the Cd partitioning must be influenced by the calcite surface structure.

Acknowledgments

References

Angus, J., Rainier J.B. and Rubstone M., 1979. Reliability of experimental partition coefficients in carbonate systems: evidence for inhomogeneous distribution of impurity cations. Chem. Geol., 271: 181-205.

Boyle, E.A., 1988. Cadmium: Chemical tracer of deepwater paleoceanography, Paleoceanography, 3: 471-489.

Burton, J.A., Prim, R.C., Schlichter, W.P., 1953. J. Chem. Phys., 21: 1987-1996.

Burton, E.A. and Walter, L.M., 1990. The role of pH in phosphate inhibition of calcite and aragonite precipitation rates in seawater. Geochim. Cosmochim. Acta 54: 797-808.

Chiang, P.P. and Donohue, M.D., 1988. A kinetic approach to crystallization from ionic solution. J. of Colloid and Interface Sci. 122: 230-250.

Christoffersen, J. and Christoffersen, M.R, 1990. Kinetics of spiral growth of calcite crystals and determination of the absolute rate constant. J. Cryst. Growth 100: 203-211.

Comans, R.N.J., Van der Sloot, H.A. and Bonouvrie, P.A., 1993. Geochemical reactions controlling the solubility of major and trace elements during the leaching of municipal solid waste incinerator residues. In: VIP -32 Municipal Waste Combustion. Proceedings of an international specialty conference, Williamsburg, Virginia, USA 667-680.

Dromgoole, E.L. and Walter, L.M., 1990. Iron and manganese incorporation into calcite: effects of growth kinetics, temperature and solution chemistry. Chem. Geol., 81: 311-326.

Gómez-Morales, J., Torrent Burgués, J., López-Macipe, A. and Rodríguez-Clemente, R., 1995. Calcium carbonate precipitation from solutions with varying Ca^{2+}/carbonate ratios. *Submitted* to J. Cryst. Growth.

Gratz, A.J., Hillner, P.E. and Hansma, P.K., 1993. Step dynamics and spiral growth on calcite. Geochim. Cosmochim. Acta, 57: 491-495.

Ichikawa, M. and Ichikuni, M.,1984. Uptake of sodium and potassium by calcite. Chem. Geol. 42: 137-146.

Lorens, R.B., 1981. Sr, Cd, Mn and Co distribution coefficients in calcite as a function of calcite precipitation rate. Geochim. Cosmochim. Acta, 45: 553-561.

Mishra, S.K., 1978. The electrokinetics of apatite and calcite in inorganic electrolyte environment. Int. J. Miner. Proc., 5: 69-83.

Morel, F.M.M., 1983. Principles of Aquatic Chemistry, Wiley, Chichester, 446 pp.

Morse, J.W. and Bender, M.L., 1990. Partition coefficients in calcite: Examination of factors influencing the validity of experimental results and their application to natural systems. Chem. Geol., 82: 265-277.

Mucci, A. and Morse, J.W., 1983. The incorporation of Mg^{2+} and Sr^{2+} into calcite overgrowths: influences of growth rate and solution composition. Geochim. Cosmochim. Acta, 47: 217-233.

Nielsen, A.E. and Toft, J.M., 1984. Electrolyte crystal growth kinetics. J. Cryst. Growth 67: 278-288.

Paquette, J. and Reeder, R.J., 1995. Relationship between surface structure, growth mechanism, and trace element incorporation in calcite. Geochim. Cosmochim. Acta, 59: 735-751.

Qiwei, W., 1991. Study on the crystal growth of calcite from solution in the presence of zinc ions. Thesis in chemistry. University of Ryukyus (China), 100 pp.

Reeder, R.J. and Grams, J.C., 1987. Sector zoning in calcite cement crystals: Implications for trace element distributions in carbonates. Geochim. Cosmochim. Acta, 51: 187-194.

Romanek, C.S., Grossman, E.L., Morse, J.W., 1992. Carbon isotopic fractionationin synthetic aragonite and calcite. Effects of temperature and precipitation rate. Geochim. Cosmochim. Acta 56: 419-430.

Sigg, L. and Stumm, W., 1991. Aquatische Chemie. Teubner Verlag, Stuttgart, Germany, 388 pp.

Staudt, W.J., Reeder, R.J. and Schoonen, M.A.A., 1994. Surface structural controls on compositional zoning of SO_4^{2-} and SeO_4^{2-} in synthetic calcite single crystals. Geochim. Cosmochim. Acta. 58: 2087-2098.

Stipp, S.L., Parks, G.A. Nordstrom, D.K. and Leckie, J.O., 1993. Solubility-product and thermodynamic properties of synthetic otavite, $CdCO_3$ (s), and aqueous association constants for the Cd (II) - CO_2-H_2O system. Geochim. Cosmochim. Acta, 57: 2699-2713.

Tai, C.Y., Chen, P. and Shih, S., 1993. Size dependent growth and contact nucleation of calcite crystals. AIChE J. 39 : 1472- 1481.

Van der Eerden, J.P. and Müller-Krumbhaar, 1986. Formation of macrosteps due to time dependent impurity adsorption. Electrochim. Acta 31: 1007-1012.

Van Gaans, P.F.M., 1989. WATEQX, version October 1989.

Van der Weijden, R.D., Van der Weijden, C.H. and Comans, R.N.J., 1994. Sorption and sorption reversibility of cadmium on calcite under simulated riverine, estuarine and marine conditions. Mar. Chem. 47: 65-74.

Van der Weijden, R.D., Van der Heijden, A.E.D., Witkamp, G.J. and Van Rosmalen, G.M., 1995. The influence of total calcium and total carbonate on the growth rate of calcite. *Accepted* by J. Cryst. Growth.

Wada, N. Yamashita, K. and Umegaki, T, 1995. Effects of divalent cations upon nucleation, growth and transformation of calcium carbonate polymorphs under conditions of double diffusion. J. Cryst. Growth, 148: 297-304.

Weijnen, M., 1986. The influence of additives on the crystallization of gypsum. Dissertation Delft Technical University, 207 pp.

White, A.F., 1977. Sodium and potassium coprecipitation in aragonite. Geochim. Cosmochim. Acta 41: 613 -625.

Zhong, S. and Mucci, A., 1989. Calcite and aragonite precipitation from seawater solutions of various salinities: Precipitation rates and overgrowth compositions. Chem. Geol. 78: 283-299.

Zhong, S. and Mucci A., 1993. Calcite precipitation in seawater using a constant addition technique: a new overall kinetic expression. Geochim. Cosmochim. Acta 57: 1409-1418.

Zhong, S. and Mucci A, 1995. Partitioning of rare earth elements (REE) between calcite and seawater solutions at 25°C and 1atm and high dissolved REE concentrations. Geochim. Cosmochim. Acta 59: 443-455.

Appendices

Appendix 1 Activities of the solution species as calculated with Wateqx (Van Gaans, 1989) at various pH with $[Ca]_T = 6\times10^{-4}$ M

pH = 7.555 $PCO_2 = 0.05$		pH = 7.655 $PCO_2 = 0.05$	
species	activity (M)	species	activity (M)
Ca^{2+}	1.44×10^{-4}	Ca^{2+}	1.40×10^{-4}
CO_3^{2-}	4.71×10^{-5}	CO_3^{2-}	7.13×10^{-5}
HCO_3-	2.98×10^{-2}	HCO_3-	3.59×10^{-2}
H_2CO_3	1.94×10^{-3}	H_2CO_3	1.86×10^{-3}
$CaCO_3^{\circ}$	0.91×10^{-5}	$CaCO_3^{\circ}$	1.33×10^{-5}
$CaHCO_3^{+}$	4.07×10^{-5}	$CaHCO_3^{+}$	4.75×10^{-5}
K^{+}	4.78×10^{-1}	K^{+}	4.84×10^{-1}
Cl^-	4.46×10^{-1}	Cl^-	4.47×10^{-1}
KCO_3-	1.13×10^{-4}	KCO_3-	1.73×10^{-4}
Cd^{2+}	3.61×10^{-9}	Cd^{2+}	3.61×10^{-9}
$CdCl^-$	1.61×10^{-7}	$CdCl^-$	1.61×10^{-7}
$CdCl_2$	2.87×10^{-7}	$CdCl_2$	2.87×10^{-7}
$CdCl_3-$	8.11×10^{-8}	$CdCl_3-$	8.11×10^{-8}
$CdCl_4^{2-}$	7.23×10^{-9}	$CdCl_4^{2-}$	7.23×10^{-9}
$CdCO_3^{\circ}$	1.71×10^{-9}	$CdCO_3^{\circ}$	2.59×10^{-9}

pH = 8.050 $PCO_2 = 0.015$		pH = 8.898 $PCO_2 = 0.000316$	
species	activity	species	activity
Ca^{2+}	1.41×10^{-4}	Ca^{2+}	1.48×10^{-4}
CO_3^{2-}	1.18×10^{-4}	CO_3^{2-}	1.36×10^{-4}
HCO_3-	2.40×10^{-2}	HCO_3-	3.91×10^{-3}
H_2CO_3	4.99×10^{-3}	H_2CO_3	1.16×10^{-5}
$CaCO_3^{\circ}$	2.22×10^{-5}	$CaCO_3^{\circ}$	2.68×10^{-5}
$CaHCO_3^{+}$	3.20×10^{-5}	$CaHCO_3^{+}$	5.47×10^{-6}
K^{+}	4.73×10^{-1}	K^{+}	4.51×10^{-1}
Cl^-	4.46×10^{-1}	Cl^-	4.47×10^{-1}
KCO_3-	2.80×10^{-4}	KCO_3-	3.07×10^{-4}
Cd^{2+}	3.60×10^{-9}	Cd^{2+}	3.57×10^{-9}
$CdCl^-$	1.60×10^{-7}	$CdCl^-$	1.60×10^{-7}
$CdCl_2$	2.86×10^{-7}	$CdCl_2$	2.85×10^{-7}
$CdCl_3-$	8.07×10^{-8}	$CdCl_3-$	8.04×10^{-8}
$CdCl_4^{2-}$	7.20×10^{-9}	$CdCl_4^{2-}$	7.16×10^{-9}
$CdCO_3^{\circ}$	4.26×10^{-9}	$CdCO_3^{\circ}$	4.90×10^{-9}

Appendix 2 Aqueous speciation reactions and equilibrium constants

Reaction					$\log K$	Source *)
CO_3^{2-}	+	H^+	=	HCO_3^-	10.3	1
CO_3^{2-}	+	$2H^+$	=	$H_2CO_3^o$	16.7	1
Ca^{2+}	+	CO_3^{2-}	=	$CaCO_3^o$	3.15	1
Ca^{2+}	+	HCO_3^-	=	$CaHCO_3^+$	11.5	1
Cd^{2+}	+	Cl^-	=	$CdCl^+$	1.97	1
Cd^{2+}	+	$2Cl^-$	=	$CdCl_2^o$	2.59	1
Cd^{2+}	+	$3Cl^-$	=	$CdCl_3^-$	2.4	1
Cd^{2+}	+	CO_3^{2-}	=	$CdCO_3^o$	4.0	1
Cd^{2+}	+	$2CO_3^{2-}$	=	$Cd(CO_3)_2^{2-}$	4.6	1
Cd^{2+}	+	$3CO_3^{2-}$	=	$Cd(CO_3)_3^{4-}$	6.24	1
Cd^{2+}	+	$H^+ + CO_3^{2-}$	=	$CdHCO_3^+$	12.4	1
Cd^{2+}	+	H_2O	=	$CdOH^+ + H^+$	10.1	1
Zn^{2+}	+	Cl^-	=	$ZnCl^+$	0.43	1
Zn^{2+}	+	$2Cl^-$	=	$ZnCl_2o$	0.45	1
Zn^{2+}	+	$3Cl^-$	=	$ZnCl_3^-$	0.56	1
Zn^{2+}	+	$4Cl^-$	=	$ZnCl_4^{2-}$	0.70	1
Zn^{2+}	+	CO_3^{2-}	=	$ZnCO_3^o$	5.23	1
Zn^{2+}	+	HCO_3^-	=	$ZnHCO_3^+$	12.54	1
Zn^{2+}	+	$2CO_3^{2-}$	=	$Zn(CO_3)_2^{2-}$	10.21	1
Cd^{2+}	+	CO_3^{2-}	=	$CdCO_3$ (s)	12.1	2
Zn^{2+}	+	CO_3^{2-}	=	$ZnCO_3$ (s)	10.0	1
Ca^{2+}	+	CO_3^{2-}	=	$CaCO_3$ (s)	8.43	3

1) Morel (1983)
2) Stipp (1993)
3) Sigg and Stumm (1991)

Appendix 3 Derivation of the expression for the partition coefficient for a semi-batch system

Let V and [Cd] denote the time-dependent reaction volume and Cd concentration respectively. The cadmium concentration in the burette equals the cadmium concentration of the reaction volume when $t = 0$, $[Cd]_{t=0}$. If K denotes the distribution coefficient between Cd in the solution and the formed calcite crystals ($[CaCO3]_{formed,t}$), the dynamic behavior of the Cd concentration in the reaction volume can be expressed by the following mass balance:

$$\frac{d(V[Cd])}{dt} = [Cd]_{t=0}\frac{dV}{dt} - K[Cd]_t[CaCO3]_{formed,t}\frac{dV}{dt} \qquad (1)$$

Dividing both sides by dV/dt, eq 1 can be rewritten as:

$$\frac{d[Cd]_t}{[Cd]_{t=0} - [Cd]_t(1 + K[CaCO3]_{formed,t})} = dlnV \qquad (2)$$

By integrating this equation with the boundary conditions $[Cd] = [Cd]_0$ and $V = V_0$ at $t = 0$, and after application of the identity $a^x = e^{x/na}$ the following solution is obtained for eq 2:

$$\frac{1 + K[CaCO_3]_{formed,t}(\frac{V_t}{V_{t=0}})^{-(K[CaCO3]_{formed,t})}}{(1 + K[CaCO_3]_{formed,t})} = \frac{[Cd]_t}{[Cd]_{t=0}} \qquad (3)$$

Now a value for K has to be found to fulfill the equality 3, by finding the root of the equation:

$$f(K) = \frac{1 + K[CaCO_3]_{formed,t}(\frac{V_t}{V_{t=0}})^{-(K[CaCO3]_{formed,t})}}{(1 + K[CaCO_3]_{formed,t})} - \frac{[Cd]_t}{[Cd]_{t=0}} \qquad (4)$$

Appendix 4 Calcite growth conditions and solution compositions of the supersaturated soluions. Cd_{solM} denotes the Cd concentration as measured in the grown calcite, whereas Cd_{solC} denotes the Cd concentration as calculated from the initial (Cd_i) and final (Cd_f) aqueous Cd concentrations.
A) Data for growth and partitioning with ripened seeds of three months old. B) Data for growth and Cd partitioning with ripened seeds of a year (5,7) and a year and a half (6) old. C) Data for growth and Zn partitioning with ripened seeds of three months old. D) Data for growth and partitioning for various amounts of seeds (3 months old)

Exp	pH	CaT	C_T	seeds	growth	σ	Cdi	Cdf	Cd$_{solC}$	Cd$_{solM}$	K(Cd)	D	Rlin
		10^{-4}M	mM	mg	mg		ppb	ppb	ppm	ppm			10^{-10} ms^{-1}
A													
1-1	7.555	9.7	50	164.3	48.4	0.74	155	42.0	1790	2040	24850	26.9	1.75
1-2	7.555	9.1	49	163.6	48.9	0.64	155	29.4	1980	2541	34289	34.8	1.12
1-3	7.565	11.0	50	164.3	48.6	0.93	155	43.0	1770	1810	24139	29.6	2.73
1-4	7.560	15.2	49	175.9	43.0	1.06	155	81.0	1370	1240	12890	21.9	4.24
2-1	7.657	8.0	60	175.5	56.0	0.93	75	15.5	850	870	29405	26.3	2.72
2-2	7.649	6.0	60	177.6	52.2	0.65	73	7.8	970	870	54008	36.2	0.99
2-3	7.653	4.9	57	162.6	52.0	0.47	78	4.0	1060	1160	104708	57.3	0.50
2-4	7.650	8.5	64	180.1	53.0	1.01	73	15.0	870	830	30596	29.1	3.23
2-5	7.654	8.1	59	151.0	52.0	0.91	76	14.1	922	1010	33153	30.0	2.45
2-6	7.650	5.5	61	162.2	51.0	0.60	72	6.0	970	920	67127	41.2	1.09
2-7	7.660	10.8	60	175.6	54.0	1.21	73	28.0	680	710	16469	19.9	6.10
2-8	7.653	5.5	60	162.9	52.0	0.55	71	5.1	950	1040	75582	46.2	0.78
2-9	7.657	9.9	61	169.2	44.9	1.12	70	23.0	790	680	21321	23.5	4.08
2-10	7.648	9.6	59	166.4	48.7	1.18	72	28.0	700	670	16786	18.1	5.11
2-11	7.666	4.8	64	159.4	46.3	0.53	77.5	6.0	1090	1400	69003	37.0	0.60
2-12	7.670	5.7	68	166.7	51.2	0.70	73	10.1	920	980	41167	26.3	0.86
3-1	8.059	6.5	44	53.3	49.7	1.33	79	10.6	1030	1230	43770	29.7	3.84
3-2	8.055	8.1	43	162.6	49.8	1.56	77	14.4	960	1280	33548	30.5	5.06
3-3	8.059	4.1	44	158.3	49.5	0.85	77	5.8	1100	1120	77995	35.7	1.60
3-4	8.049	8.1	43	148.2	49.7	1.55	77.5	14.9	960	950	32840	29.8	5.73
3-5	8.051	2.7	45	153.4	60.1	0.51	76.5	2.8	980	930	156652	41.7	0.30
4-1	8.898	8.8	6.5	171.4	51.3	1.67	75.5	9.0	1000	1280	50305	49.4	3.47
4-2	8.898	11.7	7.3	162.9	52.8	2.20	75	15.0	920	1040	38276	50.0	7.24
4-3	8.899	6.0	7.1	152.5	48.3	1.14	76.5	8.3	1050	1320	52727	35.3	2.10
4-4	8.895	5.8	7.6	165.6	51.4	1.30	76	6.3	1020	1090	66049	42.8	2.05
4-5	8.896	5.0	7.1	170.7	45.0	1.08	77	6.4	1110	1264	58649	33.0	1.44
4-6	8.898	5.5	6.9	168.2	53.0	1.15	77	7.4	980	840	65051	40.2	1.80
4-7	8.900	5.9	8	166.8	53.3	1.30	73.0	6.5	960	950	61067	40.2	2.07
4-8	8.900	11.8	6.6	154.0	47.9	2.10	70	17.4	900	1040	28327	37.3	8.86
B													
5-1	8.898	3.6	6.8	172.0	54.4	0.73	70	32.4	520	375	11536	4.7	0.43
5-2	8.893	6.4	7.3	174.5	52.5	1.30	69	24.6	640	680	16806	11.2	1.74
5-3	8.898	6.4	7.6	183.3	57.7	1.44	69	23.8	620	560	16772	12.0	2.12
5-4	8.893	4.6	6.6	187.1	57.4	0.89	69	34.7	460	N.D.	10003	5.1	0.62
5-5	8.898	3.5	6.6	158.2	48.3	0.66	70	34.0	530	640	11454	4.5	0.70
5-6	8.898	6.5	7.8	172.0	52.0	1.50	71	24.4	680	570	17770	12.9	1.80
5-7	8.898	5.8	7.7	155.6	51.1	1.30	71	23.7	690	670	18359	11.8	1.34

Exp	pH	CaT	C_T	seeds	growth	σ	Cdi	Cdf	Cd_{solC}	Cd_{solM}	$K(Cd)$	D	$Rlin$
		10^{-4} M	mM	mg	mg		ppb	ppb	ppm	ppm			10^{-10} ms^{-1}
5-8	8.892	5.2	7.7	202.6	60.7	1.19	71	22.4	630	670	17551	10.2	1.26
5-9	8.898	3.7	6.5	160.5	42.2	0.70	66	32.1	550	535	12391	5.1	0.50
5-10	8.890	10.6	6.8	159.1	44.0	1.94	68	32.0	730	870	19136	22.7	6.81
5-11	8.898	12.1	7.1	149.6	43.9	2.24	68	15.9	890	750	30771	41.7	7.49
5-12	8.898	11.7	6.9	147.8	52.3	2.14	68	21.2	740	860	21684	28.2	6.57
5-13	8.898	12.2	6.6	161.9	52.5	2.14	68	21.0	735	800	21857	29.8	8.58
5-14	8.898	11.7	6.6	154.5	48.9	2.06	67	19.0	780	915	24580	32.1	7.47
6-1	8.893	10.0	6.6	142.5	44.9	1.83	72	48.0	400	310	7039	7.7	5.34
6-2	8.900	9.8	6.5	145.3	44.7	1.79	77	51.9	420	380	6871	7.5	4.08
6-3	8.900	9.8	6.4	162.2	45.3	1.79	80	50.0	500	52	8145	8.9	4.65
6-4	8.898	3.7	6.8	149.9	45.3	0.75	75	62.0	210	185	3095	1.3	0.62
6-5	8.897	3.9	6.4	175.4	51.8	0.73	76.5	62.0	210	200	3051	1.3	0.52
7-1	7.965	6.2	39	177.5	57.8	0.97	65	22.0	590	371	17156	11.8	2.11
7-2	7.964	5.8	41	155.1	60.9	0.95	65	23.3	550	560	15593	10.1	2.47
7-3	7.985	5.8	40	166.4	55.4	1.63	65	31.0	390	390	11229	7.2	1.70
C	**(Zn)**												
8-1	8.050	7.8	43.6	145.1	45.6	1.51	20	6.0	-	196	22568	19.7	5.03
8-2	8.050	6.5	42.5	168.9	52.9	1.29	20	4.4	-	258	27517	20.3	4.11
8-3	8.053	5.7	42.8	169.9	52.8	1.14	20	<1	-	311	110899	64.6	2.78
D	**(Cd)**												
9-1	8.898	7.4	6.8	48.8	3.5	1.54	76.9	25.2	2378	-	51606	42.4	3.29
9-2	8.898	7.4	6.8	33.0	3.5	1.54	79.7	25.7	2484	-	52357	43.0	3.27
9-3	8.898	7.5	6.8	414.7	3.5	1.56	78.9	23.8	2534	-	55469	46.3	3.01
9-4	8.898	7.5	6.8	377.8	3.5	1.56	82.1	22.6	2737	-	59743	50.0	3.05

Chapter 5

Precipitation and heavy metal immobilization resulting from carbonation of filtered bottom ash leachates

Abstract— The effects of carbonation in filtered bottom ash leachates are investigated with laboratory experiments. At pH = 8.57 a precipitate is formed and a buffering effect is observed as the pH further decreases. The composition and amount of precipitate depend on the composition of the leachate and the carbonation rate. Composition, amount and formation rate of the precipitate in their turn influence the degree of heavy metal immobilization. A specific study of the removal of Cd shows a sudden decrease in concentration at the same pH at which precipitation occurs. Comparison with carbonation effects in $Al(OH)_3$ and $Ca(OH)_2$ solutions suggests that not only the trace amounts of calcite, but also the aluminumhydroxides/ hydrous aluminosilicates in the precipitate of the leachates can account for the coprecipitation of heavy metals. The quantity of calcite precipitation could be increased if levels of organic species in the leachates and carbonation rates are reduced.

R.D. van der Weijden and R.N.J. Comans

5.1. Introduction

MSWI bottom ash is a residue of municipal solid waste after incineration at 800 -1400 °C. The ash contains high levels of salts and heavy metals and therefore deposition poses a problem to the environment. After disposal or exposure in the environment of utilization, biogeochemical processes may lead to mobilization of the heavy metals. When the salts are not washed out at the early stage of weathering (pH range 10 - 12), they may aggravate leaching of heavy metals by the formation of complexes at a later stage (pH range 8 - 10). Leaching tests are customary tools to estimate the degree to which the metals are mobilized and can include study of the effects of water/ash interaction, CO_2 interaction and changes in redox potential. The experiments usually take place over a shorter period (hours) than the actual processes (years), yielding results that may differ from reality, since reactions with slow kinetics or great induction times may not have reached completion. Another setback is that batch experiments are closed systems in which the leached elements remain, whereas at the actual ash disposal site, an open system, they may be washed in or out.

Studies on the composition of the ash and the corresponding leachates show that the least volatile elements (Ca, Si, Al, Fe) make up the bulk of the solid. Glassy particles (72%) that are Si-rich, Ca,Si-rich and Al,Si-rich and hematite particles are therefore most abundant. The volatile elements usually have condensed on these particles as a coating of an oxide (Kirby and Rimstidt, 1993; Zevenbergen, 1994).

Despite the heterogeneity of bottom ashes, their leaching behavior is quite consistent (Kirby and Rimstidt, 1993; Zevenbergen, 1994; Comans et al., 1993). Upon suspension of the ash in water, portlandite, lime, and glasses that contain alkaline oxides dissolve, resulting in a very alkaline solution (pH = 10 - 12). Glasses dissolve easily at this pH and transformation of glass into clays begins. Heavy metals are either adsorbed or are present as a hydroxide at this high pH. At pH values of 10 - 12, mineral phases like ettringite, $(Ca_6Al_2(SO_4)_3(OH)_{12}.26H_2O)$ and gypsum $(CaSO_4.2H_2O)$ may determine Ca solubility (Comans and Meima, 1994). A further decrease in pH occurs, due to CO_2 infiltration (carbonation) from the atmosphere or as a result of biodegradation. The mobilization of heavy metals, however, is restricted by adsorption onto or incorporation into a $CaCO_3$ phase. The $CaCO_3$ phase, which precipitates as a result of carbonation, is slightly more soluble than calcite (Kirby and Rimstidt, 1993; Stokman, 1994; Schramke, 1992) and is thought to be monohydrocalcite or calcite containing sulfate and Mg ions (Schramke). These same ions can retard the precipitation process significantly (Meyer, 1984; Plummer and Busenberg; 1985). Therefore, the induction time for $CaCO_3$ precipitation, but also for other inorganic precipitates, may be longer than the duration of the experiment. At low pH values of 4 - 8, the carbonates will dissolve, and the heavy metals will be released.

Most leaching experiments thus far, involved the behavior of suspensions of bottom ash (Kirby and Rimstidt, 1993; Chandler et al., 1994; Schramke, 1992). In this paper a study is presented on the behavior of the filtered bottom ash leachates obtained at high pH under N_2, upon equilibration with a CO_2/N_2 stream. Primary goals were to investigate the quantity of $CaCO_3$ precipitation as a result of carbonation, and the impact it has on the mobility of heavy metals. The effects observed in the leachates were compared to those observed in calcium hydroxide, aluminum hydroxide and synthetic simulated leachate solutions. Also, the influence of the gas flow (carbonation) rate, the composition of the gas, and the composition of the leachate on the carbonation process is discussed.

5.2. Materials and Methods

5.2.1 Materials

All chemicals used, $Ca(OH)_2$, NaCl, Na_2SO_4, $NaNO_3$, $Na_3PO_4.12H_2O$, $AlCl_3.6H_2O$, NaOH, $Cd(NO_3)_2$ and $Mg(NO_3)_2.6H_2O$, were reagent grade. Radiotracers used, were ^{45}Ca (as $CaCl_2$) and ^{109}Cd (as $CdCl_2$). MSWI bottom-ash was quenched fresh incinerated waste from a Dutch incinerator. The ash was ground and sieved to a fraction < 2 mm. Water to leach the bottom-ash was nanopure Millipore water. Crystallization seeds were suprapure $CaCO_3$ rhombohedrons with an estimated surface area of 0.28 m^2/g and PTFE grains (Fluorplast, The Netherlands).

Carbonation effects in the bottom-ash leachates and in other solutions were studied in 1 l teflon (PFA) reaction vessels under continuous stirring (700 rpm) with a suspended magnetic stirrer. Reaction vessels were placed in glass mantles that were kept at a constant temperature of 22.5 °C by a Neslab Coolflow CFT-25 system. Gases (100% N_2 and 3% CO_2 in N_2) were saturated with H_2O before entering the reaction vessels. The gasflow was regulated with 2 Massflow Controllers (Bronkhorst HI TEC) for 1 l and 2 Massflow Controllers for 2 l. The pH was measured with Hamilton Gel-Plast electrodes standardized against Ingold buffer solutions of pH = 4.01, 7.00 and 11.00.

5.2.2 Methods

5.2.2.1 Solution preparation

MSWI bottom-ash was added to decarbonized nanopure water, bubbled through with N_2, and subsequently allowed to leach in a closed glass vessel for a predetermined time. $Ca(OH)_2$ solutions of a certain Ca concentration, simulating leachate solutions, were obtained by equilibrating about 10 grams of $Ca(OH)_2$ with 1 l of decarbonized water for periods > 24 hours under N_2. This yielded a Ca concentration of about 0.024 M. After filtration of the solution through a 0.22 μm Micropore filter, the desired Ca concentration was obtained by diluting with decarbonized water.

A solution of 0.01 M NaOH and 2×10^{-4} M $AlCl_3.6H_2O$ was prepared by dissolving 0.05 gram of $AlCl_3.6H_2O$ in 100 ml 0.1 M NaOH (undersaturated with respect to AlOOH) and subsequent dilution to 0.01 M NaOH with decarbonized water (slightly supersaturated with respect to AlOOH).

A simulated leachate solution was made based on the composition of a MSWI leachate at L/S = 2 after 48 hours. Thereto, 0.024 g of $AlCl_3.6H_2O$ was dissolved in 333 ml of a 0.0226 M $Ca(OH)_2$ solution (undersaturated with respect to AlOOH), together with 0.852 g Na_2SO_4, 0.011 g $Mg(NO_3)_2.6H_2O$, 0.47 g NaCl and 0.005 g $Na_3PO_4.12H_2O$ and subsequently diluted with 666 ml decarbonized nanopure water (slightly supersaturated with respect to AlOOH).

5.2.2.2. Carbonation

The leachates or solutions were filtered through a 0.22 μm Micropore filter and transferred to the (PFA) reaction vessels. Solutions were equilibrated with N_2 for half an hour. In experiments using radiotracers, the tracer was added after equilibration and a subsample was taken as counting standard before starting the CO_2/N_2 gas flow (carbonation). In experiments studying the behavior of Cd, Cd carrier (10 μg/kg) as well as Cd tracer were added. Cd carrier was added, because the leachates contained very little Cd (< 1 μg/kg). In seeded experiments, calcite seeds were added in

suspension and PTFE seeds were added dry, before carbonation. After starting the CO_2/N_2 gas flow, small (2 ml) subsamples were withdrawn with a syringe and filtered through a 0.22 μm screw-on Schleicher and Schuell filter. At the end of the experiment the solution was filtered over a 0.22 μm Micropore filter and the formed precipitate was oven-dried at 40 °C.

5.2.2.3 Analysis

Precipitates and solutions were dissolved and/or diluted, acidified and analyzed with ICP-AES. Cd in unspiked solutions was measured by means of GFAAS. The precipitates were checked for crystalline phases by means of XRD. Radiotracers were counted on a Compugamma LKB 1280 gamma-counter with a 3 inch NaI well-type detector (^{109}Cd) and on a Philips β-scintillation counter (^{45}Ca). The Ca concentrations in subsamples were determined by means of EDTA-titration. Total carbonate was determined by GRAN-plot titration for $Ca(OH)_2$ solutions. Total carbonate in the leachates was determined by addition of acid, CO_2 entrapment in a $BaClO_4$ solution, while maintaining a constant pH in the $BaClO_4$ solution by addition of NaOH.

5.3. Results and Discussion

5.3.1. Influence of L/S ratio and leaching time

In Fig. 1 the concentrations of the main elements in the MSWI-leachates at L/S ratios of 2 and 20 after different leaching times under N_2 are shown. Fig. 1 shows that both the L/S ratio and the leaching time influence the composition of the solution. In these experiments, where carbonation and its influence on the mobilization of heavy metals are studied, the solution composition can influence the magnitude of $CaCO_3$ precipitation (inhibitors) and corresponding heavy metal uptake. The mean standard deviation, due to analytical uncertainties and to the heterogeneity of the ash, in the elemental concentrations of four leachates (L/S = 2, 48 hours leaching) is 15%.

Calcium in solutions is thought to be controlled mainly by portlandite ($Ca(OH)_2$) (Schramke, 1992), and, at lower pH by gypsum ($CaSO_4.2H_2O$) and ettringite ($Ca_6Al_2(SO_4)_3(OH)_{12}.26H_2O$) (5). Since the Ca concentration at L/S = 2 is about three times higher than at L/S = 20, a greater percentage of Ca can precipitate as $CaCO_3$ at L/S = 2 as a result of carbonation. However, the greater Ca concentration at L/S = 2 is accompanied by an increase in the concentrations of sulfate (gypsum dissolution) (1.25×10^{-3} M to 6×10^{-3} M), Zn (8×10^{-7} M to 2.3×10^{-6} M) and Al (2.6×10^{-4} M to 1.8×10^{-3} M). These concentrations can reduce the calcite growth rate by over 50%. The concentrations of Mg (brucite dissolution) in these solutions ($< 3 \times 10^{-5}$ M) are too low to result in a significant reduction of the calcite growth rate according to the findings of Meyer (1984).

Silica (present in the glassy phases) shows a decrease in concentration after a long leaching time at L/S = 20. Aluminum at L/S = 20 also shows a slight decrease. Boron however, an indicator of the dissolution of the glassy phases (Schramke, 1992), increases with increasing leaching time, suggesting a continued dissolution of glassy phases. Therefore, it can be concluded that silicate dissolution continues and reaches a maximum, after which a Si(Al) precipitate, possibly a clay, is formed (Kirby and Rimstidt, 1994). Obviously, dissolution and precipitation of some elements are not necessarily coupled to a decrease in pH, but to a change in solution composition as leaching continues.
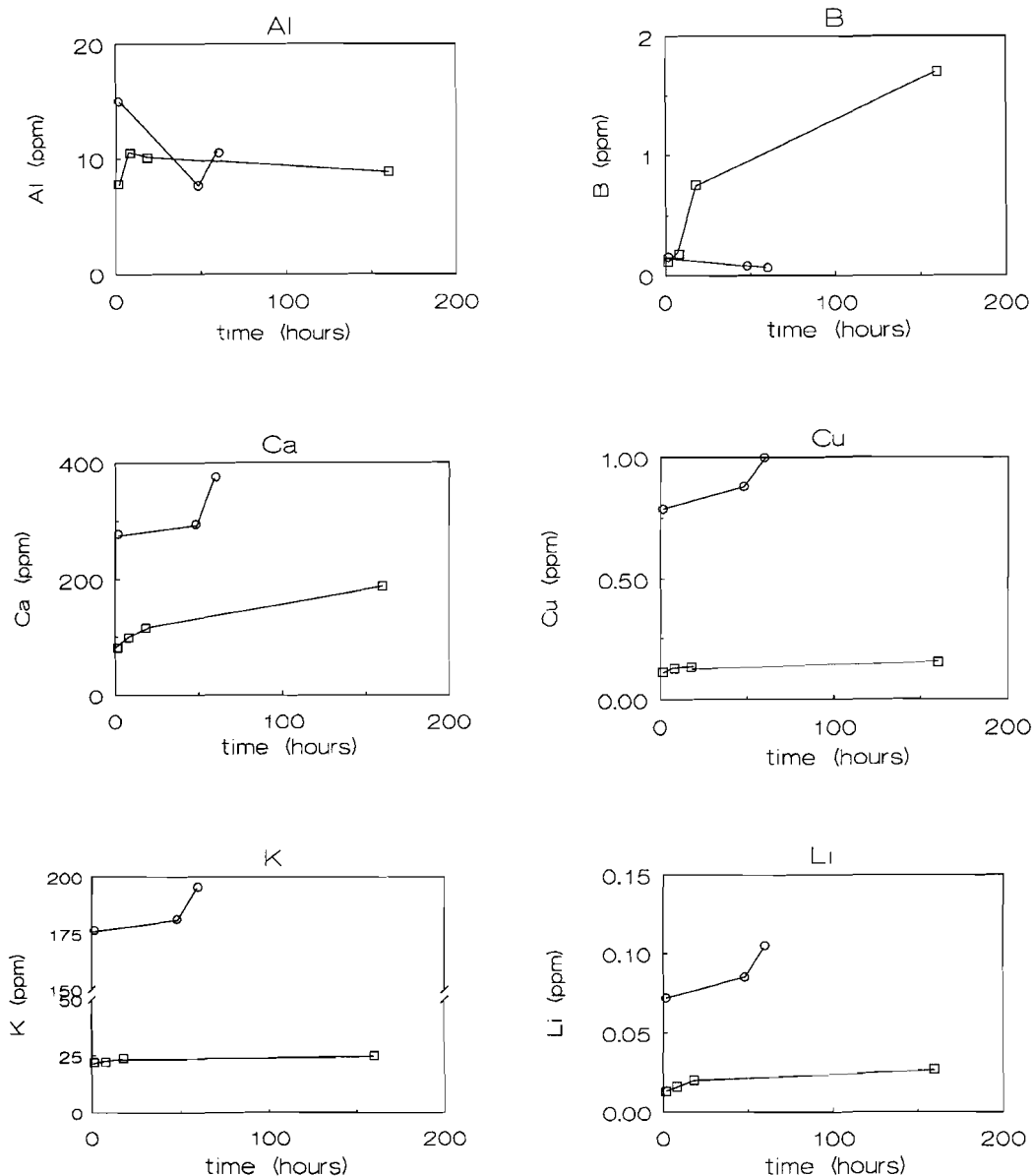
Fig. 1a Levels of elements versus leaching time in filtered AVI bottom-ash leachates at L/S ratios of 2 (O) and 20 (□), as determined with ICP-AES.
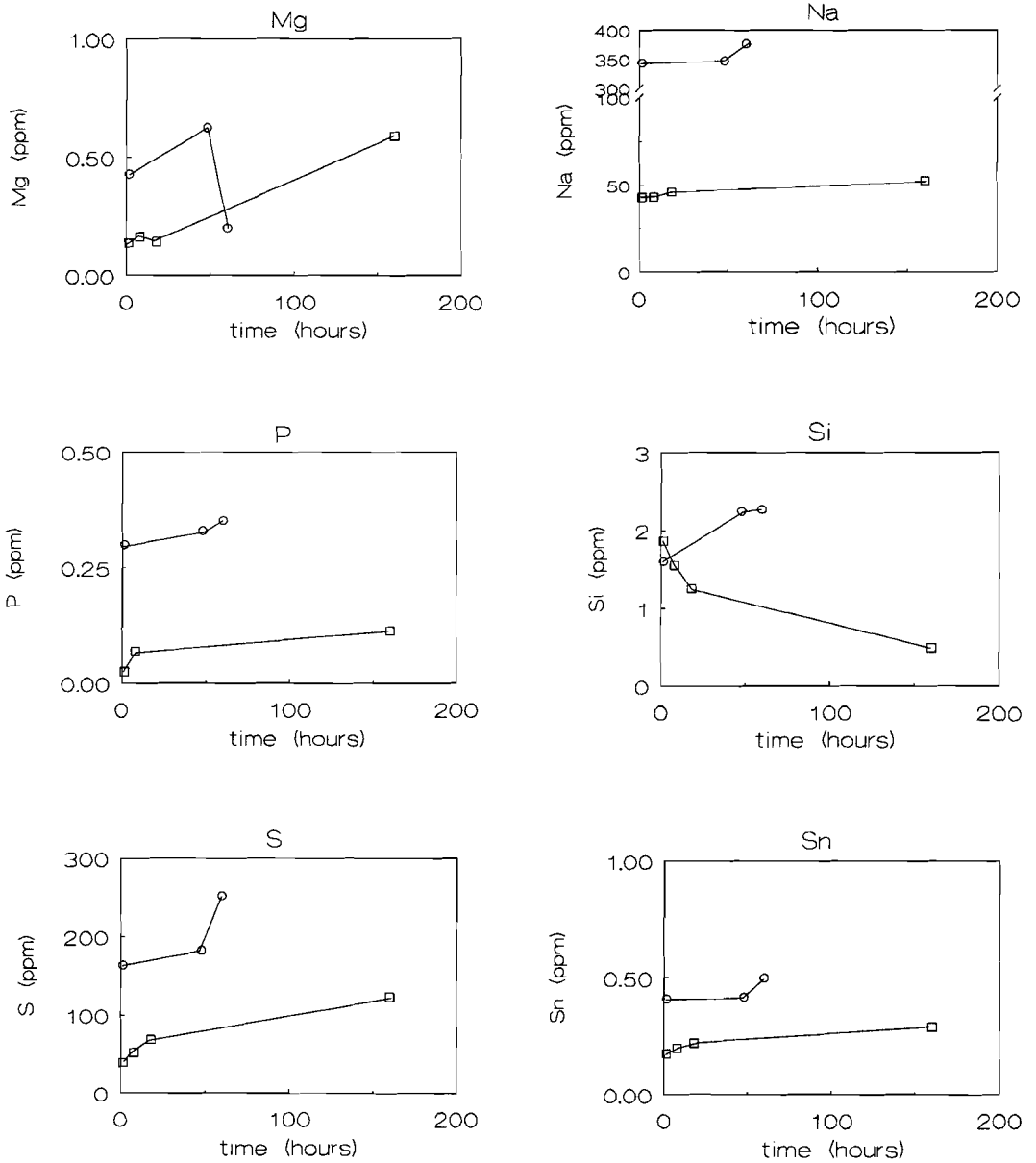
Fig. 1b Levels of elements versus leaching time in filtered AVI bottom-ash leachates at L/S ratios of 2 (O) and 20 (□), as determined with ICP-AES.
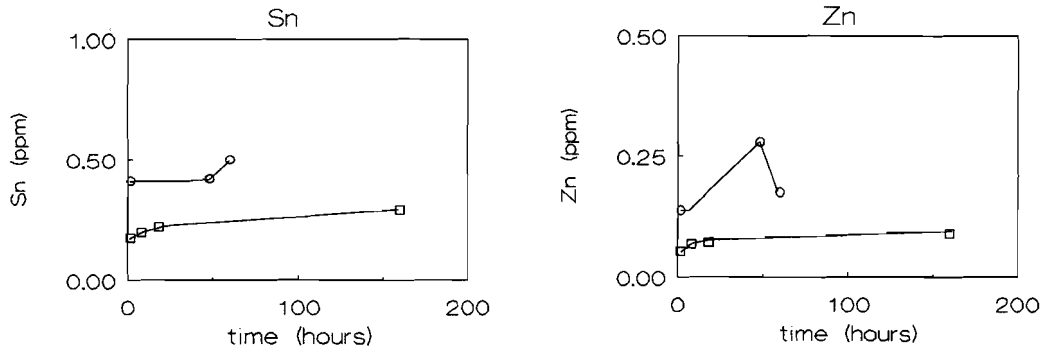
Fig. 1c Levels of elements versus leaching time in filtered AVI bottom-ash leachates at L/S ratios of 2 (O) and 20 (□), as determined with ICP-AES.

Leaching time hardly affected the amounts of Na and K in solution, suggesting that these elements are present in a very soluble phase (e.g. NaCl/KCl). The ratio of Na/K in solution is independent of L/S ratio, which indicates that their concentrations are availability-controlled (Kirby and Rimstidt, 1994). Measurable amounts of Cd (1 - 4 μg/kg) are only present at L/S = 2. Levels of Cu and Zn rise as the L/S ratio decreases and the leaching time increases. The almost instant release of Na and K (representing chloride salts) during leaching as compared to the continuous release of heavy metals, indicates that it is unlikely that the heavy metals are mobilized as chloride complexes during an early stage of weathering.

5.3.2. *Influence of carbonation*

When a mixture of CO_2/N_2 gas is bubbled through the bottom-ash leachates (carbonation), the pH decreases. In Fig. 2a the pH versus time curves of MSWI leachates are shown for various conditions. All curves have an inflection point at a pH of about 8.57, regardless of leaching time, L/S ratio, seeding with $CaCO_3$, gas flow rate, and percentage CO_2 in the gas mixture. Below pH = 8.57, the pH drops less rapidly, indicating a buffering process. Filtration of the leachate yields no precipitate right before the inflection point at pH = 8.65 and a light yellowish precipitate right after the inflection point at pH = 8.4. It can, therefore, be concluded that precipitation occurs at a pH of about 8.57 and that the buffering may be brought about by precipitation and/or dissolution of a mineral phase. The amount of precipitate increased with increasing leaching time and decreasing carbonation rates and L/S ratios (see Table 1). Carbonation in $Ca(OH)_2$ solutions shows an inflection at pH = 7.35, suggesting that the inflection point at pH = 8.57 in the leachates does not result from buffering by $CaCO_3$ (Fig. 2b). Carbonate alkalinity in the bottom ash leachates at pH = 8.6, just before precipitation, is 40.5 mg/l, and 55.2 mg/l at pH = 8.5 after precipitation. Precipitation probably occurs after the carbonate alkalinity has reached a certain level, and therefore shows the same inflection point for different conditions.

Table 1. Amount of precipitation in AVI bottom-ash leachates after carbonation (1% CO_2) under various conditions.

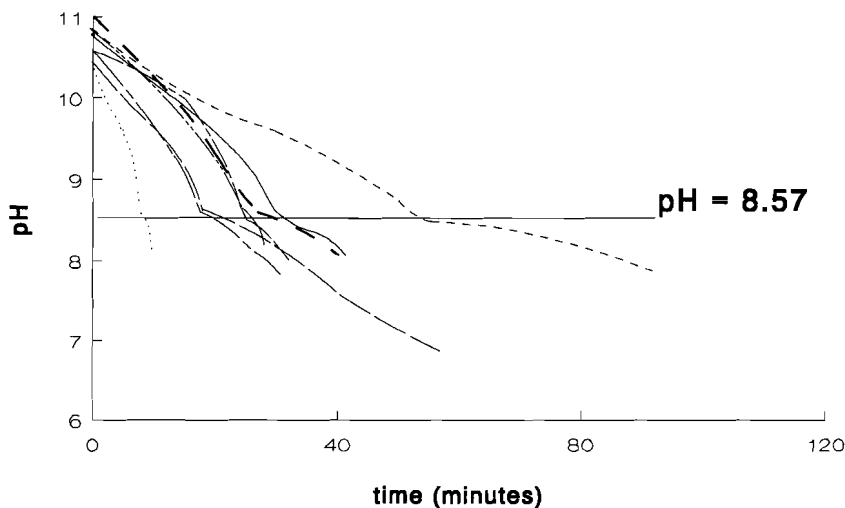| L/S	leaching time (hours)	carbonation time (min)	precipitate (mg)
20	140	100	190
20	17	80	74
20	1	30	17
20	160	30	43
2	48	30	27
2	1	30	19

Fig. 2a. pH versus time during carbonation of filtered MSWI bottom ash leachates for various L/S ratios, leaching times, gas flow rates, gas compositions and in seeded/unseeded runs. Horizontal line through inflection points of curves at pH = 8.57

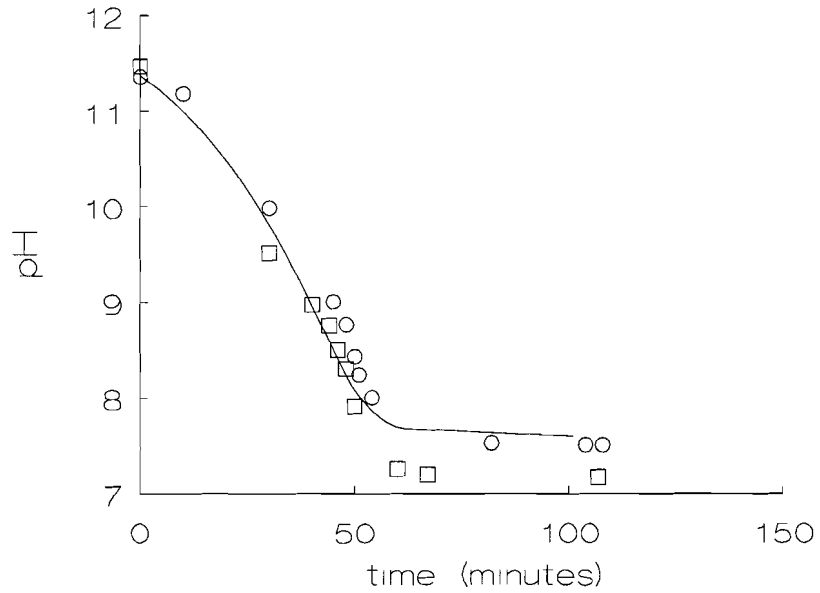|		
— — — — — — —	flow 330 ml/min 2% CO_2, L/S = 2,	48 h leaching
— ·· — ·· — ··	flow 330 ml/min 1% CO_2, L/S = 2,	48 h leaching
———————————	flow 330 ml/min 1% CO_2, L/S = 2,	1 h leaching
— — — ·· — — —	flow 300 ml/min 1% CO_2, L/S = 20,	16 h leaching
— — — — — —	flow 300 ml/min 1% CO_2, L/S = 20,	160 h leaching
— — — — — — — —	flow 330 ml/min 1% CO_2, L/S = 20,	20 h leaching
· · · · · · · · · · ·	flow 330 ml/min 1% CO_2, L/S = 2,	48 h leaching
— — — — — — — —	flow 50 ml/min 1% CO_2, L/S = 20,	16 h leaching

Fig. 2b. pH versus time during carbonation of $Ca(OH)_2$ solutions; 750 ml, 0.0024 M $Ca(OH)_2$, 0.7 M NaCl, 0.045 M $NaNO_3$, 500 ml/min 1% CO_2.

Table 2. The composition of three precipitates P1, P2 and P3 in bottom-ash leachates after carbonation (L/S=2, 48 hours leaching) in 500 ml, 330 ml/min 1% CO_2.

	P1	P2	P3
Al	732.93	736.81	787.45
Ca	128.25	106.65	137.53
Si	55.36	96.66	135.32
S	44.99	31.14	2.93
Cu	14.67	16.75	17.49
Na	8.92	9.07	8.49
K	6.2	7.09	7.59
P	4.91	5.49	5.82
Sr	0.63	0.43	0.6
Zn	1.34	<D.L.	<D.L
Mo	0.22	0.11	1.54
Ni	0.21	0.35	0.12
B	<D.L.	<D.L.	<D.L
Mg	<D.L.	<D.L.	<D.L.
V	0.39	0.33	0.43
Sn	0.25	0.19	0.20
Ti	0.07	0.04	0.07
Li	0.02	0.02	0.02

In Table 2 the composition of three precipitates (L/S = 2, 48 hours leaching) after carbonation is given. Clearly, Al and to a lesser degree Ca, Si, and sulfate contribute to the bulk of the precipitate. Especially Cu, but also Zn, Sr, Ni and Sn are removed from the leachate after carbonation. Calculations with the aqueous speciation code MINTEQA2 (Allison and Brown, 1991) show that at the start of the experiment the mineral phases diaspore, gibbsite, alunite, calcite, dolomite, cuprite, strontianite, witherite and barite are supersaturated. The (apparent) supersaturations may be maintained as a result of complexation of elements with organic species (Zevenbergen, 1994; Comans et al., 1993) or by elements/ions that inhibit nucleation (e.g. phosphate inhibits calcite precipitation). It therefore depends on the effect of inhibitors, organic species, and carbonation rates, which minerals/phases actually do precipitate.

At L/S = 2 and at L/S = 20 only after long (> 60 hours) leaching times, traces of calcite were detected in the largely amorphous precipitate with XRD. The calcite had a deviating lattice distance in one direction, which may well point to incorporation of Mg. The primary effect of Mg incorporation namely, is to shorten the c-axis dimension resulting in lattice strain and leading to a greater solubility (Lahann, 1978). The amount of $CaCO_3$ precipitation during carbonation is very small compared to the amount that could potentially precipitate. In a simulated leachate solution, containing levels of Al, Ca, sulphate, phosphate, Mg, and Cl comparable to levels in a real leachate (L/S = 2, 48 hours leaching), Ca in solution drops from 7.5 mM at pH = 12 to 1.2 mM at pH = 8.3. In the actual leachate however, Ca drops from 7.45 mM at pH = 10.87 to only 6.9 mM at pH = 8.54. Despite the presence of all possible inorganic inhibitors in the simulated leachate, $CaCO_3$ precipitates in much greater amounts than in the real leachates. Possibly, organic constituents present in bottom ash may inhibit or greatly reduce $CaCO_3$ precipitation in the real leachate. In Fig. 3, where $CaCO_3$ precipitation is monitored with ^{45}Ca, a decrease in ^{45}Ca is hardly visible, demonstrating that the amount of $CaCO_3$ precipitation is small. Seeding with teflon and suprapure calcite seeds did not yield a greater Ca decrease in solution. The presence of a surface for nucleation obviously does not influence the quantity of calcite precipitation.
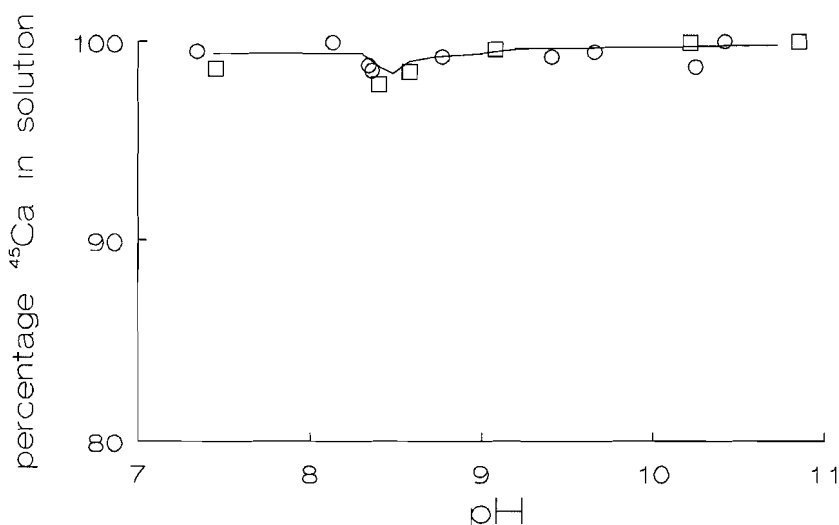

Fig. 3. ^{45}Ca versus pH during carbonation of leachate; in 500 ml, L/S = 2, 48 hours leaching, 330 ml/min 1% CO_2.

In three leachates (L/S = 20, 16 hours leaching), traces of dolomite were detected in the precipitate after carbonation. The rhombohedric planes of (100), (221) and ($\overline{1}$11) were clearly distinguishable on the XRD film. The composition of the corresponding solution before and after carbonation is given in Table 3. However, the formation of dolomite is unusual at room temperatures. Possibly the presence of organic species could permit the precipitation of dolomite.

Table 3. Solution composition (ppm) before and after carbonation in which dolomite was detected in the corresponding precipitate (L/S=20, 14-17 hours leaching); 500 ml, 330 ml/min, 1% CO_2.

	before	after
Na	44.38	44.37
Ca	98.53	93.06
S	49.51	47.35
K	23.12	23.96
Al	7.68	<D.L.
Si	2.27	0.82
Sr	0.41	0.38
Cu	0.13	0.077
Mg	0.195	0.180
Sn	0.19	0.175
P	< D.L.	<D.L.
Zn	0.07	0.057
Ba	0.22	0.178
Ni	<D.L.	<D.L.
Li	0.016	0.017
B	0.17	0.130
V	0.05	0.004
Ti	<D.L.	<D.L.

The amorphous precipitate containing Al and Si, may partly consist of allophanic material (Zevenbergen, 1994). Allophane really is a group name for noncrystalline clay minerals consisting of silica, alumina, and water (Farmer et al., 1985). The amorphous aluminum hydroxide phase is likely to be the dominant phase, since the concentration of Al outweighs the concentration of Si by far and allophanes have a Si/Al ratio of 1:2 to 1:1. Sulfate may be coprecipitated with these phases possibly as alunite ($KAl_3(SO_4)_2(OH)_6$).

Carbonation in the leachates was modelled with CHARON (De Rooij, 1991) considering the species Na, K, Al, Ca and Si, and allowing for precipitation of gibbsite ($Al(OH)_3$) and calcite. Results suggest that calcite precipitates immediately upon carbonation and that gibbsite ($Al(OH)_3$) precipitates at pH = 9.1. Also, an inflection point, similar to the inflection point in Fig. 2 is found at the pH where gibbsite precipitates. The difference with the actual leachates may come about by organic inhibitors, preventing calcite precipitation, and by the presence of sulfate, which lowers the pH at which gibbsite may precipitate (Patterson et al, 1990). Since $Al(OH)_3$ is an excellent substrate for nucleation of calcite, especially in the alkaline region (Stumm, 1992), calcite may precipitate as soon as $Al(OH)_3$ precipitates.

The heavy metals are probably coprecipitated at pH = 8.57, rather than precipitated as separate cuprite, zincite, etc. phases. ICP-AES results for zinc (L/S = 2) indicate a sudden decrease from 25 μg/kg in the pH range 8.62 - 10.7, to 7 μg/kg at pH = 8.33. From these facts, the question arises whether heavy metals coprecipitate with the small amount of $CaCO_3$, or with the Al(Si) phases. This issue will be discussed in the next paragraph.
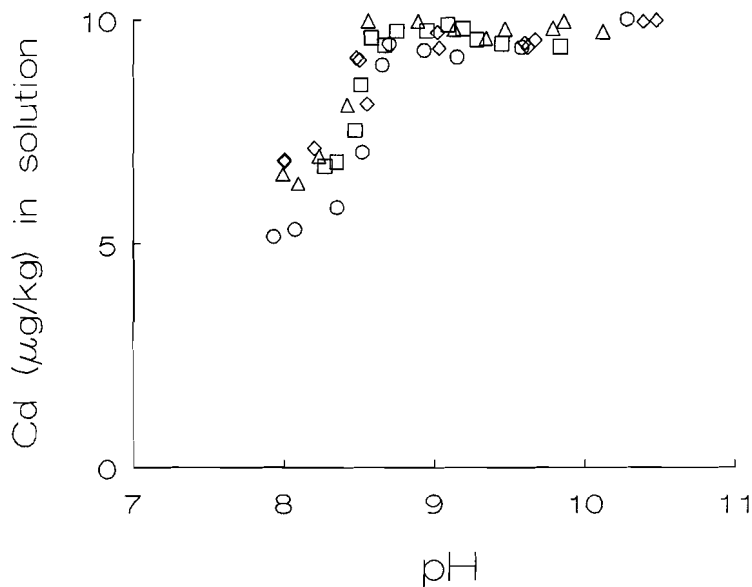
Fig. 4. Cd versus pH during carbonation (1% CO_2) of leachate (L/S = 2, 48 hours leaching), in a 15 minute (◊), a 50 minute (△,□) and a 60 minute (○) experimental run.
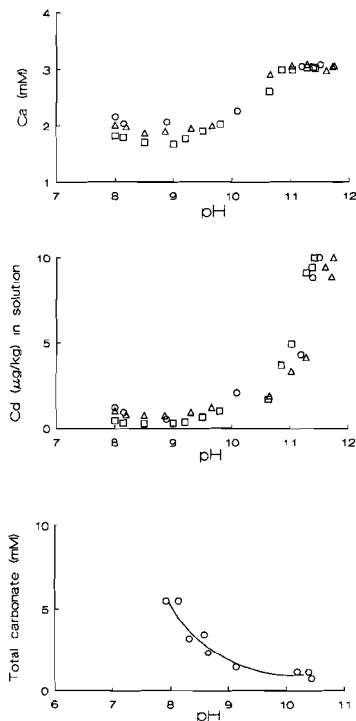

Fig. 5. Cd versus pH (a), Ca versus pH (b), and total carbonate (c) during carbonation of a Ca(OH)₂ solution; 750 ml, 0.003 M Ca(OH)₂, 0.3 M NaCl, 0.045 M NaNO₃, 500 ml/min 1% CO_2.
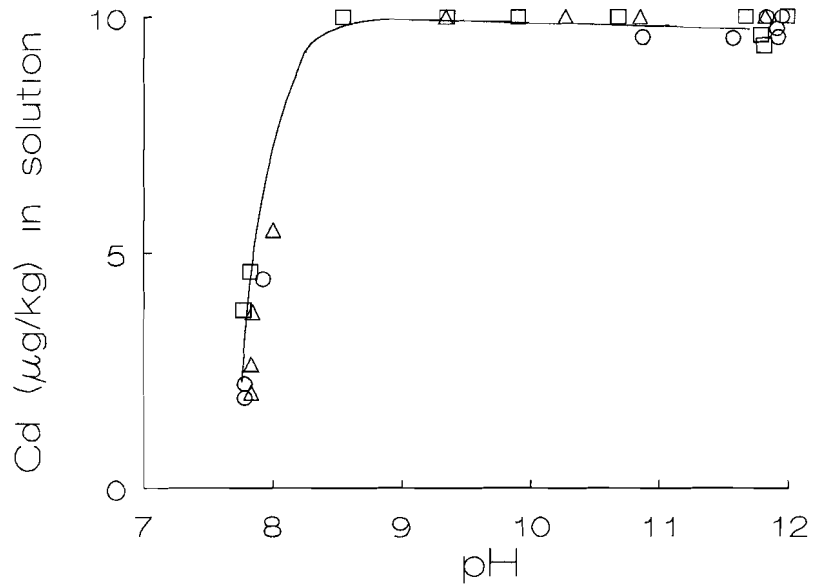
Fig. 6. Cd versus pH during carbonation in a $Al(OH)_3$ solution; in 750 ml, 0.01 M NaOH, 2×10^{-4} M $AlCl_3.6H_2O$, 50 ml/min 1% CO_2.
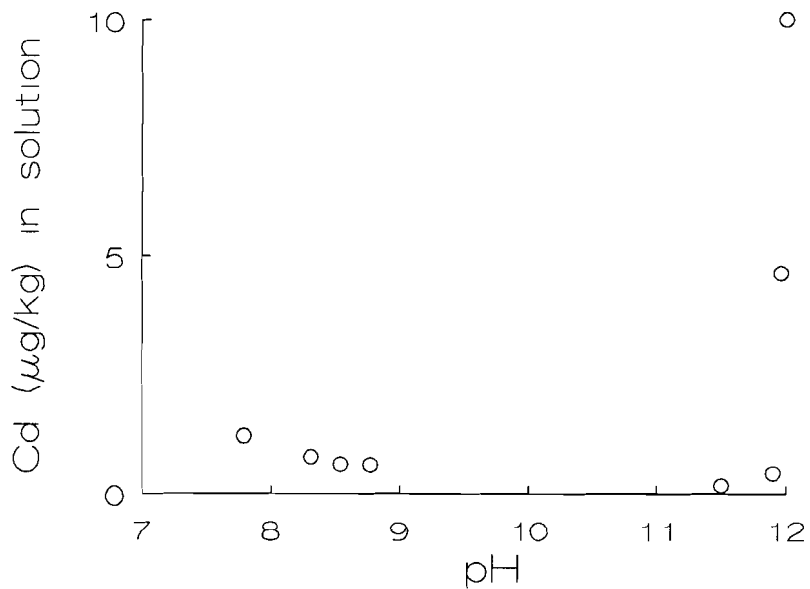

Fig. 7. Cd versus pH during carbonation in a simulated leachate (L/S = 2, 48 hours leaching) in 750 ml, 500 ml/min 1% CO_2. Exact composition is given under "Materials and methods" in text.
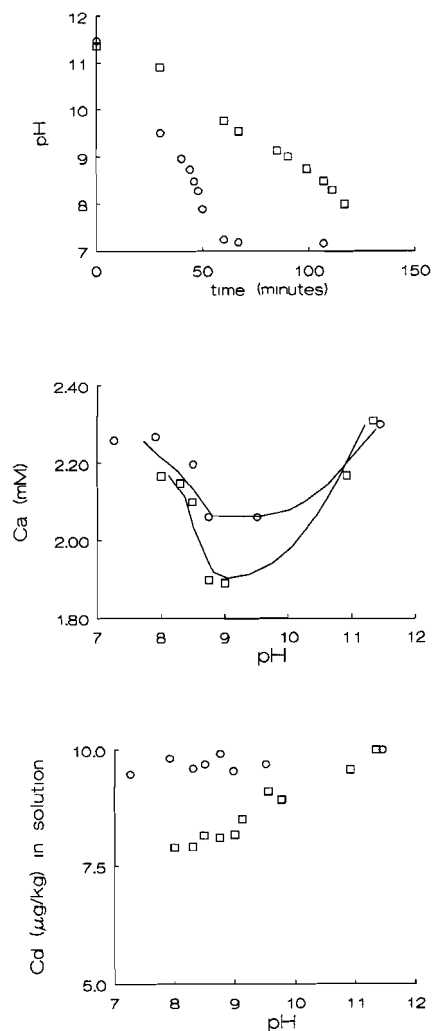
Fig. 8. pH versus time (a), Ca versus pH (b), and Cd versus pH (c) during carbonation in $Ca(OH)_2$ solutions; 0.0023 M $Ca(OH)_2$, 0.7 M NaCl, 0.045 M $NaNO_3$, 500 ml/min 1% CO_2.

The Ca concentration and the carbonate alkalinity, versus time in $Ca(OH)_2$ solutions during carbonation (Fig. 5a) is shown in Figs 5b and 5c. Obviously only a small amount (10 mg/l) of $CaCO_3$ precipitation is needed to remove most of the Cd in solution. Cd can easily replace Ca in the calcite crystal lattice because of their similar ionic radius (0.97 Å and 0.99 Å respectively). In solutions with a higher Cl concentration but equal amount of $CaCO_3$ precipitation, less Cd can be removed due to the formation of Cd-Cl complexes (Van der Weijden et al., 1994). Therefore, early washout of salts is desirable during weathering of municipal waste (compare Fig. 5a with Fig 8c).

5.3.3. Cd removal

In Fig. 4 a plot of Cd versus pH shows a sudden decrease in Cd at the same pH value as the inflection point during carbonation. It can, therefore, be concluded that Cd coprecipitates with the Al(Si)- and/or calcite precipitate at pH = 8.57. The percentage of Cd removal from solution in different runs at equal PCO_2 varies from 30 to 50% and seems to depend on the carbonation rate. For comparison, the Cd removal from solution during the carbonation in solutions of $Ca(OH)_2$ and $Al(OH)_3$ is shown in Fig. 5b and Fig. 6, respectively. While the Cd removal in $Ca(OH)_2$ solutions during carbonation is continuous as the pH decreases (Fig. 5b), the Cd removal in $Al(OH)_3$ solutions (Fig. 6) shows a pattern that closely resembles the pattern in Fig. 4, which displays a sudden decrease in Cd at a pH of about 8.3. The Cd removal in the leachates therefore appears to be associated with $Al(OH)_3$ precipitation. The amount of $Al(OH)_3$ precipitation needed for 80% Cd removal in solutions with low Cl concentrations is small (14 mg/l) (Fig. 6).

In the simulated leachate, Ca and Cd removal is continuous and associated with calcite precipitation (Fig. 7). In the actual leachates, however, organic species can inhibit calcite precipitation (see former paragraph), and therefore Cd remains in solution until a precipitate at pH = 8.57 is formed. At this pH both $CaCO_3$ and $Al(OH)_3$ can be formed. Previous studies concluded that calcite precipitation was the (only) important factor for heavy metal immobilization resulting from carbonation (e.g. Comans et al., 1993). From the results presented here it appears that precipitation of small amounts of amorphous $Al(OH)_3$ (and possibly allophanes) may be of equal importance. One has to bear in mind, though, that the processes at the disposal site may have different kinetics and that inorganic/organic species may be washed in or out, which could result in a larger amount of calcite precipitation. An example of the importance of reaction rates is shown in Figs. 8a-c where the pH versus time and the Ca and Cd concentrations versus pH are plotted for carbonation in $Ca(OH)_2$ solutions. In the slower run more $CaCO_3$ is precipitated and more Cd removed. Also, if precipitation kinetics are slow, sorption onto calcite or $Al(OH)_3$/ allophane may become an important process for heavy-metal immobilization.

5.4. Conclusions

In bottom-ash leachates, the initial composition as well as the carbonation rate influence the amount and composition of the precipitate. $CaCO_3$ precipitation resulting from carbonation is very effective for immobilization of heavy metals, but organic species may inhibit precipitation and may form complexes with the heavy metals that can be washed out. A longer incineration time for municipal waste, during which more organic material is removed, may result in more $CaCO_3$ precipitation. If $CaCO_3$ precipitation is small or inhibited, the precipitation of aluminum hydroxides or hydrous aluminosilicates and the buffering capacity of the leachates displayed after precipitation, appear to be important factors for immobilization of heavy metals.

References

Allison, J.D., Brown, D.S. and Novo-Gradac, K.J., 1991. MINTEQA2/PRODEFA2, a geochemical assessment model for environmental systems: version 3.11.

Chandler, A.J., Eighmy, T.T., Hartlén J., Hjelmar, O, Kosson D.S., Sawell, S.E., Van der Sloot H.A., and Vehlow, J. (IAWG), 1994. In: An international Perspective on Characterisation and Management of Residues from Municipal Solid Waste Incineration, 78 pp.

Comans, R.N.J. and Meima, J.A., 1994. Modelling Ca-solubility in MSWI bottom-ash leachates. In Waste Materials in Construction II. Proceedings of the International Conference on Environmental Implications of Construction with Waste Materials, Maastricht, The Netherlands; Goumans, J.J.J.M. et al. Eds; Elsevier, Amsterdam.

Comans, R.N.J., van der Sloot, H.A. and Bonouvrie, P.A., 1993. Geochemical reactions controlling the solubility of major and minor trace elements during leaching of municipal solid waste incinerator residues In: Proceedings 1993 Municipal Waste Combustion Conference, Williamsburg, VA.; Kilgroe, J. Ed.; AWMA, Pittsburg, PA.

De Rooij, N.M. and Kroot, M.P.J.M, 1991. Manual Charon, Delft Hydraulics, Delft, 458 pp.

Farmer, V.C., McHardy, W.J., Robertson, L., Walker, A. and Wilson, M.J., 1985. Micromorphology and sub-microscopy of allophane and imogolite. J. Soil Sci. 1985, 36, 87-95.

Kirby, C.S. and Rimstidt, J.D. , 1993. Mineralogy and surface properties of municipal solid waste ash. Eviron. Sci. Technol., 27: 652-660.

Kirby, C.S.; Rimstidt, J.D., 1994. Interaction of municipal solid waste ash with water. Environ. Sci. Technol., 28: 443-451.

Lahann, R.W., 1987. A chemical model for calcite growth and morphology control J. Sed. Petrol., 48: 337-344.

Meyer, H.J. J., 1984. The influence of impurities on the growth rate of calcite. J. Cryst. Growth, 66: 639-646.

Patterson, J. W., Luo, B., Marani, D. and Passino, R., 1990. In: Metals speciation, separation and recovery. Vol. III. Lewis Publishers, Chelsea, Michigan, USA, 632 pp.

Plummer, L.N.and Busenberg, E., 1985. Kinetic and thermodynamic factors controlling the distribution of SO_4^{2-} and Na^+ in calcites and selected aragonites. Geochim. Cosmochim. Acta, 49: 713-725.

Schramke, J.A., 1992. Neutralization of alkaline coal fly ash leachates by CO_2. Appl. Geochem. , 7: 481-492.

Stokman, A., 1994. Thesis Netherlands Energy Research Center, Unpublished results.

Stumm, W., 1992. Chemistry of the solid-water interface. Wiley and Sons, 428 pp.

Van der Weijden, R.D., Van der Weijden, C.H. and Comans, R.N.J., 1994. Sorption and sorption reversibility of Cd on calcite under simulated riverine, estuarine and marine conditions. Mar. Chem., 1994, 47, 65-79.

Zevenbergen, C., 1994. Natural weathering of MSWI Bottom-Ash. Ph.D. dissertation, Utrecht University, 131 pp.

Summary

The summary is divided into two parts. The first part is a compilation of the *general findings* concerning the various types of interaction between cadmium and calcite as distributed throughout the various chapters. More *specific findings* per chapter regarding these interactions in various simulated aqueous environments, are summarized in part two.

1. General findings

The high chemical affinity of cadmium (Cd) for calcite ($CaCO_3$) forms the basis for most of their interactions. This chemical affinity evolves from the similarity between the ionic radius, and ionic charge for Ca (calcium) and Cd, the similarity between the crystal lattices of calcite and otavite ($CdCO_3$), and the low solubility product of the latter.

At the calcite surface, Cd forms complexes with the carbonate groups. Usually this type of sorption, where covalent bonds are formed, is called *chemi-sorption*. The degree of Cd sorption depends on the aqueous activity of Cd^{2+}, the crystal morphology and the solution composition. Sorption can be described by a Ca-Cd exchange model. A fraction of Cd, however, may replace protons instead of Ca at the surface, since a minute increase in pH is observed after desorption.

Incorporation of Cd during calcite crystal growth is a surface reaction controlled process, where the integration in growth sites is probably the rate limiting step. Cd replaces Ca by isomorphic substitution. The degree of Cd incorporation depends on the aqueous Cd^{2+} activity, the calcite growth rate, the crystal morphology, and the solution composition.

Sorption (growth) sites are not all equally favorable for Cd sorption or incorporation, because these sites differ in size, geometry, and complexation constants of Cd with surface carbonate groups. The number of favorable sites depends on the calcite surface morphology, microtopography, and the solution composition. This non-uniformity of surface sites influences the *sorption reversibility* and, for incorporation of Cd, the partition coefficient. A low surface coverage, for instance, where only the most favorable sites are occupied by Cd, will result in a lower sorption reversibility and a higher partition coefficient.

Besides Cd sorption and Cd incorporation, *Ostwald ripening* of calcite is an important process, as it can contribute significantly to the immobilization of Cd after long sorption times. The rate of ripening (or growth) increases with increasing total aqueous concentrations of calcium and carbonate. Lower ripening (or growth) rates usually result in higher partition coefficients and lower Cd removal rates from solution. This trend may be reversed though, depending on changes in the total aqueous calcium and carbonate concentrations and/or the calcite crystal morphology.

Electrostatic forces play an insignificant role in the extent of Cd sorption and Cd incorporation. This may be concluded from the fact that despite the change in the calcite surface charge from positive to negative in the pH range 7-8.5, Cd sorption still fits the Ca-Cd exchange model. Furthermore, the decrease in Cd sorption resulting from an increase in ionic strength, can be entirely explained by the decrease in the aqueous Cd activity.

Solid-state diffusion, or *surface precipitation* at Cd concentrations below $2\times10^{-7}M$, do not significantly contribute to the removal of Cd from solution, as can be concluded from the lower sorption reversibility at lower surface coverage with Cd. Therefore, sorption, and incorporation during Ostwald ripening and growth of calcite, appear to be the main processes governing Cd removal from solution.

117

2. Specific findings

In the estuarine environment the sorption and sorption reversibility of Cd are influenced by the presence of several aqueous species (*Chapter 1*). Cd sorption decreases with increasing $Mg^{2+}$and Ca^{2+} concentrations as a result of competition with Cd^{2+} for sorption sites, and with increasing Cl^- concentrations due to complexation with Cd^{2+}. Based on these findings, a release of Cd^{2+} from riverine suspended calcite may be expected upon entry of river water in the estuary. It appears, however, that the sorption reversibility is limited, and that a great increase in the chloride concentration only results in a few percent desorption. In fact, Cd removal from the water may continue as a result of the recrystallization (Ostwald ripening) of calcite.

Phosphate and sulfate, both also present in seawater, reduce the fast initial Cd sorption and reduce the slow Cd removal rate by reducing the recrystallization rate (*Chapter 2*). The influence on the sorption of Cd is most pronounced at lower pH (lower carbonate concentrations), since sorption of PO_4^{3-}/HPO_4^{2-} and SO_4^{2-} increase with decreasing pH. The impact of phosphate on both processes is much greater than of sulfate, which is due to the greater affinity of phosphate for calcite. Experimental results show that a low Cd/Ca ratio at the crystal surface corresponds with a high aqueous phosphate concentration. This suggests that the increase in Cd/Ca ratios in benthic foraminifera with increasing phosphate concentrations in ocean deep water, probably results from biochemical rather than chemical processes.

In *Chapter 3* it is shown that no unique relationship between the calcite growth rate and the supersaturation of the solution exists. At equal supersaturation, an increase of the total aqueous carbonate concentrations causes an increase in the growth rate. This can be explained by a contribution of bicarbonate to calcite crystal growth. On the crystals macrostep formation is apparent, which is probably due to the presence of impurities. The macrostep pattern differs for various stages of outgrowth, but the calcite growth rate appears to be independent of the outgrowth factor.

Findings in *Chapter 4* reveal that no unique relationship between the growth rate of calcite and the incorporation (partitioning) of Cd exists. This is due to the fact that the total calcium and carbonate concentrations and their ratios, the crystal surface, the presence of other aqueous species, and the type of crystal seeds all influence the growth rate. Therefore, various trends of the partition coefficient versus the growth rate are conceivable.

Calcite formed as a result of carbonation of municipal incinerated waste bottom ash can very effectively immobilize Cd by incorporation and sorption (*Chapter 5*). In experiments with filtered leachates the amount of calcite that is precipitated is much less than is expected based on the solubility product of calcite. This is probably due to the presence of organic inhibitors, because inorganic inhibitors did not yield a similar effect. Precipitation of calcite and removal of Cd occur at the same pH where aluminum hydroxides precipitate. Therefore, aluminum hydroxides may well play an equally important role in the removal of Cd during carbonation.

Samenvatting

De samenvatting bestaat uit twee gedeelten. Het eerste deel is een compilatie van de *algemene resultaten* aangaande de verschillende types van interactie tussen cadmium en calciet, zoals die in de verschillende hoofdstukken aan de orde komen. In het tweede gedeelte zijn de meer *specifieke resultaten* betreffende de interacties in verschillende waterige systemen samengevat.

1. Algemene resultaten

De meeste interacties tussen cadmium (Cd) en calciet ($CaCO_3$) zijn terug te voeren op de grote chemische affiniteit van Cd voor calciet. Deze affiniteit komt voort uit de overeenkomst van de ionstraal en de ionlading van Ca (calcium) en Cd, de bijna identieke kristalroosters van calciet en otaviet ($CdCO_3$), en het lage oplosbaarheidsproduct van de laatste.

Cd vormt oppervlakte complexen met de carbonaatgroepen aan het calciet oppervlak. Dit type sorptie, waarbij covalente bindingen worden gevormd, wordt doorgaans *chemi-sorptie* genoemd. De mate van Cd sorptie hangt af van de activiteit van Cd^{2+} in de oplossing, de morfologie van de kristallen, en de samenstelling van de oplossing. Sorptie kan worden beschreven met een Ca-Cd uitwisselingsmodel. Een kleine fraktie van het Cd vervangt waarschijnlijk protonen i.p.v. Ca aan het oppervlak, omdat tijdens desorptie een lichte pH stijging wordt waargenomen.

Inbouw van Cd tijdens de groei van calciet is een oppervlak-gecontroleerd proces, waarbij de integratie in de groeiplaatsen waarschijnlijk de snelheidsbepalende stap is. De vervanging van Ca door Cd is isomorf. De mate van Cd inbouw hangt af van de Cd^{2+} activiteit in de oplossing, de kristalgroei snelheid, de morfologie van het kristal en de verdere samenstelling van de oplossing.

Niet alle sorptie (groei) plaatsen zijn even aantrekkelijk voor sorptie of inbouw van Cd, omdat de grootte, de geometrie, en complexatie constante van Cd met carbonaat, van een sorptie plek kunnen verschillen. Het aantal gunstige plaatsen is afhankelijk van de morfologie en de microtopografie van de calciet kristallen, en de samenstelling van de oplossing. De heterogeniteit van de plaatsen aan het oppervlak beïnvloedt de *sorptie reversibiliteit* en, voor inbouw, de partitiecoefficient van Cd. Een lage bedekkingsgraad van het oppervlak, waarbij alleen de meest gunstige plaatsen bezet zijn door Cd, resulteert bijvoorbeeld in een lagere reversibiliteit en een hogere partitiecoefficient.

Naast Cd sorptie en Cd inbouw tijdens groei, blijkt *Ostwald rijping* van calciet ook een belangrijke bijdrage te kunnen leveren aan de permanente immobilisatie van Cd na lange sorptietijd. De rijpings of groeisnelheid neemt toe met toenemende totaal concentraties van calcium en carbonaat in de oplossing. Lagere rijpings- of groeisnelheden resulteren gewoonlijk in hogere partitiecoefficienten en een lagere Cd-opname snelheid. Deze trend kan echter omdraaien, afhankelijk van de totaal concentraties van calcium en carbonaat in de oplossing en/of de morfologie/microtopografie van de calciet kristallen.

Electrostatische krachten spelen praktisch geen rol in de mate van Cd sorptie en Cd inbouw. Dit blijkt onder andere uit het feit dat ondanks de verandering van lading aan het calciet oppervlak van positief naar negatief in de pH range 7-8.5, de Cd sorptie nog steeds beschreven kan worden met het Ca-Cd uitwisselingsmodel. Tevens blijkt de afname van de Cd sorptie met toenemende ionsterkte uitsluitend aan de afname van de Cd activiteit in de oplossing worden toegeschreven.

Vaste stof diffusie of *oppervlakte precipitatie* bij Cd concentraties beneden 2×10^{-7}M dragen niet wezenlijk bij aan de verwijdering van Cd uit de oplossing, hetgeen geconcludeerd kan worden uit de lagere sorptie reversibiliteit bij een lagere Cd bezetting van het oppervlak. Sorptie en inbouw tijdens Ostwald rijping en calcietgroei, blijken dus de voornaamste processen te zijn voor het verwijderen van Cd uit de oplossing.

2. Specifieke resultaten

Verschillende species in het estuarine milieu kunnen de sorptie en de sorptie reversbiliteit van Cd beinvloeden. Een toename in de Mg^{2+} en Ca^{2+} concentratie veroorzaakt een afname in Cd^{2+} sorptie vanwege de grotere competitie voor sorptieplaatsen. Een toename in de Cl^- concentratie veroorzaakt eveneens een afname, doordat Cl^- complexen vormt met Cd in de oplossing. Op basis hiervan zou men verwachten dat wanneer rivierwater mengt met zeewater, remobilisatie optreedt van Cd dat aan het in rivierwater gesuspendeerde calciet geadsorbeerd is. De desorptie van Cd (en dus de reversibiliteit) blijkt echter beperkt te zijn tot slechts een paar procent. Het is zelfs zo, dat de Cd opname uit het estuariene water gewoon door kan gaan, tengevolge van de Ostwald rijping van calciet.

De in zeewater aanwezige anionen fosfaat en sulfaat, reduceren zowel de mate van Cd sorptie, alsook de inbouwsnelheid in calciet door verlaging van de snelheid van Ostwald rijping. De invloed op de Cd sorptie is het sterkst bij lage pH, omdat PO_4^{3-}/HPO_4^{2-} en SO_4^{2-} het best adsorberen bij lage pH (lagere carbonaat concentraties). Het effect van fosfaat op sorptie en inbouw is veel groter dan van sulfaat, omdat fosfaat een grotere affiniteit voor calciet heeft.

De experimentele resultaten laten zien dat een lage Cd/Ca verhouding aan het oppervlak correspondeert met een hoge fosfaat concentratie in de oplossing. Het lijkt dus aannemelijk dat de toename in de Cd/Ca ratio in benthische forams met toenemende fosfaat concentraties in het oceaan water, meer een gevolg is van biochemische dan van chemische processen.

Tussen de groeisnelheid van calciet en de oververzadiging van een oplossing bestaat geen eenduidig verband. Bij eenzelfde oververzadiging blijkt de groeisnelheid van calciet toe te nemen indien de totaal concentratie van carbonaat verhoogd wordt, door een bijdrage van bicarbonaat aan de groei van calciet. Tijdens de groei vormen zich macrosteps aan het oppervlak, waarschijnljk als gevolg van verontreinigingen. Het vóórkomen van de macrosteps is afhankelijk van de mate van uitgroei, maar de groeisnelheid lijkt onafhankelijk te zijn van de uitgroeifactor.

Er blijkt ook geen eenduidig verband te zijn tussen de groeisnelheid van calciet en de inbouw (partitie) van Cd. Dit komt doordat de groeisnelheid van calciet wordt beinvloed door de verhouding en de totaal concentraties van calcium en carbonaat, de microtopografie en morfologie van de calcietkristallen, en de aanwezigheid van verontreinigingen. Daarom zijn diverse trends denkbaar van de groeisnelheid versus de inbouw.

Tijdens de uitloging van bodemas, afkomstig van verbrand huisvuil, wordt ten gevolge van carbonatatie calciet gevormd. Door sorptie en inbouw van Cd aan/in deze gevormde calciet, kan de mobiliteit van Cd tijdens de uitloging worden beperkt. De hoeveelheid calciet die gevormd wordt in gefiltreerd uitloogsap is echter minder dan op basis van het oplosbaarheidsprodukt van calciet verwacht zou mogen worden. Aangezien anorganische bestanddelen een dergelijke vermindering in de hoeveelheid gevormd calciet niet teweeg brengen, zijn organische bestanddelen hier mogelijk de oorzaak van. De vorming van calciet en de afname in de Cd concentratie in het uitloogsap vinden plaats bij eenzelfde pH als waarbij aluminium hydroxide gevormd wordt. Het is daarom mogelijk dat laatstgenoemde fase een belangrijke bijdrage levert aan de immobilisatie van Cd tijdens uitloging.

Dankwoord

Een ieder die heeft bijgedragen aan de totstandkoming van dit proefschrift wil ik van harte bedanken.

Mijn promotoren en co-promotoren dank ik voor het commentaar op de manuscripten.

Prof. G.M. van Rosmalen bood mij de kans om kristallisatie experimenten te verrichten bij Apparatenbouw en Procesindustrie (API) aan de TU Delft. Ik heb daar met veel plezier gewerkt, vanwege de collegiale sfeer die daar aanwezig is.

Antoine van der Heijden dank ik in het bijzonder. Alhoewel het niet tot zijn takenpakket behoorde, heeft hij mij zeer dikwijls met raad en daad bijgestaan. Mede daardoor is dit proefschrift toch uitgekristalliseerd!

Voor ondersteuning van de experimentele werkzaamheden bij API dank ik Paul Durville en Jan Heerens.

De directie van het ECN in Petten stelde mij een werkplek (dicht bij zee) en de benodigde faciliteiten voor het uitvoeren van de radiotracer proeven ter beschikking.

Prof. H.A. Das wil ik bedanken voor de getoonde belangstelling voor met name het radiotracer werk, waardoor een tweetal publikaties tot stand zijn gekomen.

Dr. H.A. van der Sloot gaf de voorzet tot het uitvoeren van de uitloog/carbonatatie proeven. Pieter Kleingeld (UU) hielp met de bijzondere experimentele opstelling voor deze proeven.

Dirk Hoede, Petra Bonouvrie en Dick Beuker ben ik erkentelijk voor hun helpende hand.

De opmaak van dit proefschrift is mede verzorgd door Arjen van der Weijden.

Het zijn de gunstbewijzen des Heeren dat wij niet omgekomen zijn,
want zijn barmhartigheden houden niet op,
elke morgen zijn zij nieuw,
groot is uw trouw!

Klaagliederen 3:22-23

Curriculum Vitae

Renata van der Weijden
geboren op 5 april 1962 te Doorwerth

1974-1981	vwo Atheneum B, G.S.A., Amersfoort
1975-1976	Park Forest Junior High School, State College, Pennsylvania
1981-1988	Geochemie (oude stijl), Aardwetenschappen, Universiteit Utrecht
1988-1989	Research Assistant /Chemical Oceanography, Florida State University, Florida
1989-1994	Assistent-in-opleiding, Geochemie, Universiteit Utrecht
1995	werkzaam bij Baan Research, Ede